1-1-2017

Mechanical Interventions In Soft Tissue Repair

Elizabeth Marie Meier
Wayne State University,

MECHANICAL INTERVENTIONS IN SOFT TISSUE REPAIR

by

ELIZABETH MEIER

DISSERTATION

Submitted to the Graduate School

of Wayne State University,

Detroit, Michigan

in partial fulfillment of the requirements

for the degree of

DOCTOR OF PHILOSOPHY

2017

MAJOR: BIOMEDICAL ENGINEERING

Approved By:

Advisor: Mai T. Lam, Ph.D.	Date
Karin Przyklenk, Ph.D.	Date
Wei-Ping Ren, M.D., Ph.D.	Date
Harini Sundararaghavan, Ph.D.	Date

ACKNOWLEDGMENTS

TABLE OF CONTENTS

LIST OF TABLES

LIST OF FIGURES

CHAPTER 1: INTRODUCTION

Background and Significance

Mechanical interventions in wound healing and repair have been used since the ancient Egyptians, who were the first documented cases of splinting broken or injured limbs (Fess 2002). While medical practices have advanced significantly since then, mechanical interventions have and will continue to be necessary for some injuries, at least for the foreseeable future. With this in mind, this body of work sets to investigate some of these mechanical interventions that are designed to promote wound healing, repair, or even replace an injured tissue.

Traditionally, describing the effectiveness of mechanical interventions has been simply a matter of whether or not mechanical integrity was restored to the damaged tissue. For example, the success of the earliest splints was determined by observed improvements in the healing of broken bones. However, mechanical interventions can have physiological effects, both expected and unexpected, that can drastically affect other aspects of the tissue's performance. These physiological effects can range from providing temporary support to damaged protein filaments, to directly affecting gene expression in cells, to altering system-wide physiological responses to an injury. The purpose of this work is to investigate a range of previously used mechanical interventions and determine the physiological effects, both expected and unexpected.

Firstly, one of the most widely used and simple mechanical interventions is investigated. The use of sutures to close wounds to promote faster healing is a practice familiar to the general public. Human skin samples were sutured and loaded in tension in

multiple orientations to determine how the injury and suture treatment change the tensile mechanics of our most superficial organ. Next, the cellular component of tissue engineering was addressed. Specifically, a unique biochemical and mechanical approach was take to create a meniscus cell source from human adipose-derived stem cells. Thirdly, the inflammatory (biochemical) effects of decellularized ECM in a wound healing model were analyzed. A commercially available decellularized material, porcine small intestine submucosa (SIS), was evaluated as a patch treatment in a rat myocardial infarction model. While the mechanical benefits of an SIS patch treatment have been established, it was previously unknown how this decellularized tissue would affect inflammation, and therefore wound healing, of such a critical injury. While each of these individual works focuses on a different tissue system, each tissue system presents with specific injuries that can be aided by mechanical interventions. These tissue systems and mechanical interventions are described, tested, and discussed in the following pages.

Skin Mechanics

The integument system, also known as skin, is a three-layered organ that covers the entire body and serves as a physical barrier to protect the body from its surrounding environment. To function properly, skin must be strong and durable but flexible enough to allow movement. This is accomplished through an extracellular matrix (ECM), comprised of vast networks of collagens and elastin fibers as well as a complex population of glycosaminoglycans (GAGs) and proteoglycans (Corr 2011). While all components are present in each of the three layers, it is the largest layer, the dermis, that bears the greatest responsibility for the skin's mechanical behavior. Several types of collagen are present in the skin, although collagen I has the greatest direct contribution to tissue

mechanics, and therefore will be the main focus of this analysis. Collagen I in its mature form consists of globular collagen units covalently bonded into a right-hand triple helix filament (Holzapfel et al. 2000). Collagen I is very strong and stiff when stretched along its long axis, with an elastic modulus in the range of 5- 10 GPa (Wenger et al. 2007). By dry weight, collagen I accounts for 60-80% of skin, and therefore is the dominating protein in skin's mechanical behavior (Holzapfel et al. 2000). Elastin is another fibrous ECM protein and it accounts for 5-10% of skin by dry weight (Holzapfel et al. 2000). Elastin differs from collagen I in that its fibril structure is seemingly more organized. This organization is key to its mechanical behavior. Under tension, the fibrils display entropic straightening, resulting in energy "absorption" in the filament (Holzapfel et al. 2000). The elastin fibers have various dominating orientations depending on the location of the skin on the body, yet is always aligned with the layers of the skin (Holzapfel et al. 2000). Also present in the skin are proteoglycans, the most common of which is versican (Carrino et al. 2011). Proteoglycans are heavily glycosylated proteins that act to retain water in the tissue (Carrino et al. 2011, Holzapfel et al. 2000). In tensile skin mechanics, proteoglycans act as lubricants easing movement of collagen filaments past each other as tension is applied (Carrino et al. 2011, Holzapfel et al. 2000). This unique combination of ECM proteins gives rise to viscoelastic mechanical behavior, in that the tissue behaves in a time-dependent fashion when under load (Corr et al. 2011). Under non-loading conditions, collagen I fibrils are crimped and disorganized among proteoglycans and elastin fibrils (Holzapfel et al. 2011). The crimped, random organization of collagen can be seen in Figure 1, along with the organization of elastin fibrils.

When a load is applied in tension, the ECM proteins undergo three distinct phases. The first phase involves primarily the uncoiling and straightening of elastin filaments. The absorption of energy by elastin filaments results in minimal strain, or lengthening, of collagen and of the tissue as a whole. Rather, the elastin filaments straighten and stretch, preserving the overall integrity of the tissue (Holzapfel et al. 2000, Langdon et la. 2017). This phase I behavior is frequently referred to as the "toe" region on a stress-strain curve. Beyond this initial phase, the mechanical behavior of skin is primarily dominated by the
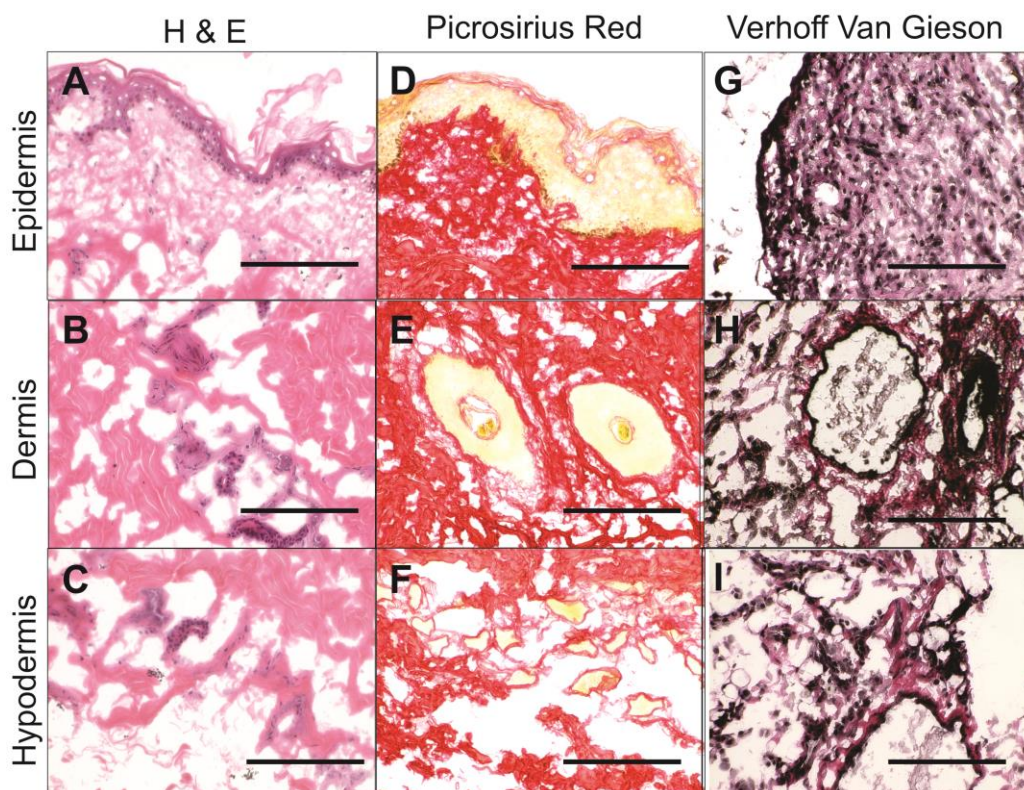
Figure 1. Histological analysis of each skin layer. Areas of cellularity and structural variation can be seen each each of the three layers (A-C). High collagen content and its disorganized structure can be seen in D-F. Elastin's orientation can be seen in the cross-sectional view, particularly in the epidermis (G) and dermis (H). Scale bar = 200 μm.

behavior of collagen (Corr et al. 2011, Holzapfel et al. 2000). This is illustrated in the

second phase, in which elastic behavior is observed and the stress-strain relationship is mostly linear. In this phase, the crimped collagen I fibers are stretched and straightened, aided in part by lubrication from proteoglycans (Holzapfel et al. 2000, Corr et al. 2011). As the collagen fibers are merely reoriented and not deformed, they will resume their original, crimped form if the stress is removed, exhibiting elastic behavior. Finally, in the third and final phase, collagen fibers are stretched, deformed and eventually break and slide past each other (Holzapfel et al. 2000). This is the plastic deformation region and it concludes when the collagen fibers break, signifying failure strength has been reached. All of this behavior is captured in Figure 2.

While this behavior is very consistent in uninjured skin samples, it is largely unknown how mechanical interventions, such as suturing may affect this behavior. The vast majority of skin mechanics studies involve computer models, xenografts, or both (Chanda et al. 2016, Levi et al. 2016, Capek et al. 2012). The few studies that have investigated suture mechanics in human skin have done so *in vivo*, which clearly limits the mechanical parameters that can be applied. As patient consent and comfort much be considered in *in vivo* work, these studies are limited to low tensile loads and strains, it is unlikely that they encompass the full mechanical behavior of sutured skin that a patient could experience. For example, one such study limits the tensile strain to 5%, which is well below the failure strain of intact human skin, which has been reported to be as high as 115% (Levi et al. 2016, Holzapfel et al. 2000). It is therefore highly likely that the reported mechanical behavior in such studies are restricted to the viscoelastic toe region of skin's stress-strain curve (Figure 2). However, skin is not limited to 5% strain in day-to-

day activities and therefore this information cannot be considered sufficient to characterize the full range of tensile mechanics of skin.

Sutures are perhaps the most commonly used and most basic mechanical intervention in regenerative medicine. While numerous materials are used for sutures, as a general rule, they have relatively high stiffness and strength, in the range of 5-50 GPa (Greenwald et al. 1994). It is unclear how sutures affect skin mechanics, as there is little to no research on the topic. As the skin's function is dependent upon its integrity, it is highly important that we understand how suturing affects the integrity, and therefore function, of skin. While numerous attempts at creating synthetic skin and computer models have been attempted, accurate information is still lacking (Chanda et al. 2016, Capek et al. 2012). Therefore, part of this body of work will focus on how sutures affect skin mechanics.

Biomechanics of the Meniscus and Cell Development

Like the skin, the meniscus is a complex tissue designed to withstand a range of forces that occur in everyday movements. Unlike skin however, the meniscus does not self-heal, even with the assistance of basic interventions,

Figure 2. Diagram showing collagen I fiber conformation relative to stress-strain behavior. Phase I ("toe region") minimally affects collagen fibers. Phase II shows the transition from viscous to elastic behavior. Phase III shows the purely elastic region leading to the plastic region (Holzapfel 2000).

such as sutures. Meniscal injuries are among the most common knee injuries

experienced by children and adults in the United States (McDermott et al. 2008, Malcris et al. 2004, Buma et al. 2004, Baker et al. 2009, Thambyah et al. 2006, Pteri et al. 2012). The meniscus is a disc-shaped tissue that lies on the surface of the tibial plateau in direct contact with the femoral condyles (McDermott et al. 2008, Malcris et al. 2004, Buma et al. 2004, Baker et al. 2009, Thambyah et al. 2006). The meniscus is a connective tissue that helps bear and distribute loads experienced by the knee during physical activity, preserving the tibial articular cartilage underneath. Injuries to the meniscus generally take the form of an abrasion or a tear and most commonly occurs during a rapid, dynamic movement in which torsion is applied to the meniscal surface (McDermott et al. 2008). Limited vasculature and exposure to high loads prevent native tissue from self-healing and current treatments are mainly restricted to partial or complete menisectomies (meniscus removal), which put the patient at very high risk for degeneration of articular cartilage and osteoarthritis (McDermott et al. 2008, Malcris et al. 2004, Buma et al. 2004, Baker et al. 2009, Thambyah et al. 2006, Son et al. 2013). Damage of the meniscus leads to increased compressive and tensile stresses on the articular cartilage and often leads to premature osteoarthritis and possible joint replacement (Buma et al. 2004). For this reason, a treatment beyond menisectomy is required. Biomaterial and tissue engineering strategies have been proposed for both repair and replacement of damaged meniscus tissue, but have so far failed to address the intricacies of this complex tissue. Biomaterial strategies have looked at allografts, natural scaffolds, and polymer-based synthetic replacements, all of which have their advantages and disadvantages. The meniscus has also been studied for possible tissue engineering solutions, with a major focus on identifying a cell source to produce adequate extracellular matrix to perform the

mechanical tasks required of this tissue. This review will address the characterization of the physiology and function of the native tissue and describe some of the current techniques and research aimed at addressing additional treatments beyond menisectomy.

Anatomy and Physiology
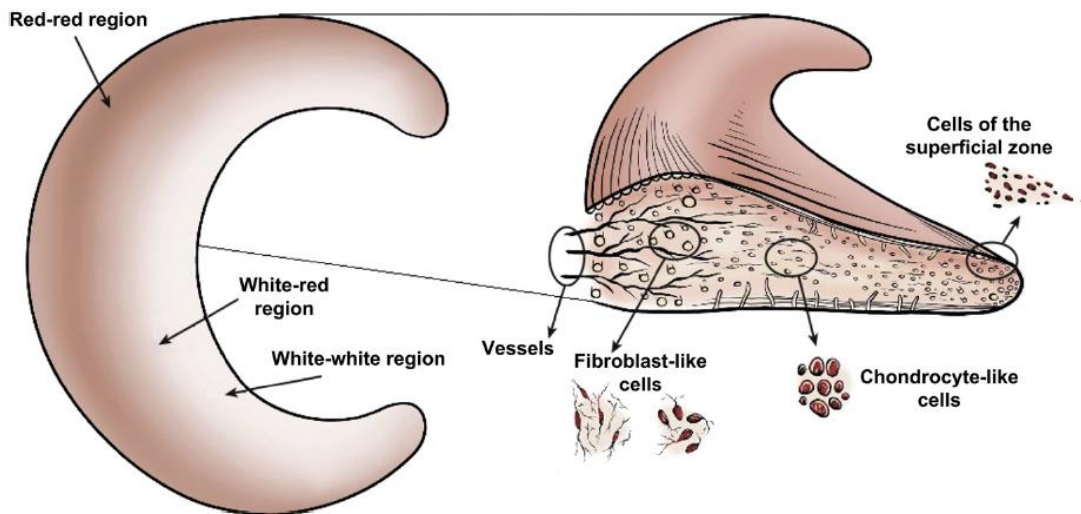
Figure 3. Diagram showing zones of the meniscus (McDermott et al. 2008)

The meniscus is a highly specific tissue, responsible for bearing and redistributing loads across the knee (McDermott et al. 2008, Makris et al. 2004, Son et al. 2013). On multiple levels, the meniscus can be divided into regions based on physiology and function. On a macroscopic level, the meniscus can be divided into three regions based on vasculature, with the greatest vasculature, "red zone", developing in the most lateral third of the meniscus (Makris et al. 2004, Buma et al. 2004, Son et al. 2013). Moving medially, the next region is a semi-vascular region commonly referred to as the red-white zone. The inner third is almost completely avascular and is known as the white zone. All of this is visually described in Figure 3. Damage to the outer, vascular, red zone tissue

can self-heal, but damage to the inner red-white or white avascular areas is generally stagnant due to the limited blood and nutrient supply (Makris et al. 2004, Buma et al. 2004). This limited vasculature is something of a double-edged sword as it indicates that establishing vasculature is not a major obstacle for tissue engineering strategies, as is almost always the case with other tissues, however the body's capacity to heal is the cornerstone of tissue engineering and regenerative medicine.

Beyond the vasculature, the meniscus structure is highly complex, consisting of two distinct regions of collagen fiber arrangement. The outer third shows circumferentially oriented collagen fibers, primarily collagen I, and experiences mostly tensile deformation under loading. These fibers help conserve the meniscus shape and contribute to resisting deformation due to the high mechanical loads (McDermott et al. 2008, Makris et al. 2004). Conversely, the inner two thirds of the meniscus display radially oriented collagen I and II fibers and experiences mainly compressive deformation under loading. These collagen fibers are accompanied by a high concentration of proteoglycans that contribute to the region's compressive stiffness through water retention (McDermott et al. 2008, Makris et al. 2004, Nishimuta et al. 2012). This complex 3D extracellular matrix structure is designed to withstand high cyclic loads. The tissue itself is composed of a gradient of cells that exhibit a mixed phenotype, with characteristics similar to cartilage and ligament. These cells are commonly called fibrochondrocytes (McDermott et al. 2008, Makris et al. 2004, Buma et al. 2004, Son et al. 2013, Kun et al. 2012, Nishimuta et al. 2012). As would be expected, meniscal cells secrete a variety of extracellular matrix proteins, including collagens I and II, versican, aggrecan, and other glycosaminoglycans and proteoglycans. Cells in the outer region have a fibroblast-like morphology and show increased expression

of collagen I and versican (McDermott et al. 2008, Makris et al. 2004, Buma et al. 2004). Cells in the inner region have a rounded morphology and behave more like chondrocytes including aggrecan and collagen II (McDermott et al. 2008, Makris et al. 2004). The cellular expression and distribution contribute to a meniscus that is 72% water and 28% organic matrix (Makris et al. 2004). Of this 28%, collagen makes up the majority (75%), then GAGs (17%), the remaining consists of cells, adhesion glycoproteins, and elastin (Makris et al. 2004). The location and population of meniscal cells, proteins, and collagens in the meniscus are critical to its mechanical function. Also of note are the anchoring ligaments that help hold the meniscus in place. The anterior intermeniscal ligament connects the anterior horns of the medial and lateral meniscus, forcing these two seemingly separate tissues to act as one (McDermott et al. 2008, Makris et al. 2004). All of these physiological features contribute directly to the mechanical integrity of the tissue and ultimately, the knee itself.

Stem Cells in Meniscus Tissue Engineering

When native tissues are incapable of providing adequate cell populations for treatments, researchers look to other donor sources and autologous stem cell sources. When dealing with connective tissues, such as the meniscus, there are several autologous stem cell sources. While human embryonic stem cells (hESCs) remain the gold standard for any stem cell-based therapy, meniscus tissue engineering strategies have often used mesenchymal stem cells (MSCs), generally from bone marrow, although adipose-derived stem cells (ASCs) have been gaining traction due to ease of harvest and patient compliance (Makris et al. 2004, Baptista et al. 2013, Kokai et al. 2014, Pak et al. 2014). MSCs have been shown to readily differentiate to various connective tissues,

including fibroblasts and chondrocytes, although a definitive differentiation protocol to the hybrid fibrochondrocyte phenotype has yet to be established. Similarly, ASCs have been shown to be capable of differentiating to cartilage and fibroblasts, with evidence suggesting that meniscus cells, or meniscus-like cells, also being very possible (Kokai et al. 2014). Many of these studies have provided much evidence to support that use of certain growth factors used in chondrogenesis, such as TGF-β, can induce expression of GAGs and biglycans in meniscal cells and MSCs in culture (Buma et al. 2004). Less well-known, platelet-derived growth factor (PDGF) has shown to counteract production of α-smooth muscle actin, which is often stimulated by TGF-β (Buma et al. 2004). Smooth muscle actin is a key indicator of scar tissue formation and can cause contraction of the scaffold, often as great as 50%, which is unacceptable for a tissue construct dependent upon its structure to fulfill its function (Buma et al. 2004). One of the more interesting findings is that culturing ASCs in chondrogenic media can yield cells with the same gene expression of Sox9, aggrecan, and collagen II as cartilage progenitor cells in the same media (Baptista et al. 2013). This indicates an unprecedented affinity for ASC differentiation to a cartilage-like phenotype and gives a strong basis for cartilage and meniscus tissue engineering techniques involving ASCs.

Beyond biochemical factors, mechanical stimulation of stem cells can encourage differentiation, especially to cell types that typically undergo high and/or cyclic loading conditions, such as muscle, ligament, bone, and cardiac tissue (Park et al. 2013). While the exact pathways are unknown, it is understood that transduction of mechanical signals are responsible for the up regulation of these proteins in the cell (Schwartz et al. 2013). During development, these mechanical stimuli can be the result of external forces on the

embryo, or forces generated from differences in tissue growth rates and/or early contraction of developing muscle and neural tissue (Schwartz et al. 2013). In fact, restricting movement in developing chick embryos results in malformation of bone and limited formation of cartilage and other connective tissues (Schwartz et al. 2013, Mikic et al. 2000). It is also known that mechanical forces are required for proper development of non-mechanical tissues such as the vasculature, kidneys, and lungs, supporting the need to investigate stem cell differentiation techniques beyond biochemical factors (Schwartz et al. 2013).

One of the more thoroughly studied effects of tensile strain is its effects on the TGF-β pathway (Meier et al 2016, Li et al 2010). An illustration of the mechanism can be viewed in Figure 4. Activation of this pathway results in activation of numerous key transcription factors within the cell (stem cell or adult cell), leading to changes in gene transcription and, often, phenotype in the case of stem cells (Li et al 2010). Activation of TGF-β pathway is crucial for differentiation of fibroblasts, chondrocytes, and osteocytes (Li et al 2010, Khani et al 2014, Saha et al 2008). Specifically, activation of TGF-β pathway leads to up regulation of collagen I and versican (Li et al 2010, Khani et al 2014). Uniaxial tension has also been shown to align F- actin and other skeletal components, increasing the elastic modulus of the cell and altering its transcription pathways (Khani et al 2014, Teramura et al 2012). Importantly, tensile strain applied to stem cells has been shown to inhibit certain differentiation pathways, particularly adipogenesis (Sen et al 2011). This is achieved through changes in the cytoskeleton which not only increase stiffness of the cell, but increase focal adhesions, which also affect the cell's transcription pathways (Teramura et al 20102, Sen et al 201). Additional focal adhesions make the cell

increasingly sensitive to tensile strain, effectively initiating a feed-forward mechanism towards differentiation to a musculoskeletal phenotype, such as fibroblasts, osteocytes, or skeletal muscle (Sen et al 2011). The specific differentiation pathway is dependent upon other factors in the cells' environment at the time of applied tension.

Numerous studies have shown that substrate stiffness can direct stem cell morphology, with softer substrates encouraging a more rounded morphology in MSCs and harder substrates directing cells towards elongation (Galie et al. 2013, Cheung et al. 2009, Lam et al. 2009). Healthy chondrocytes in the knee *in vivo* are generally subjected to repetitive cyclic loads of 3-20MPa, which can encourage increased expression of
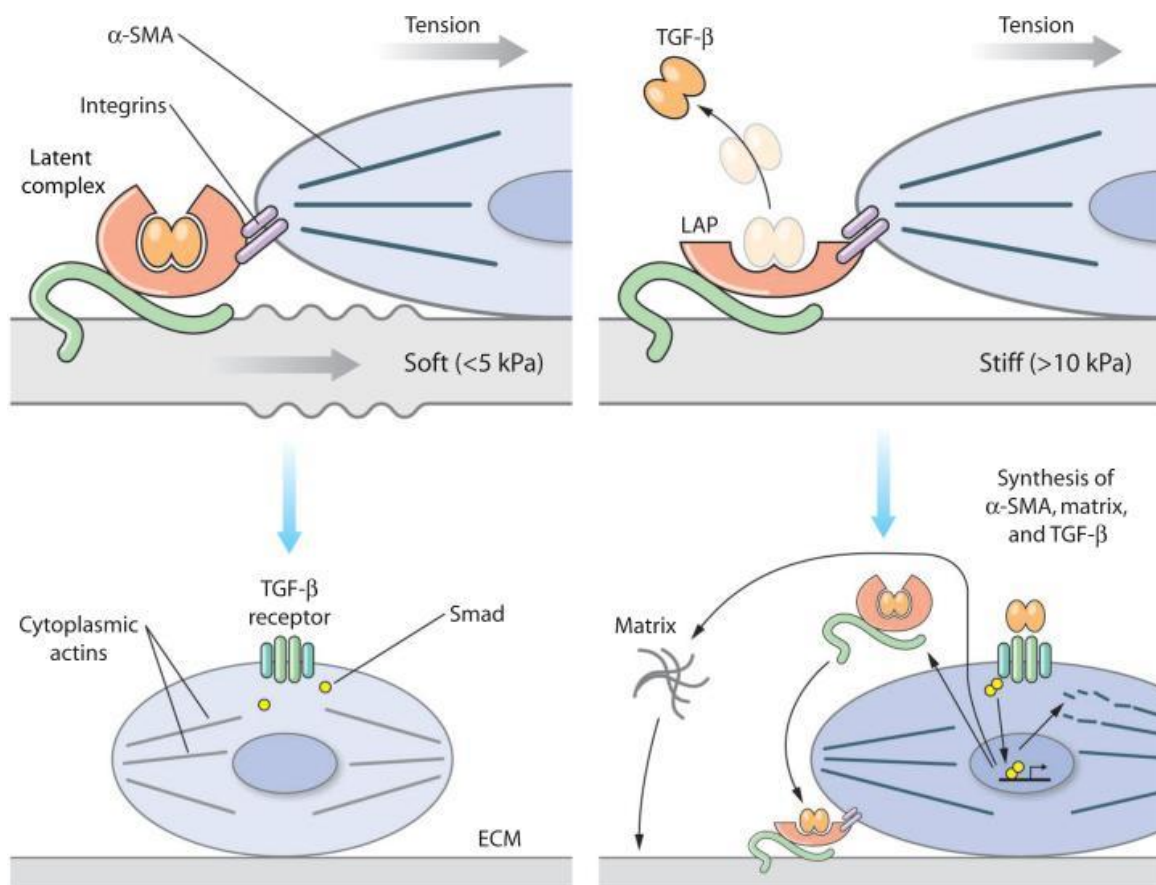
Figure 4. Diagram of how substrate stiffness and applied tension result in activation of TGF-β pathway. Expressed proteins act to resist applied tension (Wells et al. 2008).

GAGs and collagen II (Buma et al. 2004). Similar stimulation can affect differentiation of MSCs, especially in the presence of chondrogenic media including TGF-β (Petri et al. 2012, Kun et al. 2012, Nishimuta et al. 2012, Baptista et al. 2013, Buma et al. 2004). Fibroblasts can similarly be obtained, generally through tensile strains of 10-20% (Buma et al. 2004). It stands to reason then, that combinations of these growth factors and mechanical stimulation techniques could encourage features of both fibroblasts and chondrocytes in MSCs. It should be noted that the term mechanical stimulation can apply to a wide range of techniques and magnitudes of stimulation. One such study looked at combining continuous perfusion with 8 hours of cyclic compression. MSCs seeded on a collagen I fibrous scaffold were exposed to perfusion with chondrogenic media, perfusion with compression, or no stimulation at all. Compressive modulus of scaffolds that underwent perfusion and mechanical stimulation doubled that of the control group (24.7 kPa and 12.3 kPa, respectively). A significant increase in the rate of production of matrix proteins was also observed, yet levels were well below that of native tissue. It is also important to note that even the highest compression modulus is still a far cry from the native modulus, about 400 kPa, partially due to the relatively low compressive modulus of collagen I and limited time allowed for cells to replicate and produce matrix (10 days) (Petri et al. 2012, Lam et al. 2009). Another example of mechanical stimulation used MSCs with a fibrin and alginate hydrogel. By varying the concentrations of each component, researchers were able to control the differentiation and scaffold characteristics. Fibrin helps maintain gel extensibility and encouraged cell proliferation. Alginate encourages expression of chondrogenic genes, such as Sox 9 and Aggrecan, as well as production of collagen II and GAGs (Kun et al. 2012). It also resists the

contraction and shrinking of fibrin, although it is generally brittle and can tear easily (Kun et al. 2012). Based on previous work demonstrating that tensile strain increases GAG and collagen population, 1 week was found to be appropriate duration for tensile loading for optimal expression of key meniscus genes in the fibrin-alginate gel. Through measuring mechanical and biochemical properties and gene expression, they determined that a 40:8 ratio of fibrin to alginate had the best combination of net effects and would be the best composition of the two for future applications (Kun et al. 2012). This study is one of the few that combines that benefits of stem cells and adjustable materials with mechanical stimulation, an approach which will most likely be required in a long-term clinical solution. A third study looked at the effect of strain rates on healthy cartilage and meniscus explants to compare published effects of strain on developing cells and reaction of healthy cells. Cartilage and meniscus explants were subjected to several compressive strain rates (0.5%/s, 5%/s, and 50%/s) and tested for metabolic activity, water, and GAGs. Total strain was 40% for all strain rates. At the higher loading rates, cells began to lysis and no significant GAG increase was observed for any of the strain rates (Nishimuta et al. 2012). This is to be expected as normal strain rates for healthy adults is generally 19-21% (Chia et al. 2008). Loading beyond 25% strain can cause permanent deformation due to the tissue's inability to achieve full hysteresis (Chia et al 2008). This indicates that relatively higher strains than *in vivo* may be necessary for full differentiation *in vitro*.

Myocardial Infarction Injury and Wound Healing

When considering the role of mechanics in physiology, it is impossible to overlook the cardiovascular system, in which the heart serves as a pump to circulate blood throughout the body. One of the more detrimental injuries to this system is myocardial

infarction (MI), which can lead to heart failure and death (Zhang et al. 2015). Like the meniscus, the heart has limited capacity to heal. Unlike meniscus, but similar to skin, relatively simple mechanical interventions can vastly improve long term outcomes. MI occurs when an occlusion is formed in a coronary artery, restricting blood flow to a region of cardiac tissue. An illustration of this can be seen in Figure 5A. The induced ischemia results in localized cell and tissue death, with a resulting scar tissue forming over the injured area (Olivetti et al. 1990). This layer of scar tissue is stiff and exerts additional forces on the surrounding, surviving, myocytes as the ventricle contracts and distends. This cyclic tensile strain results in a condition sometimes referred to as tissue "slippage", in which the surrounding tissue is stretched and the scar tissue is thinned. Initial slippage can occur as early as a few days after the initial infarct (Olivetti et al. 1990). This tissue
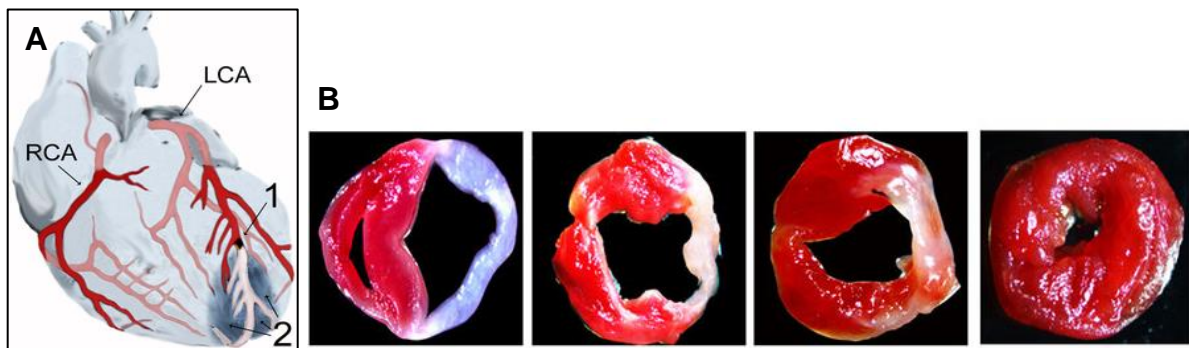
Figure 5. Myocardial infarction and post-infarct remodeling. (A) Myocardial infarction (MI) occurs when a coronary artery is obstructed (1). The ischemia results in tissue death (2) (Wan et al. 2013). **(B)** Images showing infarcted rat heart (left), two patch treatments (middle), compared to healthy tissue (right) (Wan et al. 2016).

remodeling increases the total volume of the ventricle while decreasing contractility of surviving myocytes (Olivetti et al. 1990) In rare cases, this can lead to scar rupture, but more frequently leads to long-term remodeling and complications, such as heart failure. A visual representation of this process can be seen in Figure 5B.

The formation of this scar tissue and its mechanical properties are the key to determining long term prognosis (Wan et al. 2013, Zhang et al. 2015). Tissue remodeling of the infarct area is dependent upon local inflammatory response, with "normal" healing resulting in a thin layer of scar tissue that cannot properly resist the wall pressure and will eventually distend (Zhang et al. 2015). If the scar does not provide resistance to these high pressures, it will increase wall stress on the surrounding tissue. Increased wall stress can affect cell metabolic processes, which leads to increases in the dysfunction and remodeling in the area (Zhang et al. 2015). The resulting complex tissue remodeling is dependent upon local and systemic inflammation and excessive inflammatory response can result in poor remodeling that increases the risk of development of heart failure (Wan et al. 2015). However, impeding the inflammation response can result in non-adaptive fibrosis, which can lead to cardiac rupture (Wan et al. 2015). Clearly this indicates that the components of the inflammatory response can directly predict patient outcome. A high level overview of the inflammation response can be seen in Figure 6, along with the follow written description.

Inflammation Response in MI

Upon the onset of ischemic conditions, hypoxic cardiomyocytes release danger-associated molecular pattern (DAMP) molecules (Altara 2016, Boag 2016, Feng et al. 2015). This class of molecules include DNA, heat shock proteins, and adenosine triphosphate, among others (Altara 2016, Feng et al. 2015). The release of these molecules trigger the complement system cascade and signal neutrophils to the injured area (Altara 2016, Boag 2016, Feng et al. 2015). DAMPs can activate toll-like receptors (TLRs) in other cells, leading to cytokine release (Boag 2016, Feng et al. 2015). Damage

to myocytes also results in release of reactive oxygen species (ROS), which can cause further direct industry as well as stimulate cytokine release (including TNF-α and IL-1β) (Frangogiannis 2002, Feng et al. 2015).

Injury to myocytes also activates the complement cascade via release of mitochondria membrane components that activate C1-C4 of the cascade (Frangogiannis 2002, Feng et al. 2015). Activation of the complement cascade contributes to leukocyte recruitment (Frangogiannis 2002, Feng et al. 2015). C5a has been shown to be needed for local monocyte chemotaxis to the injury area (Frangogiannis 2002, Feng et al. 2015). TNF-α is a known inducer of the cytokine cascade (Frangogiannis 2002). ROS and C5a are thought to induce Mast cell degranulation (Frangogiannis 2002). ROS can also promote neutrophil binding to endothelial cells and promote chemotaxis (Frangogiannis 2002).

Ischemic cells also release ROS and trigger release of cytokines, including TNF-α, IL-6 (Boag 2016, Frangogiannis 2016). Cytokines released, including TNF-α and IL-1β, activate the nuclear factor κβ (NF-κβ) complex (Frangogiannis 2002). TNF-α is thought to have other roles in inflammation post-MI (Frangogiannis 2002). TNF-α receptor knockout mice had significantly larger infarcts, greater myocyte necrosis, and reduced outcome compared to control animals (Frangogiannis 2002). This suggests that TNF-α may be necessary to promote and complete inflammation, likely due to activation of NF-κβ, which is known to be active in inflammation and inflammation-related pathologies (Lawrence 2009).

<u>Neutrophils in Inflammation</u>

Along with increased matrix production, these initial inflammatory pathways have an important role in recruitment of leukocytes to the area. IL-1β importantly acts to stimulate neutrophil migration into the area (Chen et al. 2013). As the first leukocyte to "arrive" to an injured area, neutrophils are an excellent indicator of the time progression of inflammation. Indeed, the beginning of inflammation is marked with a sudden influx of neutrophils to the area, especially after reperfusion (Stuart et al. 2016). Activation of the complement cascade, ROS, and TNF-α trigger circulating neutrophils to begin to arrive at the injury site (Bonaventura 2016, Boag 2016). Upon arrival, chemokines released from the injury help neutrophils adhere to the endothelial cells in the surrounding blood vessels, which contract and reduce the number of interendothelial junctions to permit the neutrophil passage (Bonaventura 2016, Boag 2016). Upon passage, they release chemokines, cytokines, inflammatory mediators, and reactive oxidative species (ROS). Cytokines and chemokines released initially include TNF-α, monocyte chemoattractant protein-1 (MCP-1), IL-6, IL-2 (Altara 2016, Bonaventura 2016, Stuart 2016). In particular, TNF-α expression and concentration directly correlates with patient mortality (Feng et al. 2015). Within a few hours, neutrophils are present in the injured area and last for the first few days of inflammation (Caimi et al. 2015, Stuart et al. 2016). In the injury area, neutrophils act to phagocytose the injured cell debris (Stuart et al. 2016).

These initial actions lay the groundwork for the overall inflammation process, particularly influencing ECM turnover and macrophage response and behavior (Altara 2016). After adhesion, neutrophil granules release MMPs, particularly MMP-2, MMP-8, and MMP-9, enabling neutrophil migration further into the tissue (Altara 2016). Matrix metalloproteinases (MMPs) are a family of zinc-dependent peptidases that actively cleave

various ECM proteins (Iyer 2016). MMPs are released by a number of cells in the heart including cardiomyocytes, macrophages, fibroblasts, neutrophils, and endothelial cells (Iyer 2016). Of particular importance are collagenases MMP-1 and -8 as well as MMP-2, which is a gelatinase (Iyer 2016). Once located in the injured area, the neutrophils release azurophilic granules, which are visible in differential-quick stains, and include serine proteases and neutrophil elastase (Altara 2016).

Neutrophil population dramatically decreases by day 7 as a result of apoptosis and phagocytosis. In chronic inflammation, neutrophil population is constantly replenished as chemokines continue to trigger attraction and migration to the injury area (Altara 2016). Indeed, neutrophil population post-MI has been identified as a clear predictor of patient death (Feng et al. 2015). Due to this, neutrophil population is frequently used as a tool to identify chronic inflammation resulting from high-risk myocardial infarction injury (Altara 2016, Stuart 2016, Feng et al. 2015).

<u>Macrophages in Inflammation</u>

Within the first hours of injury, neutrophils and monocytes are active at the injury location (Stuart 2016). The monocyte population increases are especially noticeable in ischemia-reperfusion injuries, in which perfusion occurs in fewer than 90 minutes. In these cases, circulating cells have direct access to the injury (Boag 2016). Macrophage response occurs in two phases: local monocytes in the tissue and circulating monocytes that arrive and differentiate into macrophages around day 3 of inflammation (Altara 2016). Both localized and circulating monocytes arriving in the injury area differentiate to macrophages. Macrophages exist in two distinct phenotypes (M1 and M2) (Wan et al. 2015). M1 macrophages are pro-inflammatory, while M2 macrophages are anti-

inflammatory and may have protective benefits post-remodeling (Wan et al. 2015). Polarization towards one phenotype or the other is determined, at least partially, by the inflammatory state of the injury. M1 differentiation is stimulated by high levels of IFN-γ, a result of the complement pathway, while IL-4 is required for the M2 phenotype (Geissman et al. 2010, Wan et al. 2015). Monocytes presenting shortly after ischemia differentiate to M1 phenotype (pro-inflammatory) macrophages, due to the active complement system and active cytokines. By the third day after injury, the M1 macrophages are the dominant cell type in the inflammation area (Stuart 2016, Feng et al. 2015). M1 phenotype increases the inflammatory process by releasing cytokines, including TNF-α, IL-1β, and MMPs (Altara 2016, Stuart 2016, Wan 2016). M1 macrophages also produce collagenases including matrix metalloproteinases (MMPs) (Stuart et al. 2016, Feng et al. 2015). This activity leads to fibroblast production, migration, and ECM degradation (Altara 2016). Additionally, M1 macrophages phagocytose myocytes and neutrophils, an action that is thought to trigger M2 (Altara 2016).

Later in the inflammatory phase (approximately day 5 and on) M2 macrophages are dominant, helping to induce the myofibroblast phenotype in cardiac fibroblasts, in part due to release of TGF-β (Stuart 2016, Feng et al. 2015). Stimulating myofibroblasts results in production of extracellular matrix, notably collagen, and scar formation (Stuart 2016). M2 macrophages increase expression of TGF-β1, encouraging the myofibroblast phenotype in CFs and increase matrix production (Geissman et al. 2010, Wan et al. 2015, Stuart et al. 2016). M2 macrophages have an anti-inflammatory or inflammation resolution phenotype, expressing anti-inflammatory markers that encourage collagen synthesis, myofibroblast phenotype, and angiogenesis (Altara 2016). Inflammation is resolved with

the activity of the M2 macrophage phenotype, which upregulates TGF-β, IL-10, and pro-fibrotic lipid mediators (Altara 2016). Apoptosis of macrophages indicates the end of the inflammation phase and beginning of the proliferation phase (Stuart et al. 2016).

Monocyte differentiation to macrophages and dendritic cells can also shed some light on the long term prognosis in MI. Monocyte-derived macrophages are the predominant inflammatory cell after approximately three days after injury occurs (Stuart et al. 2016). It is theorized that ideal wound healing will include a large portion of anti-inflammatory M2 macrophages compared to the pro-inflammatory M1 macrophages (Wan et al. 2015). Reduction in M2 macrophage recruitment, along with lower CD4+ T cells has been associated with weak, nonfunctional scar formation (Geissman et al. 2010, Wan et al. 2015). Furthermore, monocytes also possess the capability to differentiate into fibroblast-like progenitors in environments rich in TGF-β and other factors present with the M2 macrophage (Feng et al. 2015). Therefore, the domination of the M2 phenotype may also help increase the scar tissue formation by directing monocyte differentiation towards a fibroblast-like phenotype (progenitor) (Feng et al. 2015).

23

Figure 6. Overview of inflammation process post-MI.
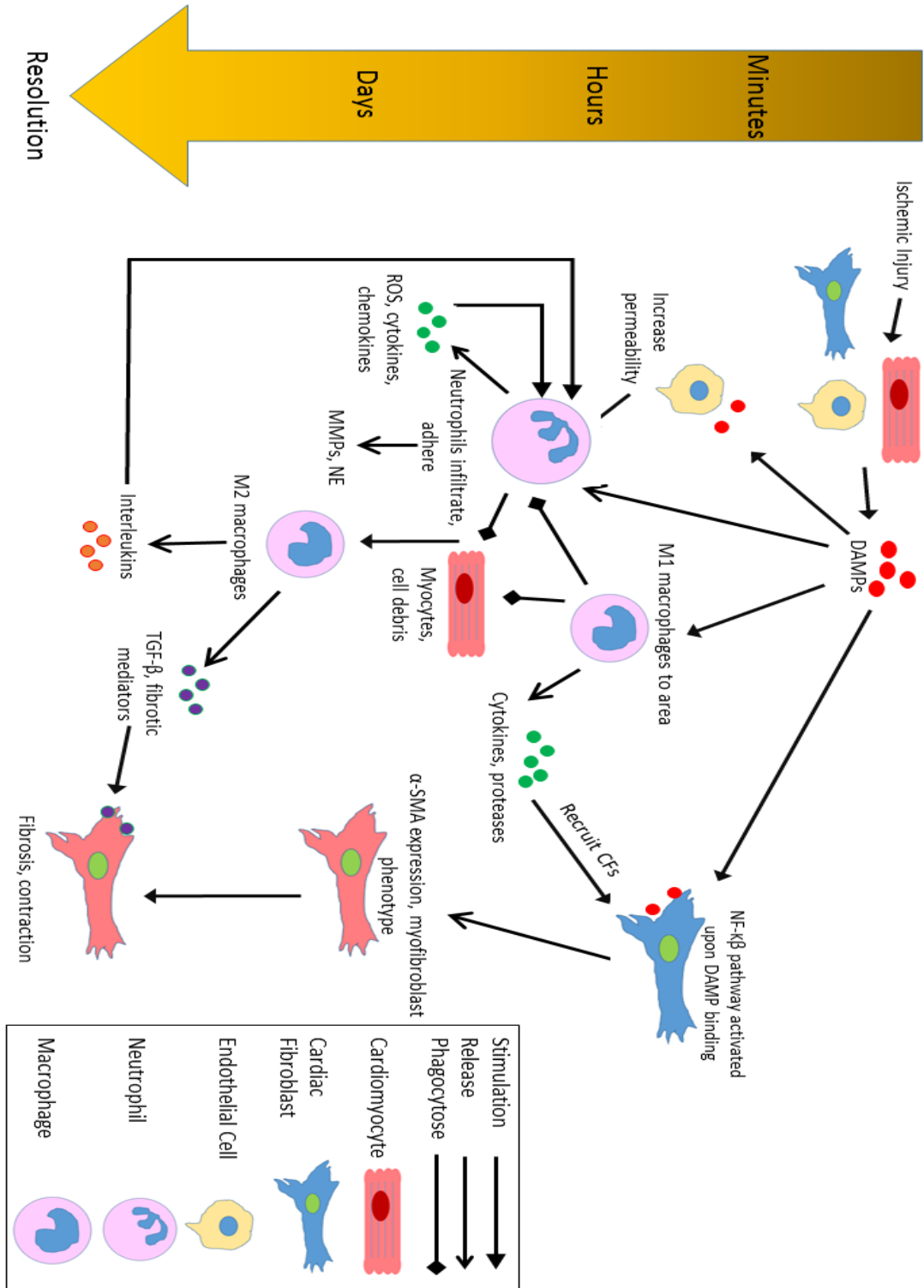
Cardiac Fibroblasts and Adoption of the Myofibroblast Phenotype

Like all injuries, cardiac ischemia due to myocardial infarction triggers an inflammatory response that helps process the damaged tissue and promote wound healing. Cardiac fibroblasts (CFs) play a significant role in directing this inflammatory response. Unlike their myocyte counterparts, CFs are relatively unharmed by temporary hypoxic conditions, and therefore generally survive the ischemic incident (Chen et al. 2013, Shinde et al. 2014). CFs are implicated in directly activating the molecular pathways that stimulate inflammation (inflammasome) (Chen et al. 2013).

As injured cardiomyocytes release DAMPs, they activate toll-like receptors (Boza 2016, Altara 2016). Toll-like receptors (TLRs) are a type of IL-R ligand that can bind DAMPs, resulting in changes to cellular behavior (Boza 2016, Altara 2016). TLRs are present on cardiac fibroblasts, and upon binding, ERK1/2 and PI3k-Akt kinases activate the NF-κβ pathway, resulting in transcription of pro-inflammatory cytokines as well as α-smooth muscle actin (α-SMA) and other genes indicative of the myofibroblast phenotype (Boza 2016). This activation also triggers activation of the complement pathway and production of reactive oxidative species (ROS) (Chen et al. 2013). These products have a very strong effect on cardiac cells in the infarct area, triggering a complex inflammatory cascade (Chen et al. 2013, Shinde et al. 2014). Both the circulating cytokines and reactive oxidative species (ROS) can act upon CFs stimulating p38k and ERK1/2 pathways (Chen et al 2013, Shinde et al 2014, Boza et al 2016). These activated pathways, along with mechanical stress and exposed fibronectin, act to alter the cells towards an anti-apoptotic, myofibrotic phenotype, with increased fibrosis and expression of α-SMA (Chen et al. 2013). This new phenotype is only observed in the injured, inflammatory state. The

myofibrotic phenotype is primarily responsible for increased release of metalloproteinases (MMPs) and inhibit production of MMP inhibitors (Chen et al. 2013). This phenotype is also affected by latent TGF-β from earlier pathways, increasing the expression and production of matrix proteins, particularly collagen (Chen et al. 2013).

This progression towards the myofibroblast phenotype simultaneously influences, and is influenced by, neutrophil and macrophage activity. During early inflammation, cardiac fibroblasts proliferate and migrate into the injured area, where they release MMPs and inflammatory cytokines to contribute to the inflammatory process, along with neutrophils (Altara 2016). TGF-β also upregulates TL4, a type of TLR, further encouraging the myofibroblast phenotype (Boza 2016). Expression of ROS and cytokines contributes to neutrophil infiltration in the area, while myofibroblast activity influences macrophage phenotype (Boza 2016, Altara 2016). Approximately three days after injury, cardiac fibroblasts in the injury area have fully adopted the myofibroblast phenotype, in parallel with arrival of M2 macrophages (Feng et al. 2015). This phenotype preferentially expresses TGF-β, α-smooth muscle actin, and collagen I and is responsible for scar formation and contraction during inflammation and maturation (Altara 2016).

Mechanical stress in the area also contributes to the differentiation to the myofibroblast phenotype. The increased tension on the cells changes the cytoskeletal structure of the myofibroblasts (Boza 2016). This tension leads to increases in focal adhesions, which along with the changes in cytoskeletal structure, leads to increased expression of collagen (Khani et al 2014, Teramura et al 2012, Boza et al 2016). Collagen expression continues until the stress experienced by the cell is balanced by the newly formed collagen scar (Boza et al 2016, Altara et al. 2016). However, if the inflammatory

process does not progress properly or is not adequately resolved, complications can occur.

<u>Complications from Improper Inflammation</u>

The inflammatory process in many animals, including humans, has evolved to place priority on speed of wound closure, rather than regeneration (Godwin 2016). While this is ideal for limiting infection and other complications, it does prevent complete tissue regeneration after myocardial infarction. How this inflammatory process unfolds can directly affect patient outcome post- MI (Boag 2016, Chen et al 2013).

The outcome of inflammation is twofold: clear the injured area of cell and tissue debris, and produce the biochemical progenitors of fibrosis and angiogenesis (Bonaventura 2016). In many injuries, including MI, resolution of inflammation occurs seamlessly. However, unresolved inflammation can result in inadequate or excessive scar tissue deposition, arrhythmias, and other complications in MI (Altara 2016).

No effective treatment for myocardial ischemia has been identified to date (Boag 2016). Current best practice is to reperfuse the injury as quickly as possible after ischemia (Boag 2016, Stuart 2016). Reperfusion is achieved through primary percutaneous coronary intervention (PPCI), which reestablishes blood flow to the area (Boag 2016). Time is of the essence after onset of ischemia, After 90 minutes of occlusion, capillaries begin to plug with thrombi and cells (Boag 2016). This is known as microvascular obstruction, in which perfusion can't be maintained even though blood flow has been reestablished (Boag 2016). The accumulated cells also contribute to ROS production and contribute to inflammation (Boag 2016).

While reperfusion is generally accepted to improve outcomes, it is not without additional complications. Injury from reperfusion may be responsible for as much as 50% of infarct size (Boag 2016, Nah et al. 2009). This is mainly due to "Lethal reperfusion injury", in which previously surviving cells die due to the changes in ROS, pH, and mitochondria collapse (Boag et al. 2016, Nah et al. 2009, Przyklenk et al. 2012, Przyklenk 2014).

T cells can be activated by danger associated molecular patterns (DAMPs) (Boag 2016). T cells help limit infarct size and limit neutrophil and macrophage populations (Boag 2016). T helper cells also produce IFN-γ and TNF-α and support macrophage activity. Mice without lymphocytes saw reduced leukocytes in the infarct area, and reduced injury from reperfusion (Boag 2016, Feng et al. 2015, Nah et al. 2009). Innate immune cells (neutrophils, monocytes, etc) are thought to play a large role in regulating inflammation (Boag 2016, Feng et al. 2015). Inadequate macrophage population can prevent full scar tissue formation, potentially resulting in rupture (Stuart et al. 2016). Clinically, high neutrophil counts have been linked to a greater risk of mortality (Boag 2016). A reduced lymphocyte population and increased neutrophil population after reperfusion is a predictor for complications 3 years post-infarct (Boag 2016). The increased risk associated with high neutrophil populations may be due to the increased expression of MMPs. Excessive MMPs reduce scar tissue deposition and cross-linking, resulting in a thinner, weaker scar, which allows for excessive left ventricle dilation (Voorhees et al. 2015).

In MI without reperfusion, neutrophil population peaked at day 3, macrophages at day 7 (Boag 2016). With reperfusion, the peaks for leukocytes remained the same

although overall cell counts were lower (Boag 2016). Neutrophil elastase (NE) is overly active in chronic inflammation, in part because the α-proteinase inhibitor that would counteract NE's activity is itself deactivated by reactive oxidative species (Doring 1994).

Proper regulation of the inflammatory phase is crucial, as inadequate inflammation can be just as detrimental as excessive inflammation. While inadequate or inappropriate inflammation can lead to underdeveloped scar tissue, excessive inflammation however, can lead to overly fibrotic tissue (Stuart et al. 2016). In these cases, scar tissue can extend well past the injured area, affect mechanical and electrophysiological heart function. This can lead to arrhythmia or cardiac arrest (Stuart et al. 2016).

Similarly, overactive and underactive leukocyte activity during inflammation can lead to impaired healing and poor left ventricular remodeling (Stuart et al. 2016, Nah et al. 2009). This poor remodeling can also result in arrhythmias due to poor electrophysiological remodeling (Stuart et al. 2016). Therefore, even patients that survive the initial infarct can be at risk for heart failure or cardiac arrest (Stuart et al. 2016). The border region of the infarct zone is at the greatest risk for inflammation-induced arrhythmias, which can affect the surrounding, healthy tissue (Stuart et al. 2016). Over expression of TNF-α reduces cardiomyocytes' ability to repolarize, directly affecting potassium channels (Stuart et al. 2016). It also affects gap junction formation and conduction velocity by limiting the promoter of the connexin 43 gene, which is responsible for gap junction formation (Stuart et al. 2016). All of this can lead to arrhythmias. Excessive fibrosis in the interstitial space of the border zone can also result in arrhythmias, due to non-conductive collagen (Stuart et al. 2016). Therefore, induction of an overly fibrotic state post-MI can be as detrimental as under-production of scar tissue.

It is also important to recognize the role of comorbidities in the inflammatory response post-MI. Patients experiencing myocardial infarction frequently do so as a result of coronary artery disease, and often with other high-inflammation pathologies, such as obesity (Przyklenk 2015). This baseline level of chronic inflammation will clearly influence the inflammation response in an injury such as MI, and this baseline level of chronic inflammation is not adequately reflected in most animal models and therefore may present some difficulty in predicting clinical effects.

Biochemical Inhibition of Inflammation

Numerous over-the-counter anti-inflammatory agents are used daily by millions of people. One of the most common of these is ibuoprofen. Ibuprofen is a nonsteroidal antiinflamatory drug (NSAID). All NSAIDs act on cyclooxygenase enzymes, which have two forms: cyclooxygenase 1 and 2 (COX 1 and COX 2) (Amer et al. 2010, Ong et al. 2013, Kirkby et al. 2016). Due to its effects on the GI tract, many NSAIDs are now designed to selectively block COX 1, which still enables the majority of the anti-inflammatory effects (Kirkby et al. 2016). However, stable presence of COX 2 in the brain and thymus require limited use of NSAIDs, including ibuprofen (Kirkby et al. 2016, Patrono 2016).

Ibuprofen blocks the catalytic site from arachidonic acid via acetylation of a serine residue near the binding site on COX 2, preventing prostaglandin formation (Amer et al. 2010). Prostaglandins are mediators of inflammation (Amer et al. 2010, Giroux et al. 2000). The large acetyl group prevents cleavage of arachidonic acid into PGG2 and PGH2, which indirectly prevents platelet formation (Amer et al. 2010). This results in reduced platelet aggregation and inhibits epithelial cell proliferation, both of which are

desirable for patients at risk for MI. This may be of special importance in situations in which reperfusion does not occur until 90 minutes or longer post-MI, as previously addressed.

COX 2 is expressed by cells involved in inflammation, including macrophages, fibroblasts, or endothelial cells (Giroux et al. 2000). Various cytokines induce COX 2 expression, including interleukins (Giroux et al. 2000). Cyclooxygenases (COX) convert arachidonic acid to prostaglandins (Giroux 2000). Therefore, synthesis of prostaglandins is inhibited due to ibuprofen's inhibition of COX 2 (Ricciotti 2011). Prostaglandins broadly act on G-protein coupled receptors that could alter the receptor structure and function, affecting cells' responses to inflammation (Ricciotti et al. 2011). NSAIDs bind to and deactivate one of the monomers of the COX 2 dimer (Ricciotti et al. 2011). Ibuprofen inhibits COX 2 without restricting the NO pathway, which is required for wound healing (Kirkby et al. 2016).

Inhibition of COX 2 has shown to have negative cardiovascular effects, specifically increased risks of MI, hypertension, and reduced outcomes of congestive heart failure (Amer et al. 2010, Kirkby et al. 2016). Because of this, NSAIDs are linked with increased mortality after MI (Amer et al. 2010). However, a study by Leshnower et. al. showed that administration of ibuprofen to rabbits and sheep after MI reperfusion did not result in any significant changes in myocyte apoptosis or infarct size (Leshnower et al. 2006). Additionally, ibuprofen is thought to induce signaling through NF-κβ pathway, which is also involved in the inflammation process (Leshnower et al. 2006). Clearly, this shows that ibuprofen could have a potential benefit in an overly inflammatory state, but may be counterproductive to normal healing. While ibuprofen, along with other NSAIDs, has been

suggested to increase risk of subsequent MI after initial MI, ibuprofen is thought to be one of the lower risk NSAIDs (Ong et al. 2013).

Naproxen (Aleve, Midol) is the only NSAID that has no risk of acute myocardial infarction (AMI) associated with its use (Vargas-Lorenzo 2013). All other NSAIDs have approximately the same small increased risk of AMI associated with daily use (Vargas-Lorenzo 2013). However, this risk was analyzed from numerous studies that looked at high-risk patient groups, which are far more likely to have an adverse event, independent of NSAID use. Newer research looking specifically at ibuprofen has shown that rats receiving ibuprofen after MI may have increased integrity in cell membranes, and reduced ROS release (Patel et al. 2016). This suggests that ibuprofen may have some benefit as a cardioprotective drug, or at least present less of a risk than other NSAIDs.

A study in which dogs with AMI were given a variety of treatments showed that infarct expansion was attenuated by ibuprofen six week post-MI (Jugdutt et al. 2007). NSAIDs can interfere with the healing and inflammatory processes, resulting in less collagen deposition and net scar thinning (Jugdutt et al. 2007). This is of particular concern clinically, where pathologies such as hypertension can lead to high intracardiac pressures, making the infarcted tissue's mechanical stability even more precarious. Animals treated with ibuprofen only saw a decrease in mechanical strength of the infarct area relative to sham, but not a significant decrease relative to infarct only animals (Jugdutt et al. 2007). No change in distensibility, ejection fraction, or contraction strength was reported relative to the control group, however a decrease in both collagen I and III was noted (Jugdutt et al. 2007). Notably, the ratio of type I to type III collagen was increased, despite this overall drop in collagen production (Jugdutt et al. 2007). These

results suggest that an NSAID, such as ibuprofen may be of some assistance in a myocardial infarction treatment in which the mechanical integrity of the infarct area is assured. Such would be the case in a patch application.

Use of Patches to Increase Mechanical Integrity Post-MI

Post-MI application of a biocompatible patch, with or without stem cells or growth factors, is one of the most commonly researched treatments in cardiac bioengineering (Lam et al. 2013, Wendel et al. 2014, Zhang et al. 2015, Tan et al. 2009, Serpooshan et al. 2013). The premise of the research is that application of a patch to the infarct area will increase wall thickness and provide mechanical support to the injured region (Zhang et al 2015, Wan et al 2013, Stuart et al 2016, Wan 2017, Tan et al. 2009). By supporting the damaged tissue, the wall stress on the remaining tissue is reduced. This prevents scar bulging during systole as well as preventing excess mechanical strain on surrounding tissue (Lam et al. 2013, Wendel et al. 2014, Zhang et al. 2015, Wan et al. 2017). Mechanical strain on the surrounding tissue has previously been described to result in infarct expansion and increase risk of arrhythmia (Stuart et al 2016, D'Amore 2016). Some studies suggest that timely application of the patch can prevent changes in ejection fraction and other measures of heart function as early as one week after infarct (Wendel et al. 2014). Furthermore, by reducing the size of the infarct, patch treatments have also been shown to increase contractility post- MI (Serpooshan et al. 2013).

Along with providing mechanical support, cardiac patch research also investigates potential uses as a delivery vehicle for cells, growth factors, or medications (Wendel et al 2014, D'Amore et al. 2016, Tan et al. 2009). For this reason, natural and/or degradable materials are preferentially investigated. However, degradation, particularly of synthetic

materials, has been cited as a potential risk for chronic inflammation in cardiac patch applications (D'Amore et al. 2016).

In one study that looked at inflammatory effects, pigs underwent myocardial infarction surgery and received with a multilaminate urinary bladder-derived ECM patch (UBM) or expanded polytetrafluoroethylene (ePTFE) patch. Inflammation was reported as increased in ePTFE compared to UBM, with UBM subjects displaying greater myofibroblast recruitment and population (Robinson et al. 2005). While this indicates that a naturally-derived collagen-based patch may result in a better prognosis for the patient, it doesn't fully explain how the inflammatory process is affected by a collagen-based patch. In order to fully understand the implications of a cardiac patch therapy, it is crucial to understand how these patches affect inflammation post-MI. These questions will be addressed in Chapter 4.

When treating myocardial infarction, the current clinical goals are to limit scar expansion, preserve contractility and encourage regeneration (Perea-Gil et al. 2015). Current approaches involve use of a patch material, either with or without stem cells, growth factors, or peptides (Perea-Gil et al. 2015, Tan et al. 2009). Collagen-based patches have been included in numerous studies and have been shown to promote angiogenesis and limit infarct expansion when administered within hours of MI (Perea-Gil et al. 2015, Mewhort et al. 2014, Tan et al. 2009, Serpooshan et al. 2013). Importantly, SIS patches have been used in murine infarct models and shown to increase ejection fraction by as much as 35% post-MI (Toeg et al. 2013, Perea-Gil et al. 2015). In general, performance changes are significant at least by 21 days post-infarct in murine models (Toeg et al. 2013, Voorhees et al. 2015, Tan et al. 2009). However, in the literature

reviewed, significant performance (i.e. ejection fraction) changes were not noted at day 7 or earlier indicating that these changes occur primarily in early proliferation phase (Toeg et al. 2013, Voorhees et al. 2015). This is logical, as it is only after inflammation that the bulk of the scar tissue is formed and full integration of the patch material can take place.

Other murine models utilizing multiple patch models, showed that all tested patches reduced infarct area size and increased wall thickness 8 weeks after infarct (D'Aleno 2016). These findings suggest that the mechanical support provided by the patch can have significant physiological improvements. Furthermore, these patch materials have shown to retain any seeded cell populations or growth factors better than synthetic counterparts, suggesting that collagen-based patches may be especially beneficial in future tissue engineering applications (Perea-Gil et al. 2015, Mewhort et al. 2014).

While there is a great deal of research to support the mechanical efficacy of this treatment, it is relatively unknown how patches directly affect the inflammatory process (Zhang et al. 2015, Wan et al. 2017). What work that has been done has focused on identifying risk of long-term chronic inflammation, and almost exclusively for synthetic patches (D'Amore et al. 2016). This suggests a large gap in literature as it is apparent from the literature that modifications to the inflammation process can greatly increase or decrease the risk for arrhythmias, rupture, or other complications. It is also well established that collagen-based patches provide excellent mechanical support, consistently increasing left ventricular wall thickness and reducing infarct size in both porcine and murine models (D'Amore et al. 2016, Zhang et al 2015, Perea-Gil et al. 2015, Lister et al. 2016). Natural materials, including SIS are decellularized before use, using a

combination of chemical and mechanical treatments that are generally proprietary. Despite these treatments, actual confirmation of removal of immunogeneic material is not conducted for SIS (Lam et al. 2009, Wu et al. 2012, Shahabiour et al. 2016, Sutherland et al. 2015). As there have not been many reports of rejection, it is a relatively safe assumption that any remaining immunogeneic material is not enough to cause rejection. However, even small amounts of such material can alter the inflammation response (Beck et al. 2016, Sutherland et al. 2015). It is therefore prudent to investigate how these patches, such as the commonly used porcine SIS patch, affect inflammation.

CHAPTER 2. MECHANICAL CHARACTERIZATION OF INTACT AND SUTURED HUMAN SKIN

Introduction

Skin acts as a physical barrier between the internal body and the environment. Part of this role includes maintenance of tissue integrity while facilitating and responding to movement, which requires a range of viscoelastic material properties. Like many tissues, skin's mechanical behavior is dependent upon the arrangement and composition of extracellular matrix (ECM). ECM composition of skin varies not only between species, but based on age, gender, size, and location on the human body as well (Edwards et al., 1995, Firooz et al. 2016, Zhu et al. 2015, Zollner et al. 2013). Due to this variation, it has been difficult to fully characterize the mechanics of skin. The few studies that have been performed with human skin *in vitro* were performed at very low strain rates in the range of 2-20 mm/min (Blackmore et al. 2014, Grady et al., 2009, Miller et al., 2000). Even within this narrow range of applied strains, large variation has been noted between properties, with elastic moduli reportedly ranging from 5-30 N/mm^2 and ultimate strains from 35-115%, although some of this variation is attributed to differences in age of the samples (Blackmore et al. 2014, Edwards et al., 1995).

Additionally, while the mechanical properties of sutures have been investigated, to our knowledge, no study has investigated how the mechanics of sutured skin compare to

those of normal skin, beyond the microscale (Flynn et al., 2010, Vesentini et al., 2003, Wang et al., 2014). Such information is critical for understanding how suturing changes the biomechanics of skin, when suturing would be considered appropriate relative to the numerous alternatives being studied in the field, and how suturing may affect other, similar soft tissues that may not be as easily tested, such as the meniscus. Most immediately, this information might be particularly important to patients who are athletes, or otherwise committed to an active lifestyle, or for patients that require physical therapy after a surgery or other injury. For these patients, it is highly important that the mechanical effects of sutures on skin are known at a macroscopic level, especially if it leads to increased risk of further injury. Currently, there is not information readily available about how sutured skin behavior may differ based on the strain rate and orientation of the injury relative to the direction of movement. Here, we investigated the tensile properties of human skin that was injured, sutured and then mechanically stretched at low (2 mm/min) and high strain (100 mm/min) rates. These loading rates were selected to encompass the range of loading human skin would be expected to withstand during a range of common movements, such as walking or stretching (Blackmore et al 2014). Our hypothesis is that if skin is injured with a linear, full thickness injury, sutured and stretched 90º to and in-line with the injury, then elastic modulus will increase relative to intact skin, due to the high stiffness of the suture material. Furthermore, it is anticipated that fracture strength and failure strain will decrease, due to the stress concentration around the skin at the bite points. Additionally, we hypothesize that these differences will be more pronounced in the high strain group, both between strain applications and within groups.

Materials and Methods

Human tissue procurement was obtained in accordance with the Wayne State University Institutional Review Board Protocol #054514M1E. Skin samples were donated from patients undergoing abdominoplasty at Henry Ford Health System (Detroit, MI) with no known diseases. Skin from 17 Caucasian female patients aged 39-52 were utilized. Patient age and sex were selected based on sample availability and predicted variations due to age and sex (Zollner et al. 2013). Male and non-Caucasian skin samples were excluded due to inadequate sample numbers and potential mechanical differences between demographic groups (Edwards et al., 1995, Firooz et al. 2016, Zhu et al. 2015, Zollner et al.

Patient	Age	Sex	Race
1	48	F	Caucasian
2	49	F	Caucasian
3	39	F	Caucasian
4	47	F	Caucasian
5	40	F	Caucasian
6	43	F	Caucasian
7	40	F	Caucasian
8	42	F	Caucasian
9	52	F	Caucasian
10	44	F	Caucasian
11	42	F	Caucasian
12	39	F	Caucasian
13	45	F	Caucasian
14	44	F	Caucasian
15	52	F	Caucasian
16	43	F	Caucasian
17	49	F	Caucasian

Table 1. Patient data for skin use.

2013). Patient data can be viewed in Table 1. All samples were taken from the abdomen, although exact location and orientation of bulk skin samples relative to the patient were unknown and therefore considered to be random. Tissue samples were received on ice and subcutaneous fat was removed using surgical scissors. Skin samples for baseline testing were cut to approximately 65 mm x 10 mm pieces, with three samples per patient sample prepared to account for any variation or slippage during testing. Skin samples that were to be sutured were cut to approximately 65 x 60 mm pieces. A scalpel was used

to apply a 40 mm incision. Incisions were sutured using a simple, interrupted suture with

6-0 Ethicon Prolene® sutures placed every 5-7 mm, per reported optimal suture spacing

for the skin location and suture type (Vesentini et al. 2003). Orientation was defined as
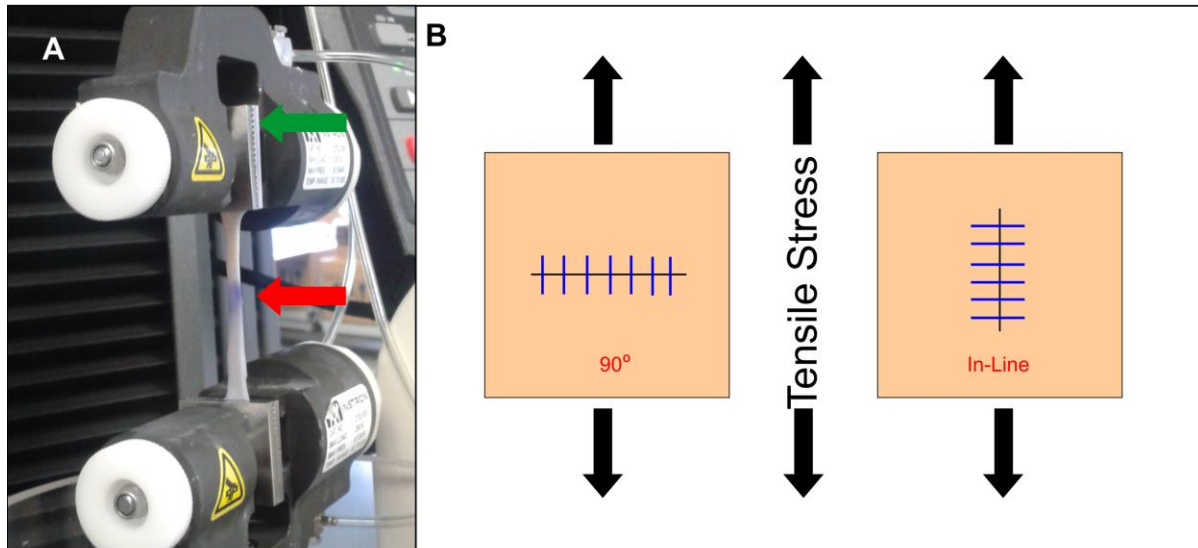
Figure 7. Installation of tissue sample in Instron. (A) Skin samples (red arrow) are

clamped into tensile device using serrated clamps (green arrow) and measured before

stretching. (B) Schematic of the suturing patterns (left – perpendicular orientation; right –

parallel orientation).

the orientation of the injury, or "cut", to the axis of applied tension. Sample orientation

would be either 90º to the injury or in-line with the injury line. Illustration of this definition

can be seen in Figure 6. Following suturing, all samples were stored in phosphate

buffered saline (PBS) at 4ºC until testing.

Tensile testing was conducted on either an Instron 5943 (low strain) or Instron

5984 (high strain) with BlueHill 3 software (Instron, Norwood, MA). Tensile testing was

performed at two strain rates: 2 mm/min and 100 mm/min. Samples were installed in the

Instron as shown in Figure 7. Prior to testing, each sample was adjusted and measured

for consistency. Following installation, samples were submerged in a PBS bath during testing to provide adequate tissue hydration. During testing analysis, failure mode in samples with sutures was defined as the first instance of failure of any individual suture. Similarly, intact skin was considered to have failed when a visible tear was able to significantly affect the applied stress as indicated by the BlueHill software during testing. Patient samples for the control, 90º, and in-line groups were n=7, n=6, and n=6, respectively. Again, each sample number consisted of three individual tissue pieces from the same donor, each tested separately to account for variations in location or installation in the Instron. All were included in data analysis unless noticeable slippage at the grips occurred, in which case the individual piece would not be counted toward the sample average. Tensile mechanics at the same strain rate (ex. 2 mm/min or 100 mm/min) were compared using one-way ANOVA with Tukey post-hoc with $p < 0.05$ for significance. Results from the power analysis yielded a β of 86.4, based on the differences from the elastic modulus calculations. This indicates that the sample size is adequate for this work. All statistics were calculated using SPSS.

Stress relaxation testing was also conducted. Samples were prepared to the same dimension and suture patterns as with tensile testing. Samples were placed in the Instron 5943 using serrated clamps and stretched to 80% of maximum strain at a rate of 2 mm/min. Maximum strain was determined from the tensile testing results at 2 mm/min. Once 80% of maximum strain was achieved, the strain gauge length was held constant for 5 min, with changes in applied stress recorded (Saulis et al., 2002). Five minutes has been used as a hold length in skin mechanical testing previously, and thus is appropriate for comparison between published results (Saulis et al. 2002, Blackmore et al. 2014).

Results were expressed as average percentage decrease in stress, rather than absolute stress, to normalize the data. Recorded decreases in stress were averaged for each of the three groups: intact (control), samples stretched 90^0 to injury, and samples stretched in-line with injury. Percent changes in stress between groups were compared using one-way ANOVA with Tukey post-hoc.

Results

Initial testing of intact skin samples at 2 mm/min, showed that human abdominal skin has an average elastic modulus of 7.76 MPa. At 100 mm/min, measured modulus significantly increased more than threefold to 29.1 MPa (p = 0.0001). However, these results fit within the range of 5-30 MPa commonly cited as the range for adult human skin, which illustrates the variation in reported data (Edwards et al., 1995, Blackstone et al. 2014). These two data sets were compared using a student's t test to illustrate the range in reported data.

Interestingly, the elastic modulus at higher strain rates reflects that of other materials that consist primarily of collagen I, such as porcine small intestine submucosa (SIS) (Roeder et al., 1999). This suggests that at higher strains, collagen I is the primary component bearing the load, while other components, such as elastin, have a greater impact on mechanical properties at lower strain rates. Such assessments can be based on the high stiffness and nearly perfectly elastic behavior of collagen, which is significantly higher than elastin or proteoglycans. This is also supported by the lack of plastic deformation under 100 mm/min strain, whereas a small region of plastic deformation was observed at 2 mm/min strain as shown in Figure 8. Samples with sutures had elastic moduli almost double that of intact skin at low strains as shown in Figure 8 and Table 1.

This is likely due to a level of stress off-loading by the stronger, stiffer suture material, protecting areas of skin from experiencing the full applied stress before the stress concentration at the bite location overwhelmed the tissue. At higher strains, skin samples stretched 90° to the injury had insignificant differences in elastic modulus measurements

as the control group (29.1 MPa), while recorded moduli for the samples stretched in-line with the injury had a significant increase to approximately 39 MPa ($p = 0.0001$). This is likely a result of the additive mechanical properties of the sutures, as well as an effect of unbroken collagen filaments in the tensile axis. Fracture strength also saw a large
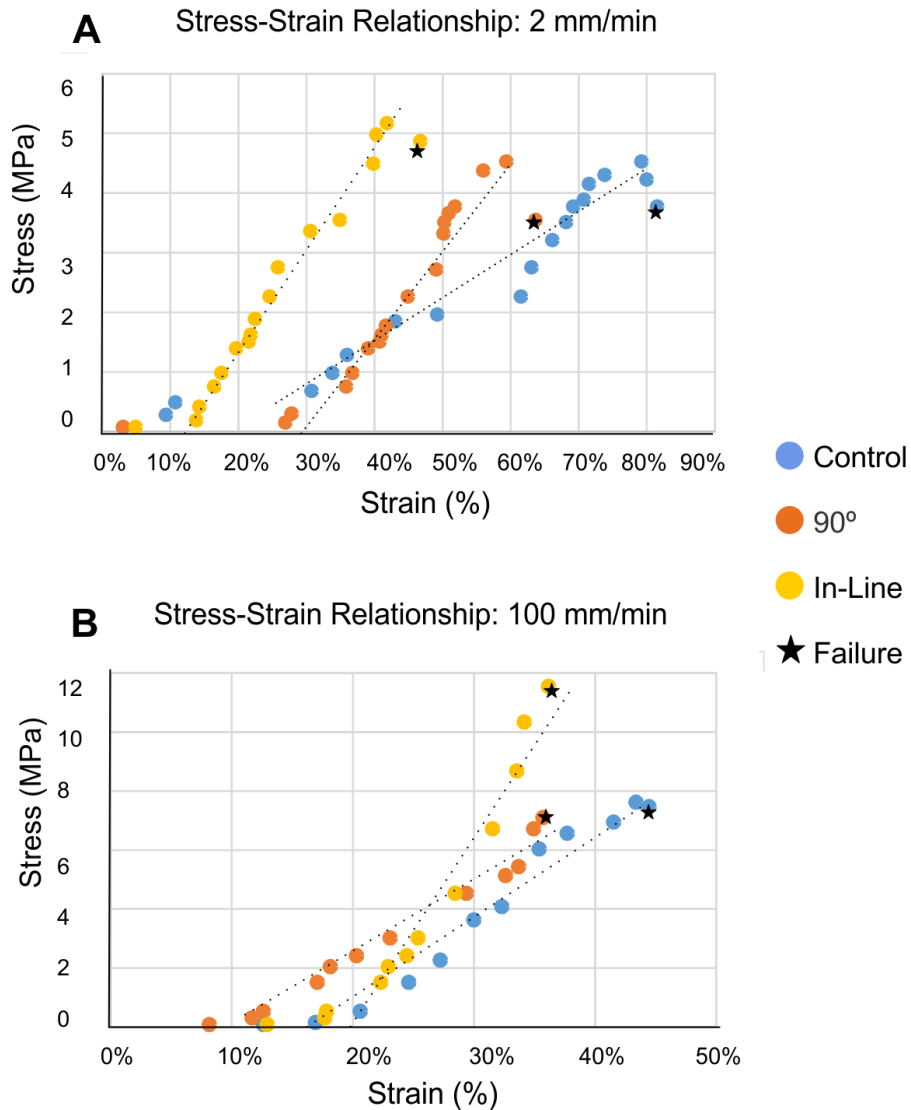
Figure 8. Tensile behavior of skin under low and high strain rates. Graph shows skin under 2 mm/min strain (A) and 100 mm/min (B). Lower strain resulted in lower elastic modulus (slope of the fitted line) and exhibited slight plastic deformation. Failure strains, or maximum strain achieved before failure, were noted to be lower at higher strain rates.

increase between the strain rate groups, an observation similar to the elastic moduli. Again, this suggests that at the higher strain rates, the mechanical behavior of collagen is dominant.

Failure strain averaged 81.54% at 2 mm/min, which falls within the age-dependent range of 35-115% strain before failure (Edwards et al., 1995). However, at 100 mm/mm, failure strain was found to average only 44.5%. The lower failure strain may be due to high strain rates' limiting collagen fibers to straighten and align before being exposed to higher levels of stress, resulting in failure at lower strains. While failure strain of the human skin samples was found to be greater when stretched at 2 mm/min, the relationship between the failure strains at each speed was found to be similar in the control (intact) and 90º groups. Both groups saw a decrease in failure strain when the strain rate increased from 2 mm/min to 100 mm/min. Samples stretched with the injury in-line with the tensile axis, however, only displayed a decrease of approximately 23% with the increase in strain rate. However, the failure strains were markedly lower in the in-line group, with failure occurring at 46.8% strain at 2 mm/min and 36.2% strain at 100 mm/min. Interestingly, the failure strains for both sutured groups at 100 mm/min are nearly identical, with failure occurring around 35% strain, regardless of suture orientation (90º to or in-line with the injury). Differences in failure strain at 2 mm/min were found to be significant, between control and 90º to the injury ($p = 0.0073$), or in-line with the injury ($p = 0.001$), and between the two suture groups ($p = 0.0057$). At 100 mm/min, none of the differences between treatment groups were statistically significant. This suggests that the generation of stress points created by the suturing process may result in early failure of sutured skin at high strain rates. The comparatively higher forces during the high strain

rate may circumvent the viscous behavior of skin. This could lead to more rapid tearing of the skin, thus resulting in undesired failure at lower strains. A summary of these results

	Elastic Modulus (MPa)		Fracture Strength (MPa)		Failure Strain	
	2mm/min	100 mm/min	2mm/min	100 mm/min	2mm/min	100 mm/min
Control	7.76 ± 0.52 *	29.1 ± 3.73	3.77 ± 0.59	7.46 ± 1.22	81.5% ± 7.82 *	44.5% ± 9.14
90⁰	14.7 ± 2.45	30.7 ± 4.30	3.54 ± 0.95	7.09 ± 2.38	63.7% ± 12.3 *	35.7% ± 7.47
In-Line	17.8 ± 1.71	39.4 ± 2.99 *	4.86 ± 0.79 *	11.5 ± 1.66 *	46.8% ± 5.01 *	36.2% ± 6.43

Table 2. Summary of tensile properties of skin samples without sutures, and with perpendicular and parallel oriented sutures. * Indicates statistical significance within strain rates ($p < 0.05$).

can be found in Table 2.

Overall, the strain rate had a statistically significant impact on elastic modulus, fracture strength and strain at failure. The elastic modulus was significantly impacted by orientation, either 90⁰ to the injury, or in-line with the injury, when stretched at 2 mm/min ($p = 0.003$ between control and 90⁰ and $p = 0.001$ between control and in-line), however at 100 mm/min significance was only observed for skin stretched in-line with the injury ($p = 0.001$). Similarly for fracture strength, only samples stretched in-line with the injury had a significant difference at both strain rates ($p = 0.0127$ at 2 mm/ min and $p = 0.002$ at 100 mm/min).

To test stress relaxation, samples were held under constant load and changes in stress over time were recorded. Stress relaxation testing showed relatively consistent relaxation proportional to the initial applied stress to achieve 80% strain as shown in Figure 9. However, due to the differences in stiffness at lower strain rates, the net stress relaxation varied between groups slightly, with samples stretched in-line with the injury having the greatest net stress relaxation, but a slightly lower proportional relaxation (39%)

than samples stretched 90º to the sutured injury (42%). However, none of the differences were significant. These stress relaxation values are slightly greater than the results published by Saulis et al., although this may be due to differences in sources of skin, as well as age and gender variations, as the cited work investigated forearm skin flaps of multiple ethnicities.

Discussion

When skin is sutured, a high-tensile strength material is used to bear tensile loads applied to the skin (Wang et al., 2014). Suturing requires induction of micro and macro tears in the surrounding tissue, creating major failure points as observed during tensile testing (Flynn 2010). Additionally, these tears are subjected to forces averaging 0.5 N-1.5 N required to pull the injury closed, further exacerbating the damage inflicted during needle driving (Capek et al. 2012). Samples with sutured injury in-line with the tensile axis had the highest average fracture strength of 4.86 MPa, compared with intact samples and sutured samples stretched 90º to the injury, which had fracture strengths of 3.77 MPa and 3.54 MPa, respectively. Samples stretched in-line with the injury had the highest fracture strength of all groups at 100 mm/min, with a fracture strength of 11.5 MPa. Additionally, stretching sutured skin in-line with injury seemed to disrupt the viscous region of the stress-strain curve, most notably at 2 mm/min. Such samples only reached 13.2% strain before displaying elastic behavior. This is a noticeable decrease from the samples stretched 90º to the injury (26.9%) and the intact skin groups (30.8%). Differences at 100 mm/min were much less noticeable, with all samples displaying strains in the range of 13-17% before experiencing elastic behavior. This is of particular interest considering the

abdomen's highly elastic behavior relative to other areas of skin, such as the head or limbs (Blackstone et al. 2014).

While loading conditions *in vivo* are rarely uniaxial, uniaxial testing is appropriate as a preliminary analysis of mechanical properties as it is more consistently and more frequently performed on soft tissues (Blackstone et al. 2014, Zhu et al. 2015, Zollner et al. 2013). In situations where loading is considered to be mainly, if not entirely, uniaxial, other approaches have been taken to reduce stress concentration around each individual bite. While simple, interrupted sutures are frequently used for closing superficial wounds, a suture button with figure 8 suture pattern has been used with great success in reducing stress concentration in patellar tendon repair (Otsubo 2016). This methodology did not restrict range of motion and yielded a 98% success rate (Otsubo 2016). Additionally, procedures such as anastomosis involve suturing of soft tissues that are very similar to skin (i.e. adventitia) and these tissues experience uniaxial loading, especially during the procedure (Roussis 2015).

Polypropylene (Prolene®) is a stiff and strong material, with an average elastic modulus of 100 MPa (Greenwald et al., 1994; Chu et al., 1989). Prolene® has a tensile strength of 40 GPa, and only minimally decreases after 6 weeks *in vivo* (Greenwald et al., 1994). Given that the stiffness and strength of the suture material is significantly greater than human skin, it is unsurprising that the sutures can increase stiffness and decrease failure strain in skin. However, injury inflicted during suturing creates new failure points. These data show that suturing can greatly affect skin's mechanical properties, and that the extent of the changes to the mechanical properties is highly dependent upon suture orientation relative to the tensile axis as well as the applied rate of strain, with

greater strain rates resulting in increased stiffness of the sample. Additionally, these data provide some interesting insights into the interaction between sutures, applied tension, and the natural structural proteins found in skin. For example, sutures applied to an injury in-line with applied tension may effectively off-load stress from viscous components, such as glycosaminoglycans, as indicated by the low strains observed in samples before engaging in purely elastic behavior. This also suggests that the high strength and stiffness of sutures may dominate the local mechanics of a given tissue, but may be counteracted by damage inflicted during the suturing process as indicated by the similarities in behavior between the control group and samples stretched 90^0 to the injury. These data suggest that we can partially accept our hypothesis that mechanical strength of injured skin with sutures will increase relative to intact skin, as injured skin stretched in-line with the injury displayed an increase in fracture strength. However, injured, sutured skin stretched 90o to the injury showed a slight (non-significant) decrease in fracture strength, although elastic moduli were increased for both sutured groups relative to intact skin. It is also important to note that the maximum strain for both sutured groups was much lower than intact skin, which may be the limiting factor in addressing potential for further injury during physical activity.

Conclusion and future work

By assessing comparative data under various strain rates and injury orientation relative to movement axis, we aim to supply vital information for assessing potential risk and complications for patients with injuries requiring sutures, particularly athletes returning to training or physical therapy. By thoroughly understanding the effects of sutures on skin's biomechanical properties, the medical community can better advise

patients with injuries or procedures requiring sutures. Furthermore, the data presented here can be extrapolated to predict behavior of other soft tissues used in tissue engineering. In particular, decellularized dermis tissue, such as commercially available AlloDerm ® are used constantly in plastic surgery procedures (Oh 2011, Shahabiour 2016, Jansen 2013). The decellularized dermis' success has led to its investigated use in abdominal repair surgeries, as well as providing the adventitia layer in vascular tissue engineering (Jansen 2013). In both of these examples, a clear understanding of the failure mechanism of suturing and tissue strength is crucial for patient outcome, yet these scenarios are much more challenging to study using conventional technology. This study can provide a reference for research such as this.
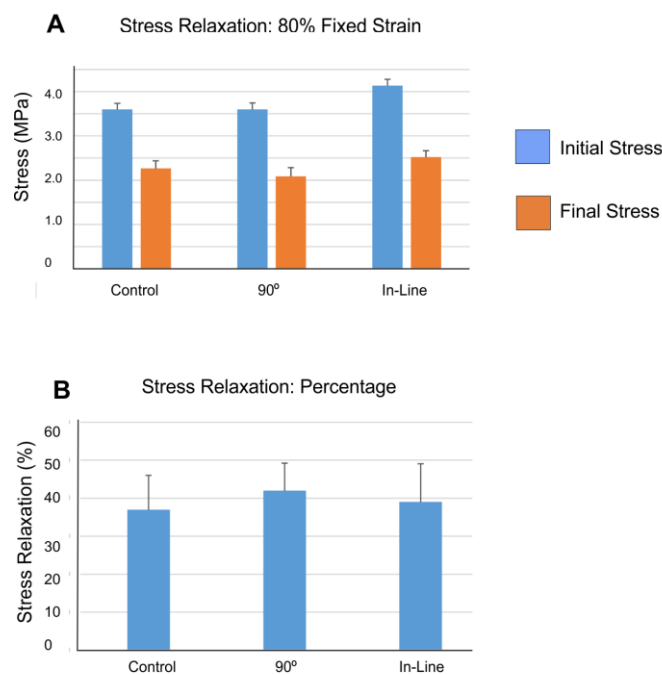
Figure 9. Stress relaxation results. A.) Initial and final stresses recorded for skin samples without sutures, perpendicular sutures, and sutures in parallel. B.) Percent decrease in applied stress after five minutes for each of the three groups. No significant differences were noted between the groups.

CHAPTER 3. MECHANICAL STIMULATION DRIVES ADIPOSE STEM CELL DIFFERENTIATION TOWARDS A MENISCUS PHENOTYPE

Elizabeth Meier was responsible for conducting experiments, including biochemical stimulation and combined biochemical and mechanical stimulation. She compiled data and assisted with statistical analysis and manuscript preparation.

Introduction

While the high tensile strength of sutures make suturing an attractive modality to help facilitate repair, they are only practical in injuries capable of self-healing. In tissues with limited ability to self-repair, such as the meniscus, other approaches must be considered in order to facilitate wound repair. One such option is the use of stem cells to create a new cell source to produce the correct proteins to develop a tissue with comparable mechanical properties as native tissue. In tissues such as the meniscus, which require mechanical loading to develop properly, it is imperative that mechanical stimulation be included. Here, we seek to develop a protocol using a combined mechanical and biochemical stimulus package to promote production of crucial structural proteins.

One in six knee surgeries are due to meniscus related issues, and many meniscal injuries are left untreated due to the lack of effective repair methods, causing long-term damage and accelerated osteoarthritis (Brophy et al. 2012, Arendt et al. 2014, Hasan et al. 2014, Rothrauff et al. 2016). Successful attempts to repair the meniscus with materials, cells, or engineered tissues have been limited due to the difficulty of mimicking this structurally and mechanically complex, heterogeneous tissue (Higashioka et al. 2014,

Rongen et al. 2014, Scotti et al. 2013, Yuan et al. 2014). Tissue donation from cadaver sources are often ill-fitting with minimal improvement in mechanical function long-term (Schuttler et al. 2014). Most meniscus engineering efforts are based on cell-populated scaffolds but this approach has shown limited success (Schuttler et al. 2014, Bouyarmane et al. 2014, Longo et al. 2013). Finding a viable cell source for meniscus tissue engineering remains an issue. Stem cells are a promising option due to proven viability in clinical trials (Pak et al. 2014).

Bone marrow mesenchymal stem cells (MSCs) have been a common cell type for study in osteochondral applications, but are not practical for clinical use (Hatsushika et al. 2014, Nerurkar et al. 2011, Okuno et al. 2014, Vangsness et al. 2014). Adipose-derived stromal cells (ASCs) are abundant and easily obtainable, capable of being isolated from fat tissue aspirated from the same patient. Our laboratory has previously shown successful differentiation of ASCs down the chondrogenic pathway (Xu et al. 2007). ASCs exhibit fibrogenic qualities, thus, we investigated the potential of ASCs to differentiate into a mixed fibrogenic and chondrogenic phenotype. Furthermore, undifferentiated ASCs have already been used in clinical trials, with some success (Pak et al. 2014)

Due to the knee's dependence on mechanical loading in function and development, mechanical strain may stimulate stem cells to differentiate into mechanoresponsive cells (Arendt et al. 2014) Mechanical effects on bone marrow MSCs has been studied extensively with inconclusive results (Byrne et al. 2008, Case et al. 2013, Kisiday et al. 2009). Here, we investigate the effects of mechanical stimulation on the differentiation of human adipose-derived stromal cells (hASCs) towards a meniscus phenotype. Biochemical factors were examined individually, then combined with uniaxial,

cyclic mechanical strain. Our results show that biochemical factors and mechanical strain are capable of promoting fibrochrondrogenesis.

Materials and Methods

Stromal cell isolation and media

Human adipose-derived stromal cells (hASCs) were isolated from discarded fat obtained from elective abdominoplasty and liposuction procedures. Specimens were obtained with informed consent from patients in accordance with Stanford University, Wayne State University, and the Henry Ford Health System human IRB guidelines. All lipoaspiration and abdominoplasty procedures were performed by a board-certified plastic surgeon. Patient age ranged from 18 to 65 years old, and adipose tissue for this study were acquired from the flank or abdomen region. Cells from these regions were selected based on their robust proliferation capability and morphological consistency. Participating patients had no prior knowledge or evidence of ongoing systemic disease at the time of operation. All specimens were immediately placed on ice and processed as follows.

Lipoaspirates were washed twice in Betadine, followed by three rinses in phosphate buffered saline (PBS). Whole fat was digested in 0.1% type II collagenase diluted in Hank's Buffered Salt Solution for 3 hours in a shaking water bath, assisted with additional mechanical digestion via vigorous hand shaking every 30 min. The digest was then neutralized by the addition of media with fetal bovine serum and centrifuged at 1000 rpm for 5 min. Supernatant with undigested fat was discarded and the remaining pellet with stromal cells were resuspended in growth media (GM) and plated at 15 ml of original tissue volume per 100 mm tissue culture dish.

The media formulations used are outlined in Table 3. Media components consisted of Dulbecco's modified Eagle's medium with GlutaMax (DMEM, 10569, Gibco, Life Technologies, Carlsbad, CA), fetal bovine serum (FBS, 26140079, Gibco), penicillin streptomycin (PS, 15140163, Gibco), ITS+ universal culture supplemental premix (ITS+, 354352, BD Biosciences, Bedford, MA), L-Ascorbic acid 2-phosphate sesquimagnesium salt hydrate (ASP, A8960, Sigma, St. Louis, MO), dexamethasone (Dex, D4902, Sigma), and recombinant human transforming growth factor- β3 (TGF-β, 243-B3, R&D systems, Minneapolis, MN).

FM	CM	FM1	FM2
1% P/S	1% P/S	1% P/S	1% P/S
10% FBS	0% FBS	1% FBS	10% FBS
-	ITS+ (1:1000)	ITS+ (1:1000)	ITS+ (1:1000)
-	ASP (37.5 µg/mL)	ASP (37.5 µg/mL)	ASP (37.5 µg/mL)
-	Dex (100nM)	Dex (100nM)	Dex (100nM)
-	TGF-β (10 ng/mL)	TGF-β (10 ng/mL)	TGF-β (10 ng/mL)

Table 3. Summary of media components and concentrations.

Biochemical differentiation

Culture media for encouraging ASC differentiation into fibrocartilage-like cells was determined from base fibrogenic and chondrogenic media formulations (Table 3). ASCs were media differentiated for the customary 21 day culture typically used in chondrogenic differentiation studies (Mandal et al. 2011). Cells of passage 1-4 were used for these experiments and pooled. Fibrogenic media (FM) traditionally contains basal media and fetal bovine serum to promote differentiation into fibroblasts. Chondrogenic media (CM) is significantly more complex, with the addition of several chondrogenic growth factors- insulin (ITS+), ascorbic acid (ASP), dexamethasone (Dex), and TGF-β. Two different

variations of combined fibrogenic and chondrogenic media were tested, composed of all components of both medias with either 1% (FCM1) or 10% (FCM2) FBS. Serial media differentiation was also assessed, by subjecting the cells to fibrogenic media followed by chondrogenic media (FM-CM) switched halfway through the differentiation period (i.e. at 10 days), and vice versa (chondrogenic to fibrogenic media, CM-FM). Complete media formulations and concentrations of supplements are listed in Table 3. Control media consisted of minimal essential ingredients for cell survival, i.e. basal media and 1% FBS, and was termed maintenance media (MM). All media contained 1% penicillin streptomycin to prevent contamination. Media was changed in all groups every 3 days.

Mechanical strain device

A custom system was built for applying mechanical stimulation to the stromal cells in the form of uniaxial, cyclic tension (Figure 10). Desired system build features included an overall small device footprint, the ability to be completely housed in a traditional incubator, and multiple sample chambers. The system was built to house four separate culture chambers to enable simultaneous stimulation of multiple samples of cells of varying parameters. The culture chamber consists of a disposable, commercially available rectangular culture plate (Thermo Scientific Nunc Dishes, 267061, Waltham, MA), which ensures sterility with each experiment at low cost. Silicone elastomer substrates (polydimethylsiloxane or PDMS) were added into the culture chambers as a stretchable cell culture surface as a means for applying mechanical strain. Inserts were designed and machined out of acrylic to attach the silicone substrates to an actuating stage. An actuating stage connects the culture substrates to the actuator, which applies uniaxial, cyclic tensile strain to the cells. A bottom plate for holding the culture and

actuator setup together was fabricated out of Plexiglas, and allowed the entire system to fit easily onto a single incubator shelf as a single unit.

Cell loading and mechanical strain regimes

The human adipose-derived stromal cells were subjected to several different strain regimes to determine the ideal stimulation protocol for encouraging fibrochondrogenic differentiation. To enable cell attachment to the non-cell adherent silicone elastomer stretch surface, the substrate was functionalized with an attachment protein prior to mechanical stimulation. Laminin (natural mouse laminin, 23017, Invitrogen, Life Technologies, Carlsbad, CA) reconstituted in phosphate-buffered saline (PBS, 10010, Gibco) was deposited onto the substrate at a concentration of 2 $\mu g/cm^2$, enabling cell adherence to the surface. Pooled ASCs between passages 1-4 were then plated onto the polymer substrate. Following overnight attachment, the cells were loaded into the ethanol-sterilized stretch device in preparation for mechanical strain application.

Mechanical stimulation parameters were varied one at a time to determine their individual effects. Parameters varied were time of stretching, applied strain and frequency of strain. First, cells were mechanically stretched for hourly durations of 1, 2, 3, 4, 5, and 6 hours, while parameters kept constant were strain at 10% and frequency at 1 Hz. At each hour time point, cells were harvested for gene expression analysis. Based on results from the biochemical differentiation (described in the **Results** section), ASCs were stretched in fibrogenic and chondrogenic medias, separately. The second parameter varied was strain. Strains of 5%, 10%, 15%, 20%, and 25% were applied to the ASCs for 3 h and 6 h, while frequency was kept constant at 1 Hz. Strain rates were chosen based on the calculations below. Time points are based on results from the time varying

experiments. Lastly, frequency was varied from 0.5 Hz, 1.0 Hz to 1.5 Hz for 3 h and 6 h under 10% strain. Unstretched ASCs served as controls for all experiments.

Gene expression

To determine fibrogenic and chondrogenic differentiation of the ASCs under the various biochemical and mechanical stimulation parameters, quantitative reverse transcription polymerase chain reaction (qRT-PCR) was performed. qRT-PCR was carried out on each sample at the conclusion of each experiment: 21 d for media differentiation, at the end of each time interval for mechanical strain (i.e. after each hour time point), and after 3 h and 6 h after the various strain rates and frequencies were applied. Briefly, total ribonucleic acid (RNA) was harvested from the cells using an RNAeasy Mini Kit (Qiagen, Valencia, CA), the samples treated with DNAse I (Ambion, Austin, TX), and the RNA amount quantified with a Qubit 2.0 fluorometer (Q32866, Life Technologies). To convert total RNA to cDNA, reverse transcription (RT) was performed by prepping samples using a Taqman Reverse Transcription Kit (Applied Biosystems, Foster City, CA) and subsequently running the samples on a reverse transcription system (GeneAmp PCR System 9700, Applied Biosystems). qRT-PCR was performed on an Applied Biosystems Prism 7900HT Sequence Detection System. All reactions were conducted in triplicate to verify technical robustness. All results were normalized to GAPDH. Fibrogenic genes probed were collagen I (Col I) and versican (VCAN). Chondrogenic genes probed were collagen II (Col II), Sox 9 and aggrecan (ACAN). Collagen X (Col X) was also probed to mark cell hypertrophy, indicating the beginning stages of endochondral ossification (Shen 2005).

Histological analysis

Hematoxylin & eosin (H&E) and Masson's trichrome stains were performed on cells following stretching for the strain rate and frequency varying studies. Immediately following stretching, PDMS substrates with cells attached were removed from the stretch device and fixed with 10% formalin. Following formalin fixation, samples to be stained with Masson's trichrome were re-fixed in Bouin's solution for one hour at 56°C. Each sample was then placed onto a glass slide. Slides were stained using hemotoxylin and eosin and Masson's trichrome protocols, with the omission of xylene from both protocols. During preliminary studies, it was determined that removal of xylene from the staining protocols produced higher quality images and so was not included. Exclusion of xylene did not adversely affect the stains. Samples were allowed to dry fully prior to imaging.

Statistics

All averages were calculated as mean values ± standard error. Statistical significance of the media treatments alone was determined with one factor ANOVA tests with ($p < 0.05$). All other experiments used a two-factor ANOVA to determine statistical significance. Tukey post hoc analysis was performed to ascertain significance between groups, with p-values set at < 0.05. Each stimulation trial was conducted a minimum of
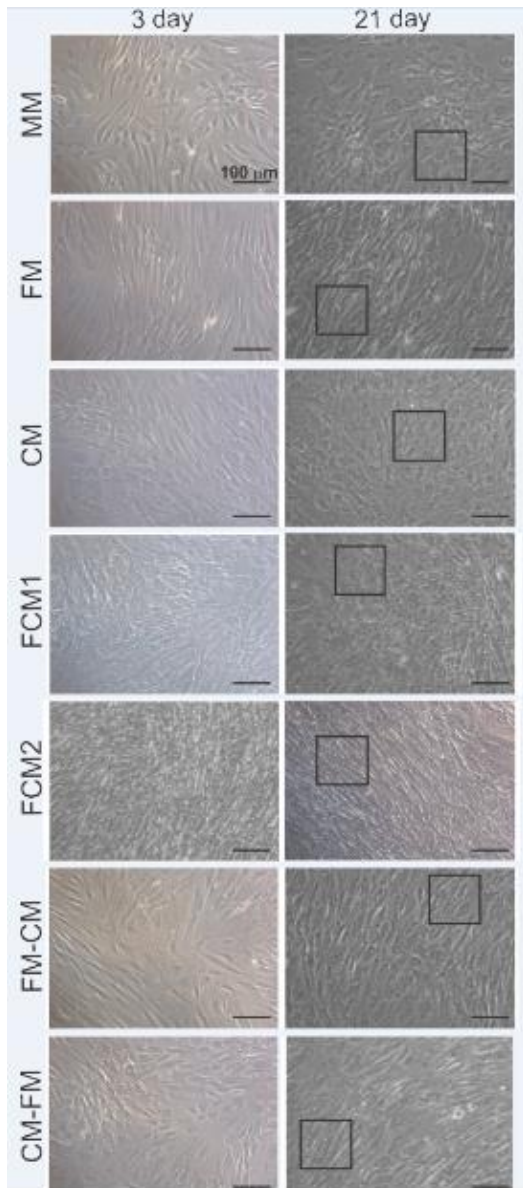
Figure 11. Cell morphology under the different media types. Black boxes indicate the cells. In the FM media, cells were elongated similar to normal fibroblast morphology. In the FM-CM media, cells were more rounded like chondrocytes, whereas in the CM-FM media cells were more elongated like fibroblasts. Scale bars = 100 μm.

three times (to ensure n=3 for each data point) and utilized ASCs from eleven different donors. Donor cells were pooled so that ΔΔCt calculations were comparing treated ASCs and control ASCs from the same donor.

Results

Media Formulation

To determine the appropriate conditions for promoting the fibrocartilage phenotype, the human adipose stromal cells were cultured in seven different media formulations consisting of variations of fibrogenic and chondrogenic biochemical factors (media descriptions are listed in the **Methods** section; formulations listed in Table 3). Cell morphology was observed throughout the 21 day culture period. Fibroblasts are characterized by elongated, narrow cells whereas chondrocytes are more rounded in shape. In the different biochemical

combinations, the stromal cells exhibited morphologies consistent with fibroblasts, chondrocytes and a combination thereof.

Maintenance media (MM) was formulated to contain the minimum essential nutrients for cell survival, i.e. basal media with 1% FBS. This media served as the control, however 1% FBS was not sufficient for cell survival for the entire 21 day culture period, shown by cell degeneration and death (Figure 11). ASCs in fibrogenic media (FM) consisting of basal media plus 10% FBS displayed morphology similar to fibroblasts. Similarly, cells in chondrogenic media (CM) were rounded, resembling chondrocytes. In the mixed fibrogenic and chondrogenic media (FCM1 and FCM2), cells were initially rounded in appearance but gradually acquired a more elongated morphology similar to fibroblasts, with few rounded cells evident in the culture. In FCM2 where the FBS content was higher than in FCM1, cells were more fibroblast-like with very few rounded cells, suggesting that cells mostly differentiated towards the fibrogenic phenotype under this media due to the higher FBS amount. In the media switched from fibrogenic to chondrogenic media (FM-CM), by 21 days cells were more rounded with some elongated, fibroblastic-like cells intertwined. When media was switched from chondrogenic to fibrogenic media (CM-FM), cells took on a more fibrogenic morphology by the end of the culture period. In both cases of changing media halfway through the culture period, the ASCs primarily acquired morphology similar to the latter media, indicating that the dominating differentiation factor was the last media formulation to which the cells were exposed. Specifically, CM-FM media produced more fibroblast-like cells and conversely FM-CM media resulted in more chondrocyte-like cells. Although morphology is a useful

marker, a more quantitative measure is necessary for determining cell phenotype, hence gene expression of the cells in the different medias was also investigated.

Biochemical formulations induce both fibrogenic and chondrogenic phenotypes

Expression of key fibrogenic and chondrogenic genes were probed to determine the direction of ASC differentiation towards the fibrocartilage phenotype under the different medias (Figure 12). Gene expression is presented relative to control, undifferentiated ASCs. All medias resulted in expression to some degree of fibrogenic and chondrogenic genes, even in pure fibrogenic or chondrogenic media. In fibrogenic media (FM), the key fibrogenic gene collagen I increased in expression the most, followed by a slight increase (100x) in the chondrogenic marker aggrecan. Chondrogenic media (CM) resulted in a significant increase in the key chondrogenic gene collagen II expression, and included increase in expression of chondrogenic Sox9 and fibrogenic versican. Fibro-chondrogenic media mix 1 (FCM1, containing 1% FBS) and the fibrogenic-to-chondrogenic media (FM-CM) only increased expression of collagen I, and also showed increased levels of collagen X indicating cell hypertrophy. Fibro-chondrogenic media mix 2 (FCM2, containing 10% FBS) only increased collagen X expression. Chondrogenic-to-fibrogenic media (CM-FM) increased expression of collagen I, Sox9, aggrecan, and collagen X. Overall, the significant difference in the presence of the essential collagen II protein with combined increased expression of other main chondrogenic and fibrogenic genes indicates that the chondrogenic media

formulation best promotes the mixed fibrochondrogenic phenotype. Hence, chondrogenic media was used in the mechanical stimulation studies.

Figure 12. ASCs exhibit increased chondrogen
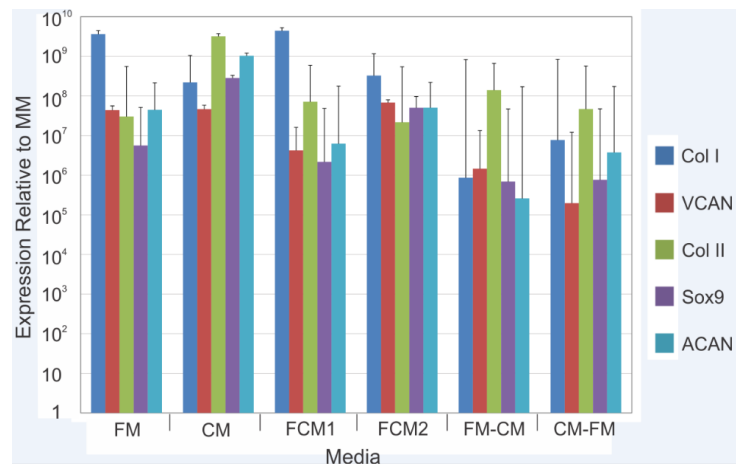
ic and fibrogenic gene expression after culture in the varying media combinations. Gene expression represented relative to the control maintenance media (MM). Gene upregulation of the major chondrocytic

Mechanical strain device

For applying mechanical strain with the desired parameters, a device was custom built as described in the Methods section. The device is able to apply up to 25% strain and up to 1.5 Hz as required by our experiments. The device had no issues operating for the 6 hour time span of the experiments and could be run for longer periods of time. The polymeric substrate was fabricated at a 1:15 polymer base to curing agent ratio, rather than the traditional 1:10 ratio to ensure that the substrate had enough strength to be able to withstand the tensile forces applied to it while still remaining compliant. PDMS is an inherently hydrophobic material and thus does not permit cell attachment. Thus, the substrates were pre-functionalized with the attachment protein laminin to enable cell adhesion, allowing the cells to remain attached to the substrate under the applied cyclic strain. For RNA extraction for gene expression evaluation, cells were easily detached with a cell scraper. Cells could potentially be

detached from the substrates and collected using trypsin. This would allow for their use in tissue engineering a knee meniscus.

Mechanical Loading Results

The components that comprise the knee joint are highly dependent on mechanical cues for proper development. It is believed that these mechanical cues participate in differentiation of the local stem cells into the fibrocartilage cells of the knee, though the precise mechanism remains to be elucidated. Thus, mechanical strain was investigated as a potential stimulant of differentiation of adipose-derived stromal cells (ASCs), a mesenchymal derived cell, down the fibrocartilaginous pathway. Mechanical stretch was applied via uniaxial cyclic strain using the custom-built cell stretching device. FM was used in all mechanical stimulation studies as the control media as it is the conventional media ASCs are cultured in. CM was used because ASCs expressed the highest levels of fibrochondrogenic genes in that media (Figure 12), and the greatest differentiation towards fibrocartilage was desired.

Stretch duration effects

Cells were subjected to mechanical stimulation for hourly increments ranging between 1 and 6 hours, while keeping constant strain at 10% and frequency at 1 Hz. The cells were stretched in fibrogenic and chondrogenic media separately. Expression of relevant fibrogenic and chondrogenic genes by cells subjected to stretch for varying time durations in each fibrogenic and chondrogenic media is shown in Figure 13. In fibrogenic media, collagen II expression was increased at early time points and versican increased at 2, 3, 5, and 6 hours. Collagen X was increased at 3 and 4 hours, showing cell

hypertrophy. In contrast, in chondrogenic media collagen I and Sox9 expression were distinctly increased across all time points. At 3 h of stretch, most fibrogenic and chondrogenic genes were noticeably increased, suggesting that 3 h of stretch in CM improved fibrochondrogenic differentiation the most.

Strain magnitude effects

ASC were subjected to mechanical strains of 5%, 10%, 15%, 20%, and 25% for 3 h
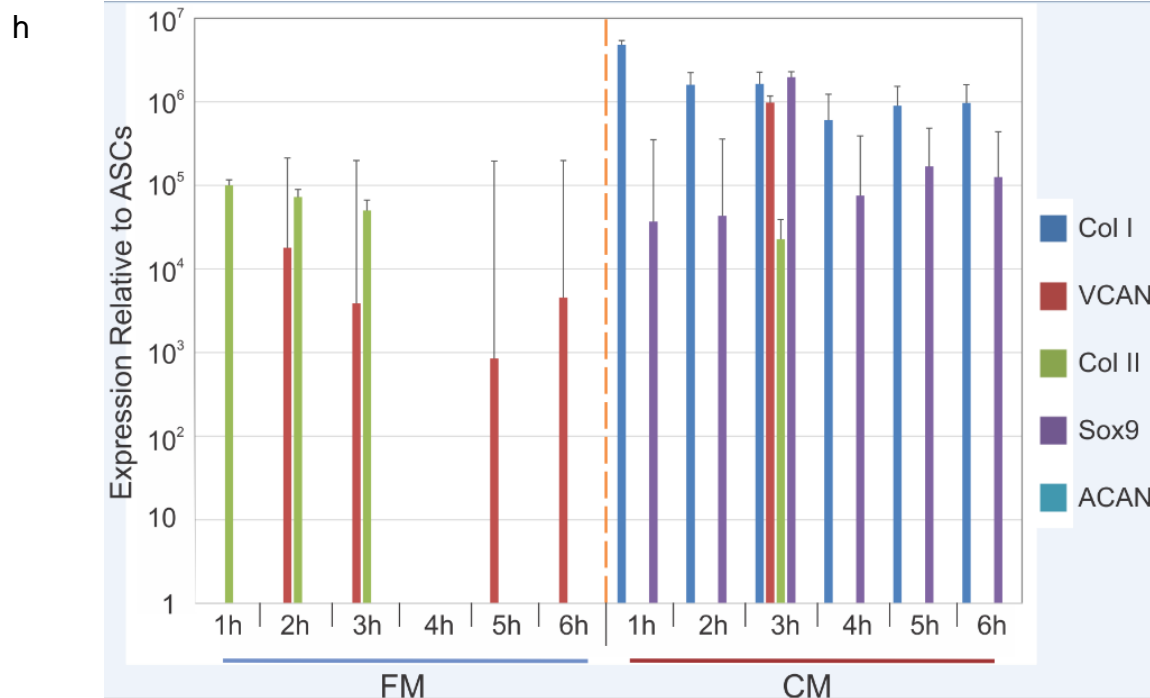
Figure 13. Mechanical stimulation for 1-6 hours promotes varying expression of both chondrogenic and fibrogenic genes. Gene expression represented as relative values compared to control ASCs. Strain was kept constant at 10% and frequency at 1.0 Hz. Mechanical stimulation in chondrogenic media mainly promoted increased expression of fibrogenic gene collagen I and chondrogenic gene Sox 9. Statistical significance (p<0.05) was not observed for these data.
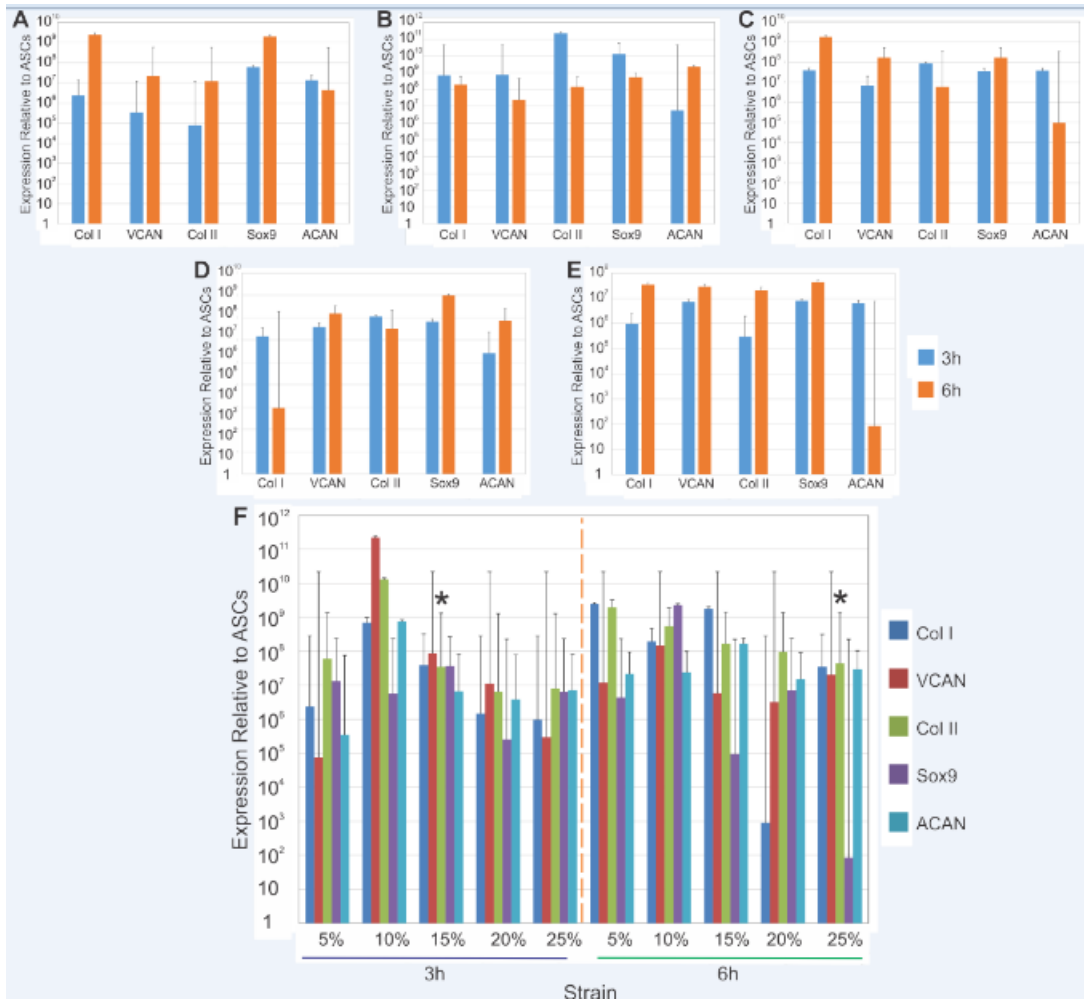
Figure 14. Phenotype expression varied with varying strain rates during mechanical stimulation. Gene expression relative to ASC only controls under 5% -25% strain. Callouts show 5% strain (A), 10% strain (B), 15% strain (C), 20% strain (D), and 25% (E). Frequency was kept constant at 1.0 Hz. The data clearly shows a peak of genetic expression at 3 h of stretch under 10% strain. Error bars represent standard error. * denotes statistical

and 6 h; in FM and CM; and at a frequency of 1 Hz. Results are shown in Figure 14. Gene expression was clearly increased in comparison to the time varying studies, showing that magnitude of strain had a greater effect on cell differentiation than time duration. At 5% strain, fibrocartilage genes were more highly expressed after 6 h of stretch compared to 3 h. At 10% strain, 3 h of stretch resulted in higher fibrocartilage gene expression. At 15%

strain, most genes increased in expression at nearly the same amounts. At 20% strain, gene expression was slightly higher at 3 h compared to 6 h, with a noticeable increase in cell hypertrophy at 6 h of stretch. At 25% strain, gene expressed was lower than at other strain rates shown by a maximum relative expression of 10^7 as opposed to 10^{10}. This result indicates that the cells were exposed to too high of a strain rate, hindering their differentiation potential. In the combined graph (Figure 14F), the greatest overall increase in fibrocartilage gene expression was at 10% strain for 3 h, supporting the use of the
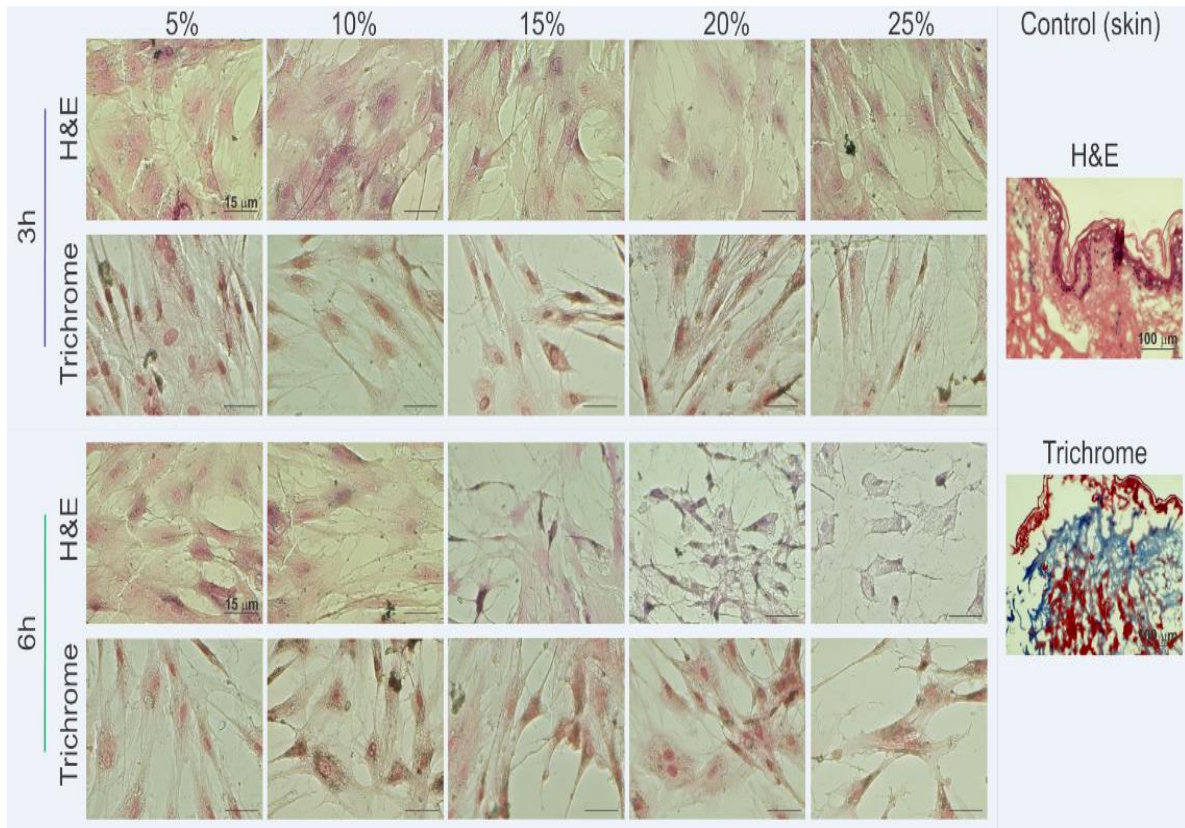
Figure 15. Strain rates do not affect protein level collagen expression. Protein level expression of collagen as seen in H&E (pink) and Masson's Trichrome (blue) stains. Control tissue with collagen present (i.e. skin) served as the positive control and is displayed for comparison. Images taken at 40x reveal undetectable protein levels. This data provides further evidence of the difficulty to achieve full translation of collagen genetic expression into protein expression when differentiating from stem cells. H&E and Trichrome stains display mostly cytoplasm and that cells survived at most strains rates, except cell death can be observed after 6 h of mechanical stimulation at 20% and 25% strains.

parameters of 10% strain and 3 h to promote the meniscal phenotype. Data at 15% strain for 3 h and 25% strain for 6 h was statistically significant.

Histological analysis using H&E and Masson's trichrome stains were used to identify the presence of collagen at the protein level in the cells after stretching (Figure

15). In H&E, collagen is demarcated by dark pink and the cytoplasm by lighter pink. In the trichrome stain, collagen is indicated by the color blue. For both time durations across all strain rates, collagen could not be detected at the protein level. Only light pink indicating cytoplasm was seen in the H&E stains, and no blue appeared in the trichrome stains. At 6 h of stretch and 20% and 25% strain, cell necrosis and death can be seen in the stain, supporting the data showing a decrease in gene expression under these parameters, likely due to overstretching. Positive control stains of skin samples are shown in Figure 15 to show that the lack of collagen staining in the tissue samples was not due to technical issues.

<u>Frequency effects</u>

Cells were mechanically stimulated at varying strain frequencies of 0.5 Hz, 1.0 Hz and 1.5 Hz at 10% strain for 3 h and 6 h in chondrogenic media (Figure 16). Relative to control, undifferentiated ASCs, all fibrochondrogenic genes increased in expression when strained at the applied frequency range. A strain frequency of 1.0 Hz promoted the highest increase in gene expression, resulting in a statistically significant increase.

Histological analysis of the cells stretched at varying frequencies show undetectable levels of collagen protein expression (Figure 17). Light pink stains in the H&E samples indicate cytoplasm, with very little dark pink areas indicating possible collagen protein content. Similarly, in the trichrome stains, blue stain indicating collagen could not be seen. The cells appeared healthy in all frequency groups. In comparison, cell death could be seen at higher strain rates (Fig. X). This difference suggests that the cells were able to adapt to the range of frequencies used, whereas strains over 20% overstretched the cells and caused cell death.
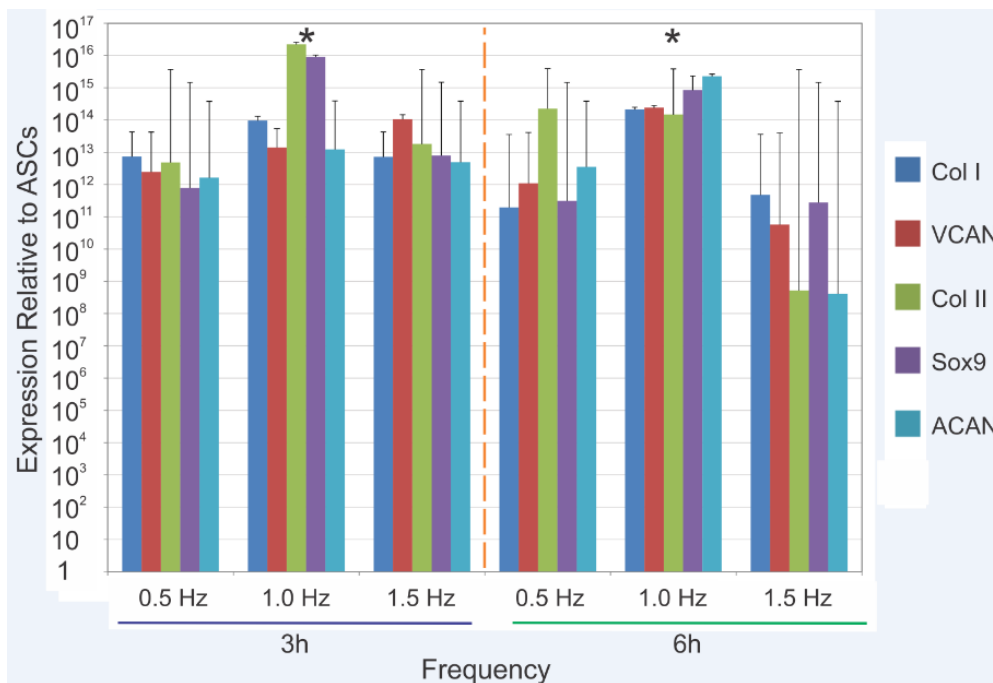
Figure 16. Mechanical stimulation frequency affects phenotype. Stimulation frequencies of 0.5, 1.0 and 1.5 Hz were applied to the ASCs for 3 h and 6 h. Strain was kept constant at 10%. Gene expression was significantly increased under 1.0 Hz stimulation for both time points, suggesting that 1.0 Hz is the ideal strain frequency to subject stem cells to for inducing fibrochondrogenesis. Error bars represent standard error. * denotes statistical significance.

Overall, the ideal parameters to promote fibrochondrogenic differentiation of adipose-derived stem cells is 3 hours of stretch at 10% strain and a frequency of 1.0 Hz in chondrogenic media, as shown by the greatest increase in expression levels of fibrogenic and chondrogenic genes.

Discussion

Multipotent stromal cells from adipose tissue were chosen due to their abundance, non-controversial nature, and potential for ease of harvest and transplantation to the same patient. Human ASCs can be easily obtained through minimally invasive liposuction procedures, and even a small amount of adipose tissue can yield millions of stromal cells. For these experiments, unwanted adipose tissue was donated from liposuction procedures in the clinic. More importantly, phenotypically, ASCs are similar to fibroblasts and have been reported to differentiate into chondrocytes (Xu et al. 2007). This combination of phenotypic characteristics make the ASC an attractive candidate for fibrocartilage differentiation.

Fibrogenic proteins collagen I and versican were used as fibrocartilage markers as they are critical to the function of fibrogenic tissues. Collagen I (Col I) plays a key role in a tissues' ability to withstand tensile forces and is found in tendons, ligaments, and other connective tissues that experience large tensile loads. Collagen I's role in the meniscus is thus to allow the tissue to withstand tensile loads exerted onto it. Versican (VCAN) is a proteoglycan that plays a large role in adhesion of cells to the extracellular matrix, and is present in large amounts in fibrocartilage (Naal et al. 2008).

Chondrogenic proteins collagen II, Sox9, aggrecan, and collagen X were used to suggest chondrogenic phenotype because of their significant presence in the meniscus and their key functional roles. Collagen II (Col I) is an especially important component in the meniscus as it allows for the tissue to withstand tensile forces. Sox9 is a key chondrogenic differentiation factor. Aggrecan (ACAN) an extracellular matrix
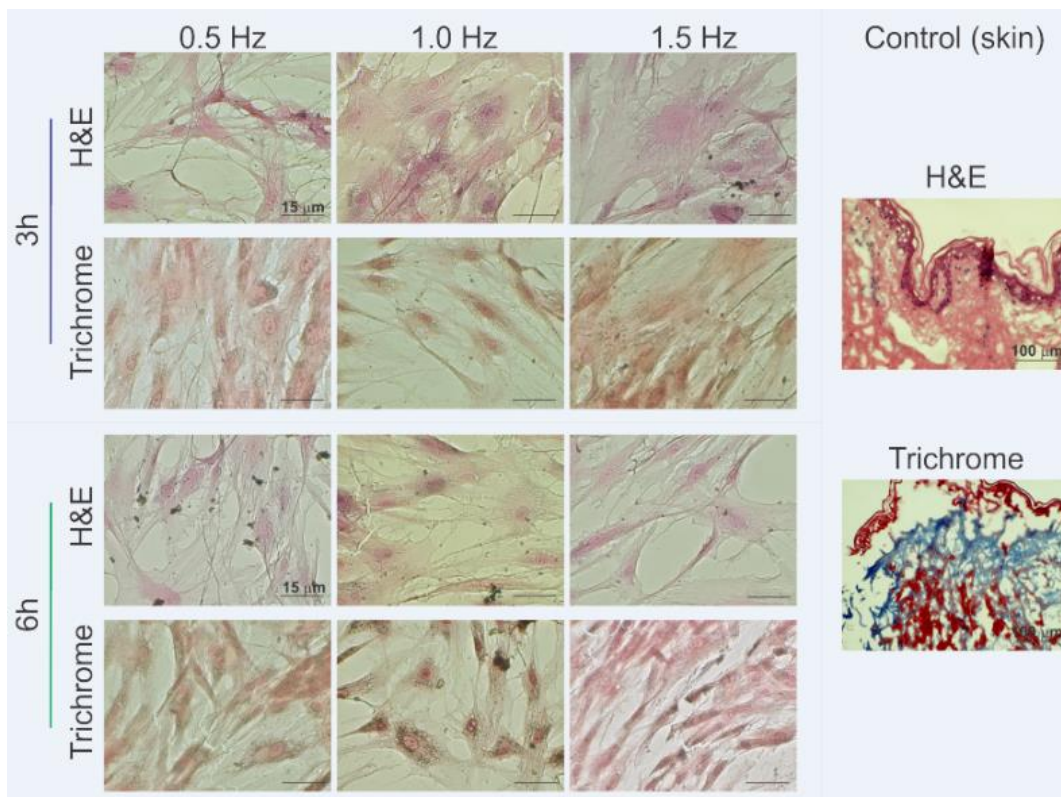
Figure 17. Stimulation frequency does not affect protein level collagen expression. Protein level expression of collagen as identified by H&E (pink) and Masson's Trichrome (blue) stains. Control tissue with collagen present (i.e. skin) served as the positive control and is displayed for comparison. Collagen protein was not observable at 40x magnification, indicating the insignificant amounts of collagen protein present in the differentiated stem cells, which is in clear contrast to the noticeable increase in collagen gene expression found in the PCR analysis.

proteoglycan that also aids cartilage in bearing compressive loads. Lastly, collagen X demarcates endochondral ossification.

Protein expression and presence after differentiation treatments is often included to strengthen claims of full or partial stem cell differentiation. Although protein expression was attempted, protein quantities were too low to be detected in mechanically-stimulated trials. This is expected, as treatment times ranged from 1-6 hours, which is considered too brief of a period given the amount of cells used for any significant protein production in adult chondrocytes, let alone pre-differentiated or immature cells (Pelaez et al. 2009). Continuation of culture after treatment was considered, but ultimately rejected as gene expression changes were dependent upon mechanical stimulation. Therefore, the cells would risk de-differentiation if allowed to continue to culture after stimulation and effects of mechanical stimulation would be lost.

The combination of the aforementioned fibrogenic and chondrogenic proteins give the knee meniscus its unique phenotype, allowing it to meet its functional demands. The meniscus experiences tensile and compressive loads- collagen I, collagen II and aggrecan allow the meniscus to bear these loads. The concentration of these proteins vary within different regions of the meniscus in relation to concentrations of tensile, compressive, hoop, and shear stresses, further contributing to the heterogeneity and uniqueness of the fibrocartilage phenotype.

Adipose-derived stromal cells were treated in the various media formulations over a period of 3 weeks to allow for progress towards chondrogenic differentiation. By comparison, pre-fibrogenic differentiation occurs at a much faster rate, taking from a few

days to a week. Progression towards a differentiated state, or "pre-differentiation" was evidenced by a changed morphology and enhanced relative gene expression by the cells. For pre-chondrogenic differentiation, the ASCs would appear more rounded in shape, indicative of chondrocytes. Under fibrogenic media, ASCs assumed a more elongated shape with many new cellular extensions, resembling natural fibroblast morphology.

For the fibrogenic-to-chondrogenic (FM-CM) and chondrogenic-to-fibrogenic (CM-FM) medias, the objective was to promote the mixed fibrochondrogenic phenotype. The media was switched between the two media types halfway through the culture period, i.e. 10-11 days through the total 21 day culture, to maximize time exposure of the cells to each media. Interestingly, the ASCs appeared to acquire characteristics of the latter media, suggesting that maintaining stromal cell adaptations is dependent upon continuous stimulation. Switching medias did not result in a mixed phenotype.

Expression of collagen I was seen in nearly all media groups that contained fibrogenic media components. This may indicate that 1) adipose-derived stromal cells have a tendency for fibrogenic differentiation given the correct fibrogenic media conditions, 2) fibrogenesis may be the dominate differentiation direction given traditional media components (since FM is the conventional media for culturing ASCs), and 3) the presence of fetal bovine serum may be an adequate stimulus to encourage fibrogenesis-like differentiation. No increase in collagen I expression was seen in the fibro-chondrogenic media 2 (FCM2) compared to increased collagen I expression in the fibro-chondrogenic media 1 (FCM1), indicating more fibrogenesis even though the serum level was lower. This was possibly due to the fact that in FCM2, and under the conditions of 10% FBS and 3 weeks of culture, the cells began to overgrow and may have transformed

into other, unknown phenotypes as commonly seen in cell culture overgrowth. Collagen II expression, a chondrogenic marker, was understandably highest in the chondrogenic media group (CM). No relative increase in collagen II expression levels was seen in the FCM1, FCM2, FM-CM, and CM-FM groups, despite the presence of chondrogenic factors. This effect is most likely due to the dominance of the fibrogenic components in the medias.

Considering that chondrogenic media resulted in the highest relative expression of both multiple fibrogenic and chondrogenic genes, this media was determined as the optimal media formulation to obtain the mixed phenotype during the tensile strain testing. Although Collagen I expression was minimal under Chondrogenic Media, cyclic, tensile strain has been shown to increase Collagen I gene expression and encourage fibrogenesis (Connelly et al. 2010, Kessler et al 2001). This suggests that using chondrogenic media, which exhibited the highest collagen II expression while still expressing the fibrogenic gene versican, has the greatest potential for obtaining a mixed fibrocartilage phenotype when combined with cyclic tensile strain.

Following comparison of biochemical factors, tensile strain was added as a second stimuli. Strains of 10% at 1Hz for 1-6 hours were initially applied, based both on our preliminary calculations in Appendix A as well as support from other studies investigating mechanical stimulation in connective tissue formation (Connelly et al. 2010, Kessler et al. 2001, Pelaez et al. 2009). In CM, ASCs subjected to mechanical stretch consistently displayed higher levels of fibrogenic gene collagen I than in CM or FM alone, supporting our hypothesis that the tensile strain would support expression of collagen I in the presence of CM. At 3 hours of stretch in CM, the combination of fibrogenic and

chondrogenic gene expression was highest. At longer stretch duration, chondrogenic gene expression decreased, while fibrogenic gene expression remained relatively high. This is likely due to the dominance of mechanical stretch to produce more fibrogenic cells, and at longer stretch times fibrogenesis gradually dominated over chondrogenesis resulting in lower chondrogenic gene expression.

The three mechanical stimulation parameters investigated of stretching time duration, strain rate and stimulation frequency showed different levels of effect on the ASCs. The greatest increase in gene expression was seen in the frequency varying data, followed by the strain rate data. Thus, frequency had the greatest effect on fibrocartilage phenotype changes. Strain had the next greatest effect, and time duration had the least relative effect.

There were no issues with removing cells from the stretching substrates for RNA extraction, but a method will need to be determined in order to remove the cells as a cell sheet for subsequent whole tissue meniscus tissue engineering. The cells cannot be simply dissociated from the substrate as differentiated cells will not retain their phenotype once dissociated and/or will simply apoptosis.

Chondrogenic differentiation is traditionally performed in a 3D culture, and usually as a pellet culture. This is because chondrocytes require high cell density and close proximity between cells. Hence, there is a level of difficulty in attempting to induce the chondrogenic phenotype on a 2D surface, i.e. that of the stretch device substrate. There is some evidence that chondrocytes and bone marrow mesenchymal stromal cells (MSCs) are able to differentiate into cartilage under certain 2D conditions (Galle et al.

2010). While the factors of 2D culture and tensile stretch favor fibrogenesis, they do not encourage chondrogenesis. Hence, chondrogenesis was mainly induced by the use of chondrogenic media and by the chondrogenic growth factors within it. In this way, we were able to still achieve a chondrogenic phenotype on a 2D surface.

Conclusion

We demonstrated for the first time, to our knowledge, the ability to encourage fibrocartilage-like differentiation from human adipose-derived stromal cells using tensile strain. Mechanical stretch along with biochemical factors promoted this mixed phenotype. The challenge of producing the chondrogenic phenotype on a 2D surface, i.e. the stretch substrate, was overcome by stretching in chondrogenic media. These fibrocartilage-like cells provide a valuable stepping stone towards obtaining a fully mature, differentiated fibrocartilage phenotype that could be used in tissue engineering applications down the road.

CHAPTER 4. IMPACT OF CARDIAC PATCH AND IBUPROFEN ON INFLAMMATION FOLLOWING MYOCARDIAL INFARCTION

Publication: Meier EM, Wu B, Xu Z, Lam MT.

Tissue Engineering A- Submitted

Elizabeth Meier assisted with experimental design. She was responsible for approximately half of all surgeries as well as post-operative care. She conducted PCR, IF analysis, histology, and blood smear sample preparation. Bin Wu conducted the remaining surgeries. Zhengfan Xu assisted with histology, immunofluorescence, and sample preparation. Ashley Apil, Tiara Heard and Bijal Patel assisted with cell counts and double blinding, respectively.

Introduction

So far we have determined that direct mechanical intervention can assist in wound healing in certain tissues (ex. skin), but not in other tissues with limited capacity to heal (ex. meniscus). Like the meniscus, heart tissue has limited capacity to regenerate, due to extremely low cell replication. However, unlike the meniscus, heart tissue is highly vascularized, resulting in a high capacity for inflammation and scar tissue formation. These are the physiological events that occur in major cardiac tissue injuries, including myocardial infarction. Myocardial infarction (MI), commonly known as heart attack, is a sometimes deadly injury that can lead to heart failure and death.

One of the major complications of MI is cardiac remodeling and improper scar tissue formation. One of the more popular research topics to address this remodeling is to suture a biomaterial patch to the cardiac tissue to increase wall thickness and increase cardiac function. Natural, decelluarized tissues, such as porcine small intestine

submucosa (SIS) are frequently used. These materials are attractive for MI treatments because they have been shown to promote angiogenesis and retain delivered cells and growth factors (Vanoos et al. 2016 Zhang et al. 2015, Mewhort et al. 2016).

However, it is largely unknown how addition of a collagen-based patch affects the inflammatory process of the tissue. Collagen-based decellularized tissues have been used in a wide variety of reconstruction surgeries (Jansen et al. 2013, Ibrahim et al. 2013), with a wide range of inflammatory responses reported. Furthermore, many of these materials incite a different inflammatory response between locations and applications in the body, making extrapolation of results between applications ill-advised. For example, AlloDerm, a collagen-based decellularized dermal layer, has minimal reaction when used in breast reconstruction, but is quickly encapsulated and infiltrated by macrophages when used in abdominal reconstruction (Broderick 2012, Ibrahim 2013). It stands to reason that in the case of a myocardial infarction treatment, the physiological response would differ from either of the two previous applications. While none of the documented responses to SIS, AlloDerm, or any other similar decellularized tissue, have been severe enough to warrant discontinuing use of the material, this variation suggests further study is needed before any such material is used to treat severe injuries, like myocardial infarction.

To address this gap in knowledge, we propose to use a porcine small intestine submucosa (SIS) patch on a rat infarct model. The SIS material has been used successfully in infarct studies (Lam et al. 2013, Wendel et al. 2014, Zhang et al. 2015). These studies have proven that a porcine SIS patch can improve cardiac mechanical measures, such as ejection fraction, at least as well as other patch materials (Lam et al. 2013, Wendel et al. 2014, Zhang et al. 2015, Mewhort et al. 2016). Porcine SIS is

commercially available through Cormatrix, which has supplied the material for clinical heart valve repair and pericardium replacement, among other uses (Gerdisch et al. 2014). While it is an approved material with numerous studies conducted on its efficacy and safety, its effects on the inflammatory response in an injury state, such as myocardial infarction, are currently unknown. Due to the addition of a foreign material, we expect that initial inflammation may be increased relative to infarct without any patch treatment. To attenuate the increased inflammation, we expect that inclusion of an anti-inflammatory agent, ibuprofen, may counteract this. To effectively evaluate how application of an SIS patch may influence the inflammatory response post- MI, we plan to observe multiple aspects of the inflammatory response in a rat MI model, with use of an SIS patch with and without ibuprofen to determine how inflammation will be affected through day 7 post-MI. Seven days was selected as the duration for the experiment as it has been suggested as a rough timeline of the inflammatory response conclusion in a rat MI model (Turer 2011, Altara 2016).

Three subject groups will be used; infarct-only (control), infarct + patch, and infarct + patch +ibuprofen. Each group will be evaluated daily through seven days for gene expression, protein expression, histology, and leukocyte counts. It is our expectation that this analysis will present a clear view of the impact of a porcine SIS cardiac patch on the inflammatory response after myocardial infarction.

Methods

<u>Myocardial Infarction Model</u>

Rats were selected for the infarct model due to their similar healing mechanisms to humans. Myocardial infarction surgery was be performed in 200-225g female Sprague-Dawley rats through left coronary artery ligation. Surgical procedures will be conducted as outlined in the approved IACUC protocol A-03-06-14. Immediately prior to the surgery, a baseline echocardiogram was performed, after which the animal would be randomly assigned to a group. Animals were allotted into groups using a random number generator (RANDBETWEEN function) in Microsoft Excel. A return value of "1" designated the animal as infarct-only, "2" corresponded to patch only, and "3" received patch and supplemental ibuprofen. Animals were anesthetized with isoflurane and intubated. The heart was exposed via thoracotomy and the left descending coronary artery was occluded using a 6-0 suture slipknot with thread. The artery was occluded for 45 minutes, during which moist sterile gauze was placed over the opening to limit dehydration. After the 45 minutes, the slipknot was removed to allow for reperfusion and the patch applied (where applicable). For designated animals, the SIS patch was visually aligned over the infarct area and sutured into place using two 6-0 sutures. This process can be seen in Figure 18. After the patch is applied, the wound is closed and the animal will receive pain medication and a bolus of saline to prevent dehydration. Analgesics were provided every 12 hours and MI confirmed via echocardiogram after 24 hours. Animals in the patch+ ibuprofen group will be given children's ibuprofen daily via syringe feeding. Dosage of supplemental ibuprofen was 30 mg/kg body weight/ day. Dosing was determined based on pharmacokinetic analysis of ibuprofen in Sprague-Dawley rats (Fu 1991). Animals not receiving ibuprofen were syringe fed with a placebo. Animals were sacrificed at days 1, 2, 3, 4 5, 6, or 7, with death confirmed via heart removal.

Gene Expression

PCR analysis was performed to assess the state of the tissue at each time point. Key inflammatory markers MMP 1, MMP 2, and MMP 8 were examined. Collagen I will be investigated for fibrosis and scar formation. TGF-β and TNF-α were reviewed for information about the presence and type of inflammation, along with IL-1RA. Neutrophil presence and activity were indicated with neutrophil elastase and neutrophil chemotactic factor (CF) 2. Primers were identified from Harvard Primer Bank and the corresponding custom DNA oligos will be ordered from Life Technologies. Primer sequences are outlined in Table 4.
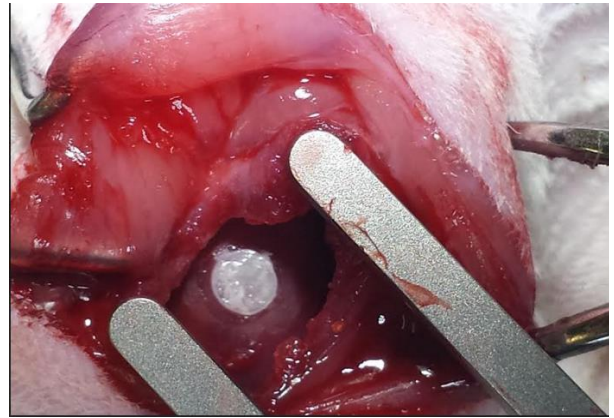
Figure 18. Placement of the SIS patch on infarct area. After reperfusion, 6 mm patch will be manually placed over the infarct and held in place with sutures.

Following sacrifice, rat heart tissue will be crushed using a mortar and pestle. Then, the steps outlined in the RNeasy minikit instruction manual (page 6-7) will be performed to extract RNA. A Beckman Coulter Microfuge 18 Centrifuge will be used for this process. Following the RNA extraction process, RNA will be stored in -80C or immediately used in downstream steps. Before cDNA production can take place, we will determine the concentration of RNA in each sample using a Qubit 2.0 Fluorometer and reagents (Invitrogen/Life Technologies). To quantify RNA, 199 uL of Qubit RNA buffer solution and 1 mL of Qubit RNA fluorescent reagent will be added to a 250 uL tubule. Eight microliters will be extracted from the 200 uL mixture and 8 uL of the RNA solution will be added. The quantity of 8 uL was selected due to the potential for low RNA

quantities in the infarct tissue. The tubule will be vortexed and then placed in the Fluorometer for quantification. If RNA quantities are undetectable, the process will be repeated with 20 uL solution removed from the 200 uL mixture and replaced with 20 uL of RNA solution. Once the quantity of RNA is determined, preparations for cDNA will begin.

Complementary DNA will be produced using Taqman Reverse Transcription Reagents kit (Applied Biosystems Branchburg, NJ). The reagents will be mixed as indicated in the kit instructions. Once the solution had been prepared, 6.525 uL will be added to four 0.2 mL flat cap tubules (Fischer Scientific). RNA will be mixed with a calculated amount of RNase-free water. Calculations are conducted so that equal

Gene	Abbreviation	Description	Sequences
Collagen I	Col I	Expressed during fibrosis.	GTTGCTGCTTGCAGTA AGGGCCAAGTCCAAC
MMP-1	MMP-1	Collagenase I, II, III MMP. Seen during remodeling and inflammation.	AAAATTACACGCCAGA GGTGTGACATTACTCC
MMP-2	MMP-2	Collagenase IV, gelatinase. Seen during remodeling and angiogenesis.	TACAGGATCATTGGCT GGTCACATCGCTCCA
MMP-8	MMP-8	Neutrophil collagenase.	TGCTCTTACTCCATGT TCCAGGTAGTCCTGA
TGF-β	TGF-β	Involved in inflammation and other processes. Produced by macrophages during inflammatory response.	AACTGCTTCCTGTATG AAGGCGTCGTCAATG
TNF-α	TNF-α	Tumor necrosis factor, released by macrophages during inflammatory response.	CCTCTCTCTAATCAGC GAGGACCTGGGAGTA
Neutrophil Elastase	NE	Serine protease released by neutrophils and macrophages during inflammation.	CTCGCGTGTCTTTTCC GCCGACATGACGAAG
CD14	CD14	Monocyte, macrophage marker	ACGCCAGAACCTTGT GCATGGATCTCCACC
Chemotactic Factor 2	CF2	Neutrophil chemotactic factor 2. Factor released during chemotaxis.	CCCACTCCCGGATTT GTCTCGGTTAATGCTT
IL-RA	IL-RA	Interleukin receptor antagonist 1. Produced by M2 macrophages.	GCGAGAACAGAAAGC CCTTCGTCAGGCATAT

Table 4. List of inflammatory marker genes and primer sequences.

amounts of RNA are included in each sample. Once the water is added to the RNA solution, 3.475 uL of the resulting mixture will be added to each tube, totaling 10 uL. Once the cDNA reagents are prepped, each reagent should be placed within a 2720 Thermocycler (Applied Biosystems). Once the program has finished its run, cDNA will be stored at -20C for up to 24 hours, or used immediately in downstream applications.

PCR

PCR was conducted using StepOne Plus Real-Time PCR (Applied Biosystems). The accompanying StepOne v2.2.2 software was used to set up the experiment. Each gene and sample were assessed in triplicate and two controls used: negative control with no cDNA, and cDNA from the MI-only tissue.

The plate design was executed in a MicroAmp Fast Optical 96-well reaction plate from Applied Biosystems. Each well received 2.0 uL of the cDNA sample and 0.4 uL of both the forward and reverse primers. Negative controls received 2.0 uL of RNase-free water in lieu of cDNA. All wells received 7.6 uL of RNase-free water, for a total of 10 uL of solutions. The plate was then covered with aluminum foil to block light as 10 uL Power SYBR Green PCR Master Mix (Applied Biosystems) was added to each well. Once the plate was loaded and cycles completed, gene expression fold-increase was calculated from CT values provided by the software.

Differential Quick Stain

In order to determine the proportion of inflammatory cells within each time point and group, a Differential Quik (Diff-Quik) blood smear stain was performed. This stain is commonly used in immunology and inflammation studies to assess different inflammatory responses (Van Hout et al. 2015, Geissman, et al. 2010, Godwin et al. 2016). Coronary

and ventricular blood was extracted from each tissue sample using a syringe immediately after sacrifice. Blood was dropped onto labeled slides and spread using a spreader slide.

Each slide was fixed and stained using a three step process using PolyScience's Differential-Quik Stain (Warrington, PA). Once the stains set, groups of one hundred cells were counted and neutrophils and monocytes were tallied. Neutrophils are signified by dark blue nucleus and granules with pink cytoplasm. Monocytes appear with lobulated, violet nuclei with light blue cytoplasm, an
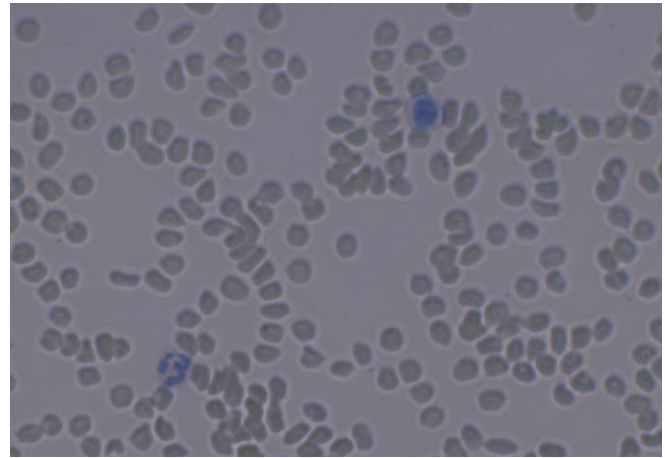
Figure 19. Diff-Quik stain of example blood smear. This smear shows a neutrophil and a lymphocyte in the 100-cell count of the smear.

example is shown in Figure 19. Following staining, each slide was relabeled by another researcher blinded to the study to prevent bias during data collection and analysis. In order to ascertain quantitative differences, each smear was viewed at 6 different locations, selected at random by two double blinded researchers with no relation to the study. The leukocytes were tallied per approximately 100 cells, with the exact cell count being included. The tallies at each location were averaged per sample, with three samples being assessed per each treatment group at each time point, for six points for blood smears from animals receiving infarct only, infarct + patch, and infarct with patch and ibuprofen groups at days 1-7 post-infarct. Six sham animal smears were included as an additional control.

<u>Histology and Immunofluorescence</u>

Samples for histological examination will be excised and frozen at -80C in OCT for a minimum of 24 hours. After samples have been thoroughly frozen, samples will be sliced in 6 um sections using a Cryotome. Section thickness was determined during preliminary staining to determine optimal thickness for staining visibility. Section slicing will be done starting with the apex of the heart, near the infarct area, moving upwards along the heart through the infarct zone. Each slice will be numbered, with every other slice being allotted to either histology stain or immunofluorescence for a total of thirty slices equidistant throughout the heart. Ten slices will be allotted for IF, while the rest will be allotted for picrosirius red, and hematoxylin and eosin. This way, each stain will have an equal representation of the infarct area while minimizing the number of animals needed. By analyzing multiple slices throughout the infarct region, we will be able to evaluate the distribution of key inflammatory cells throughout.

<u>Histology</u>

Histological evaluation provides qualitative evidence of tissue damage and infarct size. Hemotoxylin and Eosin (H&E) and Picrosirius Red was used to delineate the infarct area, healthy muscle, deposited collagen and the SIS patch, where applicable. H&E staining was performed with 6 μm sections from two animals to confirm qualitative evaluation. The same size slices was used for Picrosirius Red evaluation. Tissue samples stained with Picrosirius Red were also observed under polarized light to aid in collagen deposition and maturity analysis.

<u>Immunofluorescence</u>

Immunofluorescence (IF) staining was conducted to identify CD45AB, and was used to assess the presence, location, and density of inflammatory cells (leukocytes) in the infarct area. To separate collagen's autofluorescence from the CD45AB signal, the slides were imaged prior to IF staining and assessed for brightness using ImageJ (U.S. National Institutes of Health, Bethesda, MD). The samples were then assessed using ImageJ after staining to determine the difference in brightness, and therefore the presence of leukocytes. The quantitative differences between the before and after images were used to determine the relative presence of leukocytes between time points and treatment groups. This was conducted for nine slices within each sample, with the same corresponding slices evaluated between the groups. For example, if the tenth slice was analyzed for one sample, it was analyzed for the remaining samples. Each slice was imaged at a minimum of three locations to account for local variability. All brightness measurements were included in the analysis.

Tensile Testing

It is well established that healed wounds exhibit different mechanical behavior than that of native, intact tissues. Of particular note is the presence of scar tissue, which increases the elastic modulus of the tissue and can alter the anisotropy of the tissue. However, thick, intact scar tissue is not fully formed during the inflammation process and therefore little is known about the immediate changes in mechanical properties following an infarct. To evaluate the mechanical changes in the heart post-MI and how a collagen-based SIS patch may affect these changes, tensile testing was conducted on all day 7 tissue samples. Tensile testing was conducted on a Cell Scale UStretch uniaxial mechanical tester (CellScale, Ontario, Canada). Samples were stretched at a rate of 2

mm/min with data collected five times per second. Three tissue sections were procured from each heart sample with three hearts used for each treatment group plus a sham group. SIS patches were gently removed with forceps prior to tensile testing for applicable samples. Elastic modulus, ultimate tensile strength and failure strength were calculated and compared using one-way ANOVA with Tukey post-hoc tests.

Statistics

All averages will be calculated as mean values ± standard error. Statistical significance for PCR was determined with two factor ANOVA with an alpha value of 0.05. Tukey post hoc analysis was performed to ascertain significance within groups, with p-values set at 0.05. Ad hoc power analysis was included to ensure sample size accuracy, with a post-data power analysis yielding $\beta= 0.76$, which is close to the 0.80 used to calculate the sample size. The same statistics were used for the leukocyte counts in the blood smears. Brightness, or leukocyte presence in the tissue, was also assessed using a two-factor ANOVA with the same parameters. Elastic modulus, ultimate tensile strength and failure strength from tensile testing were calculated and compared using one-way ANOVA with Tukey post-hoc tests. Sample sizes for quantitative measurements were determined completing a power analysis. Initial sample sizes were estimated based on published data from similar studies that confirmed the sensitivity of Differential Quik staining (Selvi et al. 2000, Silverman 1995) and cell and gene expression in inflammatory studies (van Hout 2015, Vuohelainen 2014). Histology, and polarized light microscopy were evaluated qualitatively. All statistical design and analysis were completed with the assistance of Wayne State University's Research Design and Analysis (RDA) consulting unit.

Results

Expression of Inflammatory Genes

PCR results were compiled and organized into groups of related inflammation factors. Matrix metalloprotease (MMP) expression is shown in Figure 20A-D. MMP expression overall showed minimal difference between the groups, with the exception of significant down-regulation of MMP-2 at day 7 relative to infarct-only (Figure 20). As seen in Figures 20E-H, neutrophil activity is overall elevated in the first 5-6 days post-injury relative to the infarct-only group. However, by day 7, expression of all neutrophil markers was below that of infarct-only. This, along with the elevated MMP expression during this time, suggests that neutrophil activity, and potentially population, is elevated at approximately days 3 – 6 in animals receiving the patch, relative to animals that received only the infarct. The overall lack of difference in expression between the patch groups suggests that the ibuprofen, either through mechanism or dosage, does not significantly affect neutrophil gene expression post-infarct.

Figure 20I-L shows increased expression of key inflammatory markers in the patch treatment groups at days 2-3 and at days 5-6 relative to the other time points. These markers are expressed by, but not exclusively by, macrophages and thus only limited conclusions of macrophage activity can be drawn. That said, these data suggests that gene expression of these key genes can somewhat effectively "track" macrophage presence, while providing information about the inflammatory process, as the gene
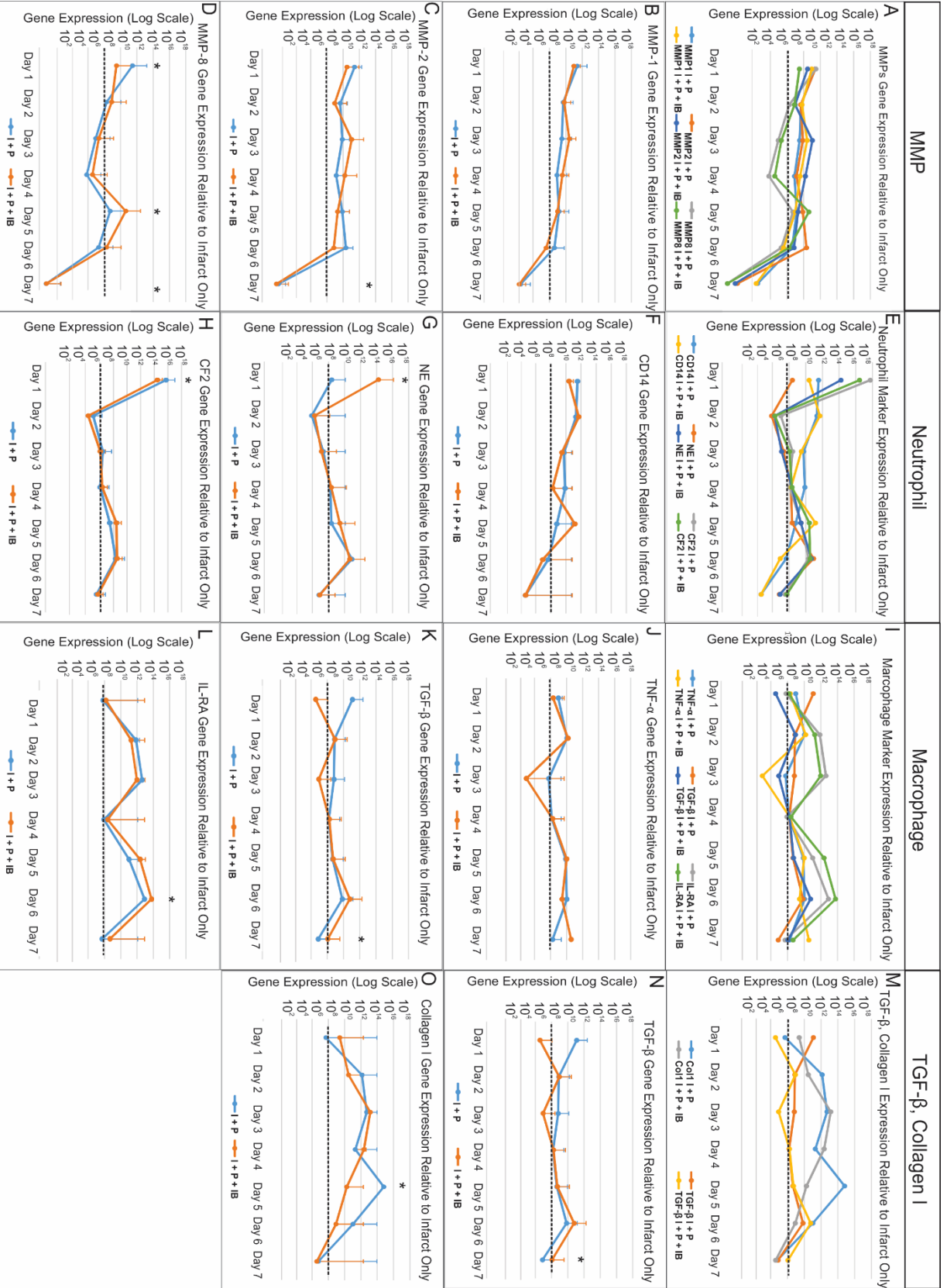
Figure 20. PCR results plotted over time relative to infarct only. Dotted lines indicate infarct only expression. All significant results were relative to infarct only, indicated by * (P < 0.05). Genes were grouped based on physiological relevance. MMPs 1, 2, and 8 are shown in **A-D**. MMPs showed a clear decline in expression over time. Neutrophil genes CD14, neutrophil elastase and CF 2 are shown in **E-H**. Neutrophil markers have a net decrease in expression over time, and expression levels remain consistently lower than infarct only expression levels at the end of day 7. Macrophage markers are shown in **I-L**, with TGF-β and collagen I in **M-O**. Macrophage expression shows higher expression around day 2-3 and 5-6 relative to the other time points. Error bars have been removed from combined graphs (**A, E, I, M**) for clarity. I + P = patch only; I + P + IB = patch and ibuprofen.

expression neatly follows the timeline of macrophage activity in inflammation outlined in literature (Altara et al. 2016). This is particularly apparent when reviewing IL-RA expression, which has clear peaks at expected macrophage infiltration times. Specifically, the expression peaks during the first few days of inflammation, when the local, pro-inflammatory macrophages (M1) are most often active, and then peaks again towards the end of inflammation when the population of circulating, anti-inflammatory macrophages (M2) is highest. Figure 20M-O supports the increased macrophage expression, as collagen I expression is lower in the later stages of inflammation in both treatment groups relative to the infarct-only group. Interestingly, during the middle days of inflammation, collagen I expression is increased relative to the infarct-only group. This suggests that overall collagen I expression is not lower between groups, but rather may be expressed on an accelerated timeline in groups receiving the patch treatment after infarct. As shown in Figure 20M, the expression of collagen I is related closely to the expression of TGF-β, which is expressed by macrophages as well as other cell types in the area. Clearly, these

data cannot give a complete picture of the differences in the inflammatory process between the groups, however it can provide valuable evidence when combined with other data, as described next.

<u>Evaluation of Leukocyte Populations</u>

Analysis of the neutrophil and macrophage cell counts was conducted using a two factor ANOVA model in SPSS. These results are outlined in Table 5. The change in neutrophil counts over time was significant for all groups ($p = 0.004$). Macrophage counts also varied significantly over the 7 day period for all groups ($p = 0.008$). Significant decreases in neutrophil counts were noted for all groups between days 2 and 6 ($p = 0.047$) and days 2 and 7 ($p = 0.014$). Similarly, macrophage counts yielded significant differences between early and later timepoints throughout the experiments for all groups. Significant differences were noted between days 1 and 6 ($p = 0.002$), 2 and 6 ($p = 0.022$), 3 and 6 ($p = 0.001$), 4 and 5 ($p = 0.049$), and 4 and 6 ($p = 0.008$). These differences are likely due to the low macrophage counts at day 4 and the higher counts at day 6. These results are similar to other inflammation studies that show the greatest macrophage population towards the end of the inflammatory period, generally around day 7 (Altara et al. 2016, Stuart et al. 2016, Giroux et al. 2000, Fu et al. 1991). Therefore, these results do not suggest significant ill effects from the treatments. Differences in neutrophil counts between groups were significant at days 4 ($p = 0.05$) and 6 ($p = 0.01$), due to the higher neutrophil presence in the patch + ibuprofen group. Differences in macrophage counts were significant between groups at day 2 ($p = 0.004$), with the patch + ibuprofen group having lower population than the other two groups. As macrophage populations remained low in the group receiving ibuprofen, it may indicate that the ibuprofen slowed the

inflammation process slightly, delaying the arrival of circulating macrophages and limiting the influx of cells. Also significant were the counts at day 4 (p = 0.03), this time due to the lower macrophage population in the infarct-only group. This may be due to a heightened response to the patch treatment, resulting in a greater population of macrophages traveling to the injury area. An example of the smears can be seen in Figure 19.

Neutrophils

	Day 1	Day 2	Day 3	Day 4	Day 5	Day 6	Day 7
Infarct Only	0.68 ± 0.48%	1.24 ± 0.69% *ᵷ	0.61 ± 0.51%	0.55 ± 0.46%	0.15 ± .13%	0.07 ± 0.08% *	0.07 ± 0.15% ᵷ
I + P	0.38 ± 0.41%	0.88 ± 0.76% *ᵷ	1.07 ± 0.87%	0.19 ± 0.21%	0.49 ± 0.57%	0.02 ± 0.03% *	0.16 ± 0.15% ᵷ
I + P + IB	0.26 ± 0.27%	0.68 ± 0.58% *ᵷ	0.98 ± 0.66%	0.40 ± 0.32%	0.37 ± 0.46%	0.33 ± 0.56% *	0.04 ± 0.07% ᵷ

Macrophages

	Day 1	Day 2	Day 3	Day 4	Day 5	Day 6	Day 7
Infarct Only	0.27 ± 0.56% ‡	0.56 ± 0.38% *	0.33 ± 0.52% ∏	0.03 ± 0.64% •ψ	0.59 ± 0.39% •	0.89 ± 0.77% ‡*∏ψ	0.34 ± 0.16%
I + P	0.24 ± 0.26% ‡	0.66 ± 0.22% *	0.36 ± 0.26% ∏	0.16 ± 0.06% •ψ	0.89 ± 0.81% •	1.28 ± 0.36% ‡*∏ψ	0.32 ± 0.24%
I + P + IB	0.47 ± 0.73% ‡	0.33 ± 0.25% *	0.36 ± 0.34% ∏	0.25 ± 0.21% •ψ	1.18 ± 0.29% •	1.48 ± 0.68% ‡*∏ψ	0.21 ± 0.22%

Table 5. Means and standard deviations for neutrophil and macrophage counts. No significant differences were noted between groups. Significant (p < 0.05) differences between days within treatment groups are designated by matching symbols. IB = Ibuprofen.
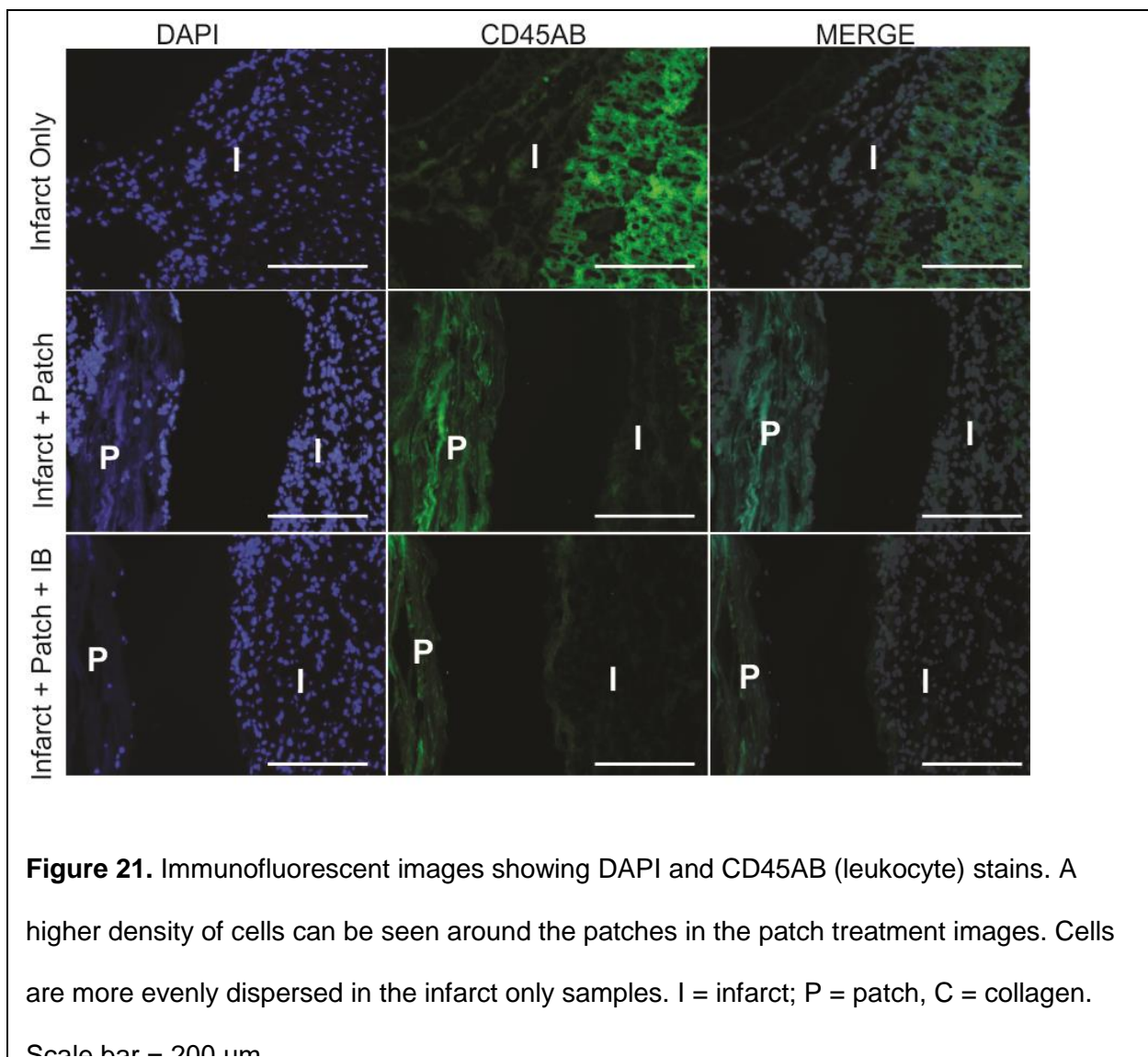
Leukocyte Location and Density

While analysis the of the Quik Diff stains yielded useful information about the cell populations, the cell counts do not provide information about the leukocytes' locations within the infarcted area. Tissue samples from day 7 stained with CD45AB antibodies were viewed under fluorescent light and cell location and density observed (Figure 21). The CD45AB antibody exclusively identifies monocytes and neutrophils in rats, although it does not allow for identification between the two cell types (van den Berg 2001). It was immediately apparent that leukocytes respond to the patch, as a high density of leukocytes are located on the periphery of the patch in both the infarct + patch and infarct + patch + ibuprofen groups (Figure 21). However, there was no clear area of high leukocyte accumulation in the infarct only tissue. It is highly likely that the majority of the cells seen in these images are macrophages, due to the low neutrophil gene expression (Fig. 20) and low neutrophil counts (Table 5) at day 7. To evaluate the differences in leukocyte population within the tissue, images were analyzed before and after fluorescent labeling of CD45AB antibody, with the resulting average difference in Table 6. The average difference is the average readout of brightness due to the antibody labeling and was performed to reduce readout error due to collagen and other background effects. This provides a more direct comparison between groups, as images had varying levels of background signal, which can influence the difference in the brightness readouts before and after fluorescent labeling. The data shown in Table 6 overall shows a strong correlation with the cell counts (Table 5). Overall, both patch groups generally had higher brightness values, or higher leukocyte populations, within the tissue, than the control tissue from the corresponding day, indicating that the addition of the patch resulted in greater migration of leukocytes. The values at Day 1 seemed to display the most variation

between the cell counts and the ImageJ analysis, likely due to the sensitivity of the inflammation process in the first 24 hours of the inflammatory process. The surgical process allowed for variations of up to 6 hours from infarct until sacrifice for 1 day animals, which may account for the variability in the leukocyte counts. Leukocytes, particularly neutrophils, are activated within the first few hours of injury, and therefore a few hours could make a large impact on population counts (Feng et al. 2015). However, after day 1, results were consistent and leukocyte population in the tissue appeared to follow the same population flux as the cell counts, with an overall peak in cell population at Day 5. These data combined suggest that the patch treatments do not necessarily prolong the

inflammatory response relative to infarct-only, but may result in an elevated inflammatory response that is resolved quickly.

Brightness Values from CD45AB Immunofluorescence							
	Day 1	Day 2	Day 3	Day 4	Day 5	Day 6	Day 7
Infarct Only	8.56 ± 7.95	6.01 ± 5.64	11.1 ± 3.49	12.3 ± 4.4	7.58 ± 5.16	11.5 ± 3.73	19.6 ± 0.381
Patch	5.67 ± 6.43	11.2 ± 7.86	18.2 ± 7.23	13.1 ± 6.31	12.2 ± 10.4	17.3 ± 8.01	24.7 ± 14.2
Patch + IBU	19.1 ± 20.8	6.54 ± 9.16	16.4 ± 3.45	30.5 ± 0.82	15.7 ± 2.89	14.4 ± 4.52	12.9 ± 7.14

Table 6. Summary of brightness difference between groups. Brightness indicates average leukocyte presence. Overall, increases in leukocytes were seen throughout the 7 days with small peaks around day 3-4 and 6-7.

Figure 21. Immunofluorescent images showing DAPI and CD45AB (leukocyte) stains. A higher density of cells can be seen around the patches in the patch treatment images. Cells are more evenly dispersed in the infarct only samples. I = infarct; P = patch, C = collagen. Scale bar = 200 µm.

Collagen Deposition in the Infarct Zone

Tissue samples from day 7 show the beginning of deposited collagen in all groups. However, the samples receiving only the SIS patch and no ibuprofen after infarct had a much more defined collagen layer than either of the other two groups. Of note is the collagen surrounding the patch itself, which may be indicative of early encapsulation. SIS implants been known to result in encapsulation in other uses (Jansen et al. 2013, Ibrahim et al. 2013). The collagen deposition on the cardiac surface, however, appears to be similar in thickness and volume between the two patch groups. Interestingly, the collagen in the infarct only group appears to be thinner, than in the treatment groups (Fig. 22).
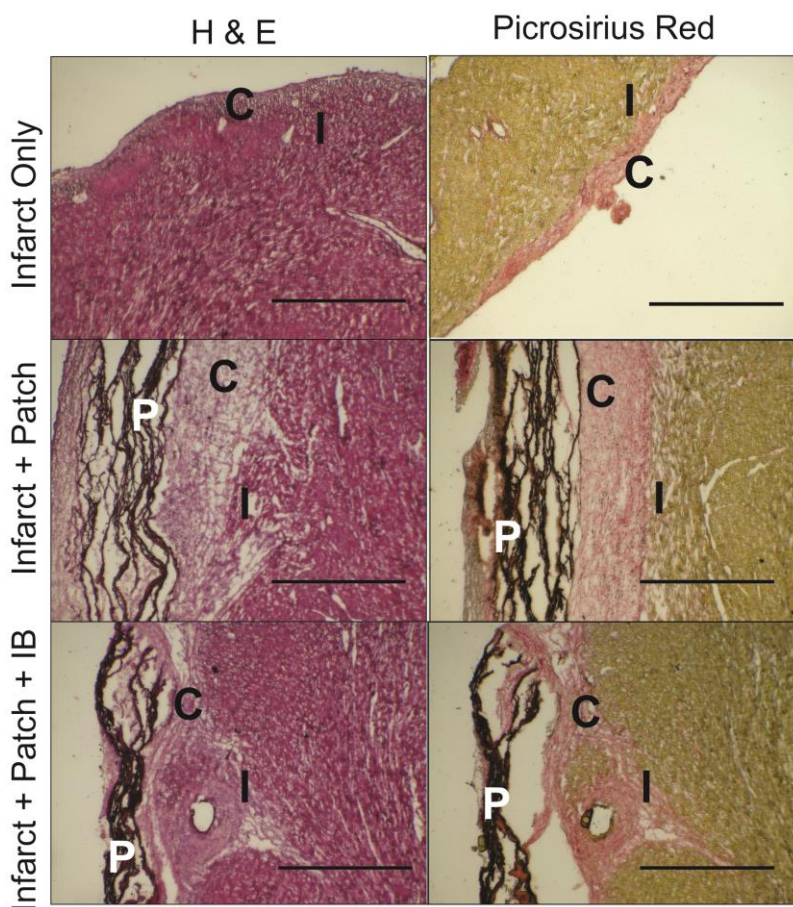

Figure 22. H&E and Picrosirius Red stained tissue samples. "I" indicates the infarct area.. I = infarct; P = patch; C = collagen. Scale bar = 1000 μm.

Collagen Maturity Analysis

Picrosirius red stained slides were viewed using a polarized filter in a Zeiss Axiovert 200. Under polarized light, mature collagen fibers appear red or orange while thinner, less mature fibers appear yellow or green. Generally, infarct models show little immature collagen fibers within the first week, but up to 95% mature collagen after 5 weeks (Wan et al. 2013, Rich et al. 2005). Figure 23 shows samples from infarct only, infarct + patch, and infarct + patch + ibuprofen. All three groups showed some signs of new collagen deposition: thin, immature green fibers in the infarct area. The most interesting difference between the three groups was not in the infarct zone itself, but in the collagen surrounding the patch in the treatment groups. As noted in the histological analysis, the infarct + patch group had a much larger layer of collagen surrounding the patch than the infarct + patch + ibuprofen group. The collagen also appeared to be more mature than the collagen in the infarct zone, as indicated by the orange color. Also of note was that the infarct + patch + ibuprofen group appeared to have more mature collagen in both the infarct zone and in the area between the patch and the cardiac surface. As the increased collagen is consistent between the two patch groups, it is likely that the patch increases local inflammatory response. As there was consistently more collagen in the patch only group relative to the patch + ibuprofen group, there is a possibility that the
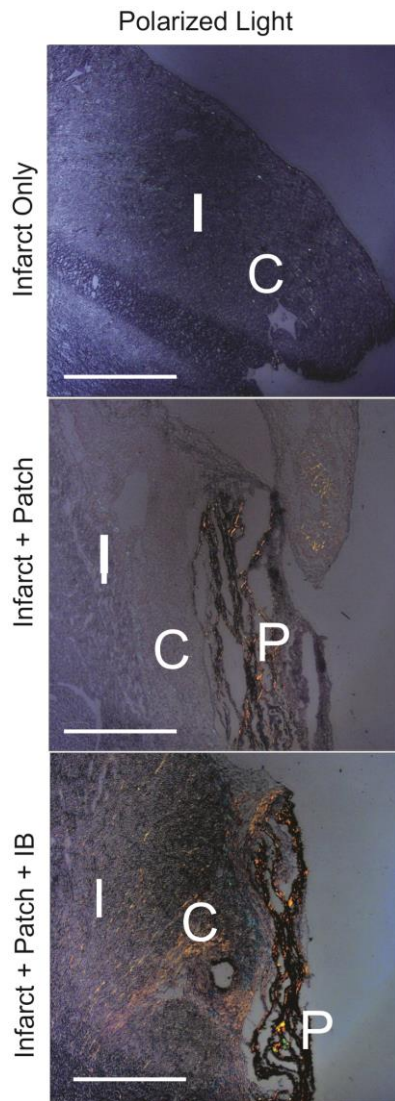
Polarized Light

Figure 23. Images show faint collagen presence in infarct area. Thicker red and orange patches can be observed around the patches. I = infarct; P = patch; C = collagen. Scale bar = 1000 μm.

ibuprofen was responsible for the difference in new collagen deposition. Collagen I expression as shown in Figure 20 O. supports these observations in that collagen I expression was elevated in the groups receiving the patch relative to the infarct only group, yet expression in the patch + ibuprofen group was lower than the patch only group, particularly during days 4 and 5. While this does not directly nor completely explain the differences in the polarized light images, it does support the overall observation that inflammation, including the end-inflammatory state collagen deposition, is increased with the patch use.

Tensile Mechanics

Tensile analysis following a seven-day period showed relatively little differences between infarct only animals and animals receiving the patch treatment. However, elastic moduli were significantly increased in animals experiencing myocardial infarction compared to sham animals (Table 8; Fig. 24). While differences in ultimate tensile strength were not determined to be statistically significant, the data suggest that cardiac tissue is weakened seven days post-MI relative to

uninjured tissue. Likewise, while statistically insignificant, a similar trend can be seen with

fracture strength, with fracture strength decreasing in samples with infarct (Fig. 24).

Interestingly, the greatest decrease in fracture strength occurred in groups that received

the patch and supplemental ibuprofen treatment after infarct. This difference was found

to be significant between the infarct + patch + ibuprofen group and the other treatment

and sham groups. Again, while not all tensile results were statistically significant, these

data do suggest that the tissue turnover and remodeling may be exacerbated or increased

in animals receiving the patch and supplemental ibuprofen after infarct. One explanation

could be that the increased exposed collagen from the patch results in an increase in

MMPs and other proteases, leading to increased removal of damaged tissue. This is also

supported by the slight increase in MMP-1 and MMP-2 during early inflammation as noted in Figure 20.

	Elastic Modulus (kPa)	Ultimate Tensile Strength (kPa)	Fracture Strength (kPa)
Control	89.3 ± 73.2	148 ± 36.8	148 ± 19.1
Infarct Only	102 ± 42.0 *	143 ± 33.7 *	140 ± 18.3 *
Infarct + Patch	108 ± 88.1 *	134 ± 39.0 *	145 ± 28.0 *
Infarct + Patch + IB	111 ± 0.0450 *	135 ± 40.3 *	111 ± 69.7 *†

Table 7. Means and standard deviations for tensile measurements. The sham groups were significantly different from the treatment groups (*). The ultimate tensile strength for the infarct + patch + IB group was also significantly lower than the other groups (†). IB = Ibuprofen.
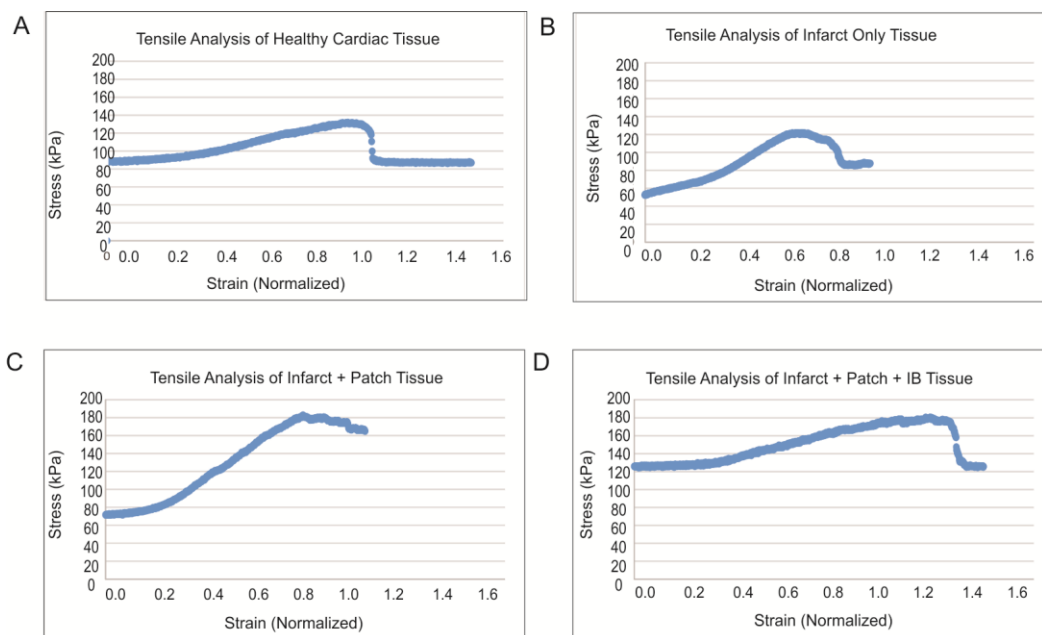

Figure 24. Raw data graphs showing samples of data output from tensile loading. All groups showed a similar toe region, indicating that overall composition is not significantly different. IB = ibuprofen.

Discussion

The function of inflammation is twofold: to clear the injured area of cell and tissue debris, and to produce the biochemical progenitors of fibrosis and angiogenesis (Jugdutt et al. 2007, Altara et al. 2016, Ricciotti et al. 2008). Unresolved or poorly managed inflammation can lead to inadequate or excessive scar tissue deposition, which can have devastating effects (Jugdutt et al. 2007, Bonaventura et al. 2016). Similarly, overactive and underactive leukocyte activity during inflammation can lead to impaired healing and poor left ventricular remodeling, resulting in arrhythmias and/or increased risk of heart failure or cardiac arrest (Wan et al. 2016, Stuart et al. 2016, Giroux et al. 2000). The border region of the infarct zone is at the greatest risk for inflammation-induced arrhythmias, in which newly formed, non-conductive, scar tissue can affect the surrounding, healthy tissue contractions and electrical signaling (Stuart et al. 2016). The primary goal when using cardiac patches is to provide mechanical support; increasing wall thickness and limiting infarct expansion. By completing these two goals, the patch indirectly leads to a third, which is reducing the size of the border region, which leads to lower incidences of arrhythmias (Stuart et al. 2016, Wan et al. 2013, Amer et al. 2010, Ong et al. 2013, Olivetti et al. 1990).

Our data suggest that the use of a porcine SIS biomaterial patch does increase the inflammation response after a 45 minute occlusion-reperfusion myocardial infarction, either with or without supplemental ibuprofen. Importantly, the addition of the patch to the infarct area does *not* appear to result in chronic inflammation, although further studies are required to conclusively confirm this assessment. Both the PCR and cell counts analyses showed minimal neutrophil presence and activity in the treatment groups at the end of the

7 day period, which is an indication of resolved inflammation. Likewise, the treatments do not appear to promote excessive or inadequate collagen production, at least within the inflammation phase. While collagen deposition was noticeable in the patch treatment groups, both Figures 22 and 23 show that this collagen deposition was limited to the area immediately surrounding the patch, and therefore is unlikely to increase the risk of pathophysiology. This is also supported by the majority of the tensile properties of all groups. The similar elastic moduli and ultimate tensile strength of all infarct groups shows that the patch's presence did not significantly affect the tissue turnover in the 7 days post-infarct, relative to the infarct-only group. As excessive inflammation would have resulted in high leukocyte infiltration and earlier deposition of collagen, the tensile testing can provide some comparative information on the state of inflammation (Chen et al. 2013, Shinde et al. 2014,). By maintaining the same stiffness and relatively similar protein composition, the patch allows inflammation to continue while providing the mechanical support for which it is intended.

It is possible that some of the variations seen between the groups are due to this mechanical support. Several studies have shown that application of a mechanically supportive cardiac patch will prevent expansion of the infarct area during wound healing (Wendel et al. 2014, Zhang et al. 2015, Robinson et al. 2005). A reduction or prevention of injury expansion in the patch groups are supported by the downregulation of inflammatory markers at day 7 relative to the infarct only group. It is also worth noting that IL-RA expression is significantly increased in both treatment groups during the times that macrophage activity is highest. This suggests that the patch presence may encourage expression of IL-RA, resulting in slightly faster resolution of inflammation, as IL-RA

prevents interleukin action as a receptor antagonist (RA). Faster resolution may be due to biochemical interactions with the patch itself or, more likely, due to the patch mechanically limiting the spread of injury and therefore, limiting the inflamed area. Supporting this conclusion is that both TGF-β and TNF-α are expressed in lower (albeit, statistically insignificant) levels in both treatment groups relative to infarct only expression. This suggests that the macrophage behavior is directed towards inflammation resolution, and not continuation as is often seen with implanted biomaterials (Wendel et al. 2014, Zhang et al. 2015, Robinson et al. 2005, Ricciotti et al. 2011).

Interestingly, these data also suggest that low-dose NSAID treatment has minimal effect, if any, on the wound healing process in myocardial infarction. NSAID administration post-MI has been reviewed in a number of studies, with non-conclusive results (Leshnower et al. 2006, Vuohelainen et al. 2016, Olivetti et al. 1990, Vargas-Lorenzo et al. 2013). The data discussed here is supported by the body of work that suggests that low doses of NSAIDs do not significantly alter inflammation in an injury as severe as MI, but may assist more so in pain modification and patient comfort (Olivetti et al. 1990, Vuohelainen et al. 2016). Importantly, these data do not suggest that ibuprofen results in improper inflammation, either excessive or inadequate, and may be safe to use post-MI.

Overall, this study provides adequate data to conclude that inflammation is heightened with the porcine SIS patch treatment. However, the data does not support the conclusion that the inflammatory process was chronic, or otherwise detrimental to moving towards the proliferation stage of wound healing, at least compared to the infarct alone. Therefore, we can conclude that while the patch treatment does increase inflammation,

the treatment does not appear to affect inflammation in a manner that poses significant

risk to the long-term wound healing process. This is particularly important when compared

to the mechanical aid that the patch has been shown to provide.

CHAPTER 5. CONCLUSION AND FUTURE WORK

Conclusions

These studies demonstrate a broad range of how mechanical interventions can affect soft tissue repair, both mechanically and biochemically. This work served to provide a crucial next step in multiple fields of biomedical research, that is, the "test engineering" phase which identifies potential complications with the design solution inside the system. First, understanding how suturing affects skin mechanics sheds light on how a mechanical intervention, sutures, can restore one function of skin (coverage of underlying tissue), yet have unintended effects on the physiology. By assessing the changes in elastic modulus, failure strength, and failure strain after suturing parallel or perpendicular to the tensile axis, we were able to ascertain potential failure modes in sutured soft tissues that differ from native tissue. This work demonstrates that even the most basic mechanical interventions can have significant effects on soft tissues at the macroscopic level.

The next study examined if mechanical interventions can affect soft tissues at a microscopic level while simultaneously investigating a novel tissue engineering strategy to replace damaged meniscus tissue. As adipose-derived stromal cells (ASCs) are highly abundant and are derived from the mesenchyme, they are an ideal source for differentiation towards a meniscus-like phenotype. By utilizing a combination of biochemical and mechanical stimulation, we were able to alter the phenotype of the ASCs and encourage gene expression and protein production of key meniscus proteins, such as collagen I, collagen II, aggrecan, and versican. By exposing the ASCs to cyclic mechanical tensile strain, we were successful in inducing fibrosis and chondrogenesis via

the TGF-β pathway. This clearly illustrated the potential and necessity of exploring mechanical intervention when assessing tissue engineering and regenerative medicine treatments.

Finally, we aim to explore how a mechanical intervention can affect the inflammation, and healing, of an active, mechanically-dependent soft tissue organ, the heart. By utilizing concepts on the impact of suturing on dynamic soft tissues as well as the effects of mechanical forces on the cellular level, we designed an experiment to assess how the addition of a collagen-based cardiac patch can affect the inflammation, and ultimately the long-term prognosis, of a rat myocardial infarction model. By comparing the inflammatory response using gene expression, histology, and inflammatory cell population and density, we can reasonably gauge how this cardiac patch model will affect inflammation, and therefore wound healing in a rat infarct model.

The implications of this body of work suggest that mechanical interventions will play a critical and prominent role in many tissue engineering and regenerative medicine applications. In particular, the future body of work concerning the use of cardiac patches to attenuate tissue necrosis and scar tissue bulging in myocardial infarction is of particular importance. After assessing the initial inflammation status in a patch model, it would be prudent to evaluate the long term impact of the patch. This analysis would consider not only mechanical benefits from the patch reinforcement, but how the presence of the patch affects the proliferation and maturation in the infarct. Furthermore, should the results of future work suggest that the patch model significantly aids in the promotion of wound healing in a myocardial infarct model, it would be prudent to optimize the size and material of the patch. Both of these parameters stand to affect the mechanics of the surrounding

tissue, including wall thickness, stiffness, and stress shielding. Altering these parameters may further improve patient outcomes.

Future Directions

Beyond the tasks of developing an ECM structure and developing an anti-immunogeneic cell source, there is still much work to be done before a reasonable tissue developed *in vitro* can be implemented *in vivo.* One of the most critical components of most tissues is vasculature, yet very few studies address vasculature when publishing work about a novel tissue. In fact, a number of highly publicized studies use decellularized tissues and stem cells to create "whole" organs to much fanfare (Guyette 2016). However, these organ structures do not contain a vascular network and would therefore fail quickly if removed from the cell culture media. This is not to criticize these great works, but to highlight how the typical approach of ECM + cells is lacking some of the most crucial elements of a functional tissue.

The lack of vasculature is one of the many reasons why connective tissues and avascular tissues, such as meniscus, are so attractive to tissue engineers. Connective tissues tend to be lower cell density, placing a higher priority on excellent ECM structure. This excellent ECM structure can be obtained through decellularization processes, while the lower cell population can be provided by stem cells.

REFERENCES

1. Altara R, Manca M, Sabra R, Eid A, Booz GW, Zouein FA. (2016) Temporal cardiac remodeling post-myocarial infarction: dynamics and prognostic implications in personalized medicine. Heart Fail Rev 21(25): 25-47.

2. Amer M, Bead VR, Bathon J, Blumenthal RS, & Edwards DN. (2010) Use of Nonsteroidal Anti-Inflammatory Drugs in Patients With Cardiovascular Disease. Cardiology in Review 18:204-212.

3. Arendt EA, Miller LE, & Block JE (2014) Early Knee Osteoarthritis Management Should First Address Mechanical Joint Overload. Orthop Rev (Pavia) 6: 5188.

4. Baker BM, Nathan AS, Huffman Russell G, & Mauck RL. (2009) Tissue engineering with meniscus cells derivced from surgical debris. Osteoarthritis and Cartilage 17: 336-345.

5. Baptista LS, Silva KR, Pedrosa CSG, Amaral RJ, Belizario JV, Borojevic R, & Granjeiro JM. (2013) Bioengineered cartilage in a scaffold-free method by human cartilage-derived progenitor cells: a comparison with human adipose-derived mesenchymal stromal cells. Artificial Organs 37(12): 1068-1075.

6. Beck EC, Barragan M, Tadros MH, Gehrke SH, Detamore MS. (2016) Approaching the compressive modulus of articular cartilage with a decellularized cartilage-based hydrogel. Acta Biomaterialia. 38: 94-105

7. Boag S, Andreano E, Spyridopoulos I. (2016) Lymphocyte Communication in Myocardial Ischemia/Reperfusion Injury. Article In Press

8. Bonaventura A, Montecucco F, & Dallegri F. (2016) Cellular recruitment in myocardial ischaemia/ reperfusion injury. Eur J Clin Invest 46 (6): 590-601.

9. Boza P, Ayala P, Vivar R, Humeres C, Cacere FT, Munoz C, Garcia L, Hermoso MA, & Diaz-Araya G. (2016). Expression and function of toll-like receptor 4 and inflammasomes in cardiac fibroblasts and myofibroblastsL IL-1β synthesis, secretion, and degradation. Mol Immunol. 74: 96-105.

10. Bouyarmane H, Beaufils P, Pujol N, Bellemans J, Roberts S, & Spalding T. (2014) Polyurethane scaffold in lateral meniscus segmental defects: clinical outcomes at 24 months follow-up. Orthop Traumatol Surg Res 100:153-157.

11. Brophy RH, & Matava MJ. (2012) Surgical options for meniscal replacement. J Am Acad Orthop Surg 20: 265.

12. Buma P, Ramrattan NN, van Tienen TG, & Veth RPH. (2004) Tissue engineering of the meniscus. Biomaterials 25(1): 1523-1532.

13. Byrne EM, Farrell E, McMahon LA, Haugh MG, O'Brien FJ, Campbell VA. (2008) Gene expression by marrow stromal cells in a porous collagen-glycosaminoglycan scaffold is affected by pore size and mechanical stimulation. J Mater Sci Mater Med 19:3455-3463.

14. Caimi G, Lo Presti R, Canino B, Ferrera E, & Hopps E. (2015) Behaviour of the neutrophil to lymphocyte ratio in young subjects with acute myocardial infarction. Clinical Hemorheology and Microcirculation. Article In Press.

15. Capek L, Jacquet E, Dzan L, Simunek A. (2012) The analysis of forces needed for the suturing of elliptical skin wounds. Med Biol Eng Comput. 50(2):193-8.

16. Carrino DA, Calabro A, Darr AB, Dours-Zimmermann MT, Sandy JD, Zimmermann DR, Sorrell JM, Hascall VC, & Caplan AI. Age-related differences in human skin proteoglycans. Glycobiology 2: 257-268.

17. Case N, Thomas J, Xie Z, Sen B, Styner M, & Rowe D. (2013) Mechanical input restrains PPARγ2 expression and action to preserve mesenchymal stem cell multipotentiality. Bone 52: 454-464.

18. Chanda A, Unnikrishnan V, Flynn Z, Lackey K. (2016) Experimental study on tissue phantoms to understand the effect of injury and suturing on human skin mechanical properties. Proceedings of the Institution of Mechanical Engineers part H. 231.

19. Chen W, & Frangogiannis NG. (2013) Fibroblasts in post-infarction inflammation and cardiac repair. Biochimica et Biophysica Acta 1833: 945-953.

20. Cheung HS, Huang CY, & Pelaez D. (2009) Cyclic compression maintains viability and induces chondrogenesis of human mesenchymal stem cells in fibrin gel scaffolds. Stem Cells and Development 18(1): 93-100.

21. Chia HN, & Hull ML. (2008) Compressive Moduli of the Human Meniscus in the Axial and Radial Direction at Equilibrium and at Physiological Strain Rate. Journal of Orthopedic Research 8: 951-956.

22. Chu B, & Deshmukh, N. (1989) The lack of effect of pentoxifylline on random skin flap survival. Plastic and Reconstructive Surgery 83: 315-318.

23. Connelly JT, Vanderploeg EJ, Mouw JK, Wilson CG, & Levenston ME. (2010) Tensile Loading Modulates Bone Marrow Stromal Cell Differentiation and the Development of Engineered Fibrocartilage Constructs. Tissue Eng A 16: 1913-1923.

24. Corr, DT, & Hart DA. (2011) Biomechanics of Scar Tissue and Uninjured Skin. Advances in Wound Care (2)2: 37-43.

25. D'Amore A, Yoshizumi T, Luketich SK, Wolf MT, Gu X, Cammarata M, Hoff R, Badylak SF, Wagner WR. (2016) Bi-layered polyurethane- Extracellular matrix cardiac patch improves ischemic ventricular wall remodeling in a rat model. Biomaterials 107: 1-14.

26. Edwards D, & Elson R. (1995) Skin closure using nylon and polydioxanone: a comparison of results. Journal of the Royal College of Surgeons of Edinburgh 40: 342-353.

27. Feng L, Moore XL, Dart AM, Wang LM. (2015) Systemic inflammatory response following acute myocardial infarction. J Geriatr Cardiol. 12:305-312.

28. Frangogiannis NG, Smith CW, Entman ML. (2002) The inflammatory response in myocardial infarction. Cardiovascular Research 53: 31-47

29. Galie PA, Khalid N, Carnahan KE, Westfall MV, & Stegemann JP. (2013) Substrate stiffness affects sarcomere and costamere structure and electrophysiological function of isolated adult cardiomyocytes. Cardiovascular Physiology 22(1): 219-227.

30. Geissman F, Gordon S, Hume DA, Mowat AM, & Randolph GJ. (2010) Unraveling mononuclear phagocyte heterogeneity. Nature Reviews Immunology 10(6): 453-460.

31. Gerdisch MW, Shea RJ, Barron MD.(2014). Clinical experience with CorMatrix extracellular matrix in the surgical treatment of mitral valve disease. J Thorac Cardiovasc Surg. 148:1370-8.

32. Grady E, Elder S, Ryan P, Swiderski C, & Rashmir-Raven A. (2009) Biomechanical and molecular characteristics of hereditary equine regional dermal asthenia in Quarter Horses. Veterinary Dermatology 20: 591-599.

33. Greenwald D, Shumway S, Albear P, & Gottlieb L. (1994) Mechanical Comparison of 10 Suture Materials before and after *in Vivo* Incubation. Journal of Surgical Research 56: 372-377.

34. Giroux M, & Descoteaux A. (2000). Cyclooxygenase-2 Expression in Macrophages. Modulation by Protein Kinase C-α. J Immunol 165: 3985-3991.

35. Godwin JW, Pinto AR, & Rosenthal NA. (2016) Chasing the recipe for a pro-regenerative immune system. Sem Cell Dev Biol. Article in Press.

36. Harries RL, Bosanquet DC, Harding KG. (2016) Wound bed preparation: TIME for an update. International Wound Journal. Article In Press.

37. Hasan J, Fisher J, & Ingham, E. (2014) Current strategies in meniscal regeneration. J Biomed Mater Res B Appl Biomater 102: 619.

38. Hatsushika D, Muneta T, Nakamura T, Horie M, Koga H, & Nakagawa, Y. (2014) Repetitive allogeneic intraarticular injections of synovial mesenchymal stem cells promote meniscus regeneration in a porcine massive meniscus defect model. Osteoarthritis Cartilage 22: 941-950.

39. Higashioka MM, Chen JA, Hu JC, & Athanasiou KA. (2014) Building an anisotropic meniscus with zonal variations. Tissue Eng Part A 20: 294.

40. Holzapfel, GA. (2000) Biomechanics of Soft Tissue. Computational Biomechanics 7(1): 1-15.

41. Ibrahim A, Ayeni OA, Hughes KB, Lee BT, Slavin SA, Lin SJ. (2013). Acellular Dermal Matrices in Breast Surgery. Annals of Plastic Surgery 70(6):732-740.

42. Iyer RP, Jung M, Lindsey ML. (2016) MMP-9 signaling in the left ventricle following myocardial infarction. Am J Physiol Heart Circ Physiol 311: H190-H198.

43. Jansen LA, De Caigny P, Guay N, Lineaweaver WC, Shokrollahi K. (2013) The Evidence Base for the Acellular Dermal Matrix AlloDerm. Ann Plast Surg 70: 587-594.

44. Jugdutt BI, Halliday I, & Uwiera RE. (2007) Therapeutic drugs during healing after myocardial infarction modify infarct collagens and ventricular distensibility at elevated pressures. Mol Cell Biochem 304: 79-91.

45. Kapellos TS, Iqbal AJ. (2016) Epigenetic control of macrophage polarisation and soluble mediator gene expression during inflammation. Mediators of Inflammation. 6(59): 1-15.

46. Kessler D, Dethlefsen S, Haase I, Plomann M, Hirche F, & Krieg, T. (2001) Fibroblasts in mechanically stressed collagen lattices assume a "synthetic" phenotype. J Biol Chem 276: 36575-36585.

47. Khani MM, Tafazzoli-Shadpour M, Goli-Malekabadi Z, Haghighipour N. Mechanical characterization of human mesenchymal stem cells subjected to cyclic uniaxial strain and TGF-B1. J Mech Behav Biomed Mater 43:18-25. 2015.

48. Kirkby NS, Tesfai A, Ahmetaj-Shala B, Gashaw HH, Sampaio W, Etelvino G, Leao NM, Santos RA, Mitchell JA. Ibuprofen arginate retains eNOS substrate activity and reverses endothelial dysfunction: implications for the COX2/ADMA axis. The FASEB Journal. 30:1-7.

49. Kisiday JD, Frisbie DD, McIlwraith CW, & Grodzinsky AJ. (2009) Dynamic compression stimulates proteoglycan synthesis by mesenchymal stem cells in the absence of chondrogenic cytokines. Tissue Eng Part A 15: 2817-2824.

50. Kokai LE, Marra KJ, & Rubin JP. (2014) Adipose stem cells: biology and clinical applications for tissue repair and regeneration. Translational Research 163(4): 399-408.

51. Kong J, Grando SA, & Li YC. (2006) Regulation of IL-1 Family Cytokines IL-1α, IL-1 Receptor Antagonist, and IL-18 by 1,25 Dihydroxyvitamin D3 in Primary Keratinocytes. The Journal of Immunology 176: 3780-3787

52. Kun M, Titan AL, Stafford M, Zheng CH, & Levenston ME. (2012) Variations in chondrogenesis of human bone marrow-derived mesenchymal stem cells in fibrin/alginate blended hydrogels. Acta Biomaterialia 8(10): 3754-3764.

53. Lam MT, Huang YC, Birla RK, & Takayama S. (2009) Microfeature guided skeletal muscle tissue engineering for highly organized 3-dimensional free-standing constructs. Biomaterials 30(6):1150-1155.

54. Lam MT, Nauta A, Meyer NP, Wu JC, & Longaker MT. (2013) Effective Delivery of Stem Cells Using an Extracellular Matrix Patch Results in Increased Cell Survival and Proliferation and Reduced Scarring in Skin Wound Healing. Tissue Engineering A 19: 738-747.

55. Lam MT, Wu JC (2012). Biomaterial applications in cardiovascular tissue repair and regeneration. Expert Rev Cardiovasc Ther. 10(8): 1039-49.

56. Langton AK, Graham HK, McConnell JC, Sherratt MJ, Griffiths CEM, Watson REB. (2017) Organisation of the dermal matrix impacts the biomechanical properties of skin. British Journal of dermatology. Article in Press.

57. Leshnower BG, Sakamoto H, Zeeshan A, Parish LM, & Gorman RC. (2006) Role of acetaminophen in acute myocardial infarction. Heart and Circulatory Physiology 290: H2424-2431.

58. Levi K, Ichiryu K, Kefel P, Keller J, Grice J, Belson O, Storne E, Safa B. (2016) Mechanics of wound closure: emerging tape-based would closure technology vs. traditional methods. Cureus. 8(10):86.

59. Li Z, Kupcsik L, Yao SJ, Alini M, Stoddart M. Mechanical load modulates chondrogenesis of human mesenchymal stem cells through the TGF-B pathway. J Cell Mol Med. 14:1338-1346. 2010.

60. Lister Z, Rayner KJ, Suuronen EJ. (2016) How Biomaterials Can Influence Various Cell Types in the Repair and Regeneration of the Heart after Myocardial Infarction. Front Bioeng Biotechnol (4):62.

61. Longo UG, Rizzello G, Berton A, Fumo C, Battaglia G, & Khan WS. (2013) A review of preclinical and clinical studies using synthetic materials for meniscus replacement. Curr Stem Cell Res Ther 8: 438-443.

62. Makris EA, Hadidi P, & Athanasious A. (2004) The knee meniscus: Structure-function, pathophysiology, current repair techniques, and prospects for regeneration. Biomaterials 32: 7411-7431.

63. Mandal BB, Park SH, Gil ES, & Kaplan DL. (2011) Stem cell-based meniscus tissue engineering. Tissue Eng Part A. 17: 2749-2761.

64. McDermott ID, Masouros SD, & Amis AA. (2008) Biomechanics of the meniscus of the knee. Current Orthopaedics 22: 193-201.

65. Meier EM, Lam MT. (2016) Role of Mechanical Stimulation in Stem Cell Differentiation. JSM Biotechnology and Biomedical Engineering. Article in Press.

66. Meier EM, Wu B, Siddiqui A, Tepper D, Lam MT. (2016) Mechanical Stimulation Increases RNA-level expression of Knee Meniscus Genes in Adipose-Derived Stromal Cells. Plastic and Reconstructive Surgery. 16;4(9):e864.

67. Mewhort HEM, Turnball JD, Meijndert HC, Ngu JMC, Fedak PWM. (2014) Epicardial infarct repair with basic fibroblast growth factor-enhanced CorMatrix-ECM biomaterial attenuates postischemic cardiac remodeling. J Thorac Cardiovasc Surg 147:1650-9.

68. Mikic B, Johnson TL, Chhabra AB, Schalet BJ, Womng M, & Hunziker EB. (2000) Differential effects of embryonic immobilization on the development of fibrocartilaginous skeletal elements. Journal of Rehabilitation Research and Development 37(2): 127-133.

69. Miller, K. (2000) Biomechanics of soft tissues. Medical Science Monitor 6: 158-167.

70. Naal FD, Schauwecker J, Steinhauser E, Milz S, von Knoch F, & Mittelmeier W. (2008) Biomechanical and immunohistochemical properties of meniscal cartilage after high hydrostatic pressure treatment. J Biomed Mater Res B Appl Biomater 87: 19-25.

71. Nah DY, Rhee MY. (2009) The Inflammatory Response and Cardiac Repair After Myocardial Infarction. The Korean Society of Cardiology. 39:393-398.

72. Nerurkar NL, Han W, Mauck RL, & Elliott DM. (2011) Homologous structure-function relationships between native fibrocartilage and tissue engineered from MSC-seeded nanofibrous scaffolds. Biomaterials 32: 461-468.

73. Nishimuta JF, & Levenston ME. (2012) Response of cartilage and meniscus tissue explants to in vitro compressive overload. Osteoarthritis and Cartilage 5(20): 422-429.

74. Oh SJ, Kim Y. (2011) Combined AlloDerm and thin skin grafting for the treatment of postburn dyspigmented scar contracture of the upper extremity. Journal of Plastic Reconstructive and Aesthetic Surgery 64, 229-233.

75. Okuno M, Muneta T, Koga H, Ozeki N, Nakagawa Y, & Tsuji K. (2014) Meniscus regeneration by syngeneic, minor mismatched, and major mismatched transplantation of synovial mesenchymal stem cells in a rat model. J Orthop Res 32: 928-936.

76. Olsen AM, Fosbol EL, Lindhardsen J, Folke F, Charlot M, Selmer C, Lambers M, Olsesen JB, Kober L, Hansen PR, Torp-Pedersen C, Gislason G. (2011). Duration of Treatment With Nonsteroidal Anti-Inflammatory Drugs and Impact on Risk of Death and Recurrent Myocardial Infarction in Patients with Prior Myocardial Infarction. Circulation. 123: 2226-2235.

77. Olivetti G, Capasso JM, Sonnenblick EH, & Anversa P. (1990) Side-to-Side Slippage of Myocytes Participates in Ventricular Wall Remodeling Acutely After Myocardial Infarction in Rats. Circulation Research 6: 23-34.

78. Ong HT, Ong LM, Tan TE, & Chean KY. (2013) Cardiovascular Effects of Common Analgesics. Med J Malaysia 68: 189- 176.

79. Otsubo H. (2016) Repair of Acute Patellar Tendon Rupture Augmented with Strong Sutures. J Knee Surg. 1538-8506.

80. Pak J, Lee JH, & Lee SH. (2014) Regenerative repair of damaged meniscus with autologous adipose tissue-derived stem cells. Biomed Res Int. 3: 436029-436039.

81. Pak J, Lee JH, & Lee SH. (2014) Regenerative repair of damaged meniscus with autologous adipose tissue-derived stem cells. BioMed Research International.

82. Park JH, Ushida T, & Akimoto T. (2013) Control of cell differentiation by mechanical stress. J Phys Fitness Sports Med 2(1): 49-62.

83. Patel P, Parikh M, Shah H, Gandhi T. (2016) Inhibition of RhoA/Rho kinase by ibuprofen exerts cardioprotective effect on isoproterenol induced myocardial infarction in rats. European Journal of Pharmacology. 791: 91-98.

84. Patrono C. Cardiovascular Effects of Nonsteroidal Anti-Inflammatory Drugs. Curr Cardiol Rep. 18:25-32.

85. Pelaez D, Huang CC, & Cheung HS. (2009) Cyclic compression maintains viability and induces chondrogenesis of human mesenchymal stem cells in fibrin gel scaffolds. Stem Cells and Development 1: 93-102.

86. Perea-Gil I, Prat-Vidal C, & Bayes-Genis A. (2015) In vivo experience with natural scaffolds for myocardial infarction: the times they are a-changin'. Stem Cell Res Ther 6: 248-256

87. Petri M, Ufer K, Toma I, & Becher C. (2012) Effects of perfusion and cyclic compression on in vitro tissue engineered meniscus implants. Knee Surg Sports Traumatal Arthrosc 20: 223-231.

88. Przyklenk K. (2013). Reduction of Myocardial Infarct Size with Ischemic "Conditioning": Physiologic and Technical Considerations. Anesth Analg. 117:891-901.

89. Przyklenk K. (2015). Ischemic conditioning: pitfalls on the path to clinical translation. British Journal of Pharmacology. 172: 1961-1973.

90. Przyklenk K, Dong Y, Undyala VV, Whittaker P. (2012) Autophagy as a therapeutic target for ischaemia/reperfusion injury? Concepts, controversies, and challenges. Cardiovascular Research. 94: 197-205.

91. Qazi SM, Sindby EJ, Norgaard MA. (2015) Ibuprofen-a Safe Analgesic During Cardiac Surgery Recovery? A Randomized Controlled Trial. J Cardiovasc Thorac Res. 7(4): 141-148.

92. Ricciotti E, & FitzGerald GA. (2011) Prostaglandins and Inflammation. Arterioscler Thromb Vasc Biol 31(5): 986-1000.

93. Rich L and Whittaker P. (2005) Collagen and Picrosirius Red staining: a polarized light assessment of fibrillary hue and spatial distribution. Journal of Morphological Sciences 22: 97-104.

94. Robinson KA, Li J, Mathison M, Redkar A, Cui J, Chronos NAF, Matheny RG, & Badylak SF. (2005) Extracellular Matrix Scaffold for Cardiac Repair. Circulation 112: I-135-I-143.

95. Roeder C, & Driesch P. (1999) Psoriatic erythroderma and bullous pemphigoid treated successfully with acitretin and azathioprine. European Journal of Dermatology 9: 537-539.

96. Rongen JJ, van Tienen TG, van Bochove B, Grijpma DW, & Buma P.(2014) Biomaterials in search of a meniscus substitute. Biomaterials 35: 3527.

97. Rothrauff BB, Numpaisal PO, Lauro BB, Alexander PG, Debski RE, Musahl V, Tuan RS. (2016) Augmented repair of radial meniscus tear with biomimetic electrospun scaffold: an in vitro mechanical analysis. J Exp Orthop 3(1):23-30.

98. Roussis PC, Giannakopoulos AE, Charalambous HP. (2015) Suture line response of end-to-side anastomosis: A stress concentration methodolody. Cardiovasc Eng Techno 6(1):36-48.

99. Saha S, Ji L, de Pablo JJ, Palecek SP. Inhibition of human embryonic stem cell differentiation by mechanical strain. J Cell Physiol. 206:126-137. 2006.

100. Saha S, Ji L, de Pablo JJ, Palecek SP. TGFB/Activin/Nodal Pathway in Inhibition of Human Embryonic Stem Cell Differentiation by Mechanical Strain. Biophys J. 94:4123-4133. 2008.

101. Saulis A, Lautenschlager E, & Mustoe T. (2002) Biomechanical and viscoelastic properties of skin, SMAS, and composite flaps as they pertain to rhytidectomy 110: 177-183.

102. Schleip R, & Muller DG. (2013) Training principles for fascial connective tissues: Scientific foundation and suggested practical applications. Journal of Bodywork and Movement Therapies 17(1): 103-155.

103. Schüttler KF, Pöttgen S, Getgood A, Rominger MB, Fuchs-Winkelmann S, & Roessler PP. (2014) Improvement in outcomes after implantation of a novel polyurethane meniscal scaffold for the treatment of medial meniscus deficiency. Knee Surg Sports Traumatol Arthrosc 7: 1929-1935.

104. Scotti C, Hirschmann MT, Antinolfi P, Martin I, & Peretti GM. (2013) Meniscus repair and regeneration: review on current methods and research potential. Eur Cell Mater 26: 150.

105. Selvi E, Manganelli S, Catenaccio M, De Stefano R, Frati E, Cucini S, & Marcolongo R. (2000) Diff Quik staining method for detection and identification of monosodium urate and calcium phosphate crystals in synovial fluids. Ann Rheum Dis 60:194-198.

106. Sen B, Guilluy C, Xie Z, Case N, Styner M, Thomas J, Oguz I, Rubin C, Burridge K, Rubin J. Mechanically Induced Focal Adhesion Assembly Amplifies Anti-Adipogenic Pathways in Mesenchymal Stem Cells. Stem Cells. 29:1829-1836. 2011.

107. Serpooshan V, Zho M, Metzler SA, Wei K, Shah PB, Wang A, Mahmoudi M, Malkovskiy AV, Rajadas J, Butte MJ, Bernstein D, Ruiz-Lozano P. (2013). The effect of bioengineered acellular collagen patch on cardiac remodeling and ventricular function post myocardial infarction. Biomaterials 34:9048-9055.

108. Shahabiour F, Banach M, Johnston TP, Pirro M, Sahebkar. (2016) Novel approaches toward the generation of bioscaffolds as a potential therapy in cardiovascular tissue engineering. International journal of cardiology. 228 319-326.

109. Shinde AV, & Frangogiannis NG. (2014) Fibroblasts in myocardial infarction: A role in inflammation and repair. Journal of Molecular and Cellular Cardiology 70:74-82.

110. Shwartz Y, Blitz E, & Zelzer E. (2013) One load to rule the all: Mechanical control of the musculoskeletal system in development and aging. Differentiation. 86(3): 104-111.

111. Silverman, JF. Inflammatory and neoplastic processes of the lung: differential diagnosis and pitfalls in FNA biopsies. Diagnostic Cytopathy 13(5): 448-462.

112. Son M, Goodman SB, Chen W, Hargreaves BA, Gold GE, & Levenston ME. (2013) Regional variation in T1p and T2 times in osteoarthritic human menisci: correlation with mechanical properties and matrix composition. Osteoarthritis and Cartilage 6(21): 796-805.

113. Stuart SD, De Jesus NM, Lindsey ML. (2016) Ripplinger, CM. The crossroads of inflammation, fibrosis, and arrhythmia following myocardial infarction. Journal of Molecular and Cellular Cardiology 91: 114-122.

114. Stuart SDF, De Jesus NM, Lindsey ML, & Ripplinger CM. (2016) The crossroads of inflammation, fibrosis, and arrhythmia following myocardial infarction. J Mol Cell Car 91: 114-122.

115. Sutherland AJ, Converse GL, Hopkins RA, Detamore MS. 2015. The bioactivity of cartilage extracellular matrix in articular cartilage regeneration. Adv Healthc Mater. 4(1): 29-39.

116. Tan MY, Zhi W, Wei RQ, Huang YC, Zhou KP, Tan B, Deng L, Luo JC, Li XQ, Xie HQ, Yang ZM. (2009). Repair of infarcted myocardium using mesenchymal stem cell seeded small intestinal submucosa in rabbits. Biomaterials. 30:3234-3240.

117. Teramura T, Takehara T, Onodera Y, Nakagawa K, Hamanishi C, Fukuda K. Mechanical stimulation of cyclic tensile strain induces reduction of pluripotent related gene expressions via activation of Rho/ROCK and subsequent decreasing of AKT phosphorylation in human induced pluripotent stem cells. Biochem Biophys Res Commun 417:836-841. 2012

118. Thambyah A, Nather A, & Goh J. (2006) Mechanical properties of articular cartilage covered by the meniscus. Osteoarthritis and Cartilage 14: 580-588.

119. Toeg HD, Tiwari-Pandey R, Seymour R, Ahmadi A, Crowe S, Vulesevic B, Suuronen EJ, Ruel M. (2013). Injectable Small Intestine Submucosal Extracellular Matrix in an Acute Myocardial Infarction Model. Ann Thorac Surg 96:1686-94.

120. Turer AT, & Hill JA. (2010) Pathogenesis of Myocardial Ischemia-Reperfusion Injurt and Rationale for Therapy. Am J Cardiol 106(3): 360- 368

121. Van den Berg TK, Puklavec MJ, Barclay AN, Dijkstra CD. (2001) Monoclonal antibodies against rat leukocyte surface antigens. Immunological Reviews. 183:109-116.

122. Van Hout GPJ, van Solinge WW, Gijsberts CM, & Hoefer IE. (2015). Elevated mean neutrophil volume represents altered neutrophil composition and reflects damage after myocardial infarction. Basic Res Cardiol 110: 58-69

123. Vangsness CT Jr., Farr J 2nd, Boyd J, Dellaero DT, Mills CR, & LeRoux-Williams M. (2014) Adult human mesenchymal stem cells delivered via intra-articular injection to the

knee following partial medial meniscectomy: a randomized, double-blind, controlled study. J Bone Joint Surg Am 96: 90-98.

124. Vargas-Lorenzo C, Riera-Guardia N, Calingaert B, Castellsague J, Salvo F, Nicotra F, Sturkenboom M, & Perez-Gutthann S. (2013) Myocardial infarction and individual nonsteroid anti-inflammatory drugs meta-analysis of observational studies. Pharamcoepidemiol Drug Saf 22(6): 559-570.

125. Vesentini S, Redalli A, & Montevecchi F. (2003) Skin Nanostructural Features Determine Suture Biomechanics. Transactions on Nanobioscience 2: 79-87.

126. Voorhees AP, DeLeon-Pennell KY, Ma Y, Halade GV, Yabluchanskiy A, Iyer RP, Flynn E, Cates CA, Lindsey ML, Han HC. (2015). Building a better infarct: Modulation of collagen cross-linking to increase infarct stiffness and reduce left ventricular dilation post-myocardial infarction. Journal of Molecular and Cellular Cardiology. 85:229-239.

127. Vuohelainen V, Paavonen T, Hamalainen M, Moilanen E, & Mennander AA. (2014) C4d Deposition Reveals Myocardial Infarction After Cardiac Arrest- Experimental Study. Adv Clin Exp Med Article in Press.

128. Wan E, Yeap XY, Dehn S, Terry R, Novak M, Zhang S, & Thorp EB. (2013) Enhanced Efferocytosis of Apoptotic Cardiomyocytes Through Myelod-Epithelial-Reproductive Tyrosine Kinase Links Acute Inflammation Resolution to Cardiac Repair After Infarction. Circulation Research 113: 1004-1012.

129. Wan F, Letavernier E, Jourdan Le Saux C, Houssani A, Abid S, Czibik G, Sawaki D, Marcos E, Dubois-Rande JL, Baud, L, Adnot S, Derumeaux G, & Gellen B. (2015) Calpastatin Overexpression Impairs Post-infarct Scar Healing in Mice by Compromising

Reparative Immune Cell Recruitment and Attachment. Am J Physiol Heart Circ Physiol. Article In Press.

130. Wan L, Chan Y, Wang Z, Wang W, Schmull S, Dong J, Xue S, Imboden H, Li J. (2017) Human heart valve- derived scaffold improves cardiac repair in a murine model of myocardial infarction. Sci Rep. Article in Press.

131. Wan Z, Zheng S, Fan Y, Liu K, Du F, Davey AM, Zhang H, Han W, Xiong C, & Liu W. (2013) B Cell Activation Is Regulated by the Stiffness Properties of the Substrate Presenting the Antigens. The Journal of Immunology 190: 4661-4675.

132. Wang A, Kleinerman R, Armstrong A, Fitzmaurice S, Pascucci A, Awasthi S, Ratnarathorn M, Sivamani R, King T, & Eisen D. (2014) Set-back buried vertical mattress suturing: results of a randomized blinded trial. Journal of American Academy of Dermatology 72: 674-680.

133. Wendel JS, Ye L, Zhang P, Tranquillo RT, & Zhang JJ. (2014) Functional Consequences of a Tissue-Engineered Myocardial Patch for Cardiac Repair in a Rat Infarct Model. Tissue Engineering A 20: 1325-1335.

134. Wenger MPE, Bozec, L, Horton MA, & Mesquida P. (2007) Mechanical Properties of Collagen Fibrils. Biophysical Journal 93: 1255-1263.

135. Whittaker P, & Przyklenk K. (2009) Fibrin architecture in clots: A quantitative polarized light microscopy analysis. Blood Cells Mol Dis 42: 51-56.

136. Xu Y, Malladi P, Chiou M, Bekerman E, Giaccia AJ, Longaker MT. (2007) In vitro expansion of adipose-derived adult stromal cells in hypoxia enhances early chondrogenesis. Tissue Eng 13: 2981-2993.

137. Yuan X, Arkonac DE, Chao PH, & Vunjak-Novakovic G. (2014) Electrical stimulation enhances cell migration and integrative repair in the meniscus. Sci Rep 4: 3674.

138. Zhang J (2015) Engineered Tissue Patch for Cardiac Cell Therapy. Curr Treat Options Cardio Med 17: 37-48.

139. Zhu F, Dong L, Jin X, Jiang B, Kalra A, Shen M, & Yang K. (2015) Testing and modeling the responses of Hybrid III Crash-Dummy Lower Extremity under high-speed vertical loading. Stapp Car Crash Journal 59: 521-536.

ABSTRACT

MECHANICAL INTERVENTIONS IN SOFT TISSUE REPAIR

by

ELIZABETH MEIER
May 2017

Advisor: Dr. Mai Lam

Major: Biomedical Engineering

Degree: Doctor of Philosophy

This body of work sets to investigate some of these mechanical interventions that are designed to promote wound healing, repair, or even replace an injured tissue. By investigating three separate tissues and three separate mechanical interventions, we can draw conclusions about the implications of including mechanical interventions in biomedical research and clinical treatments. The use of sutures to close wounds is highly common, however the effects of sutures on the tensile mechanics of human skin are largely unknown. To evaluate how sutures may affect uniaxial tensile mechanics, human skin samples were sutured and loaded in tension in multiple orientations. The data suggested that the sutured skin had a lower fracture strength and higher elastic modulus than the intact skin, particularly when loaded in-line with the injury. Next, the inflammatory effects of a decellularized ECM patch in a myocardial infarction model were analyzed. A commercially available decellularized material, porcine small intestine submucosa, was evaluated as a patch treatment in a rat myocardial infarction model, a treatment that is common in cardiac research. As anticipated, the addition of the patch in the injury area increased local inflammation as indicated by gene expression and leukocyte population

and density. However, the patch did not appear to extend the inflammation response nor affect the response in a manner that would suggest hindrance to wound healing. Thirdly, a unique biochemical and mechanical approach was used to direct human adipose stem cells to differentiate towards a meniscus-like phenotype. By using a variety of media formulations and a variation of uniaxial tensile parameters, a protocol to maximize meniscus gene expression was concluded. A chondrogenic media formulation with 10% uniaxial strain at 1 Hz for 3 hours was found to have the greatest increase in meniscus gene expression of all of the parameters tested. Together, each of these individual works contributes to the conclusion that mechanical interventions can have a significant impact on the restructuring, repair, and replacement of soft tissues.

AUTOBIOGRAPHICAL STATEMENT

.

Elizabeth majored in biomedical engineering at Michigan Technological University in Houghton, MI. Her work in the healthcare industry and as a professional engineer fueled her desire to continue her education to better contribute to the current struggles of the healthcare system. In her spare time, she enjoys training and competing in road races and triathlons.

<u>PUBLICATIONS</u>

Elizabeth M. Meier MSE, Bin Wu, Aamir Siddiqui MD, Donna Tepper MD, Mai T Lam PhD. Mechanical Stimulation Increases RNA-level expression of Knee Meniscus Genes in Adipose-Derived Stromal Cells. Plastic and Reconstructive Surgery. 2016 Sep 16;4(9):e864.

Elizabeth M. Meier MSE, Mai T Lam PhD. Role of Mechanical Stimulation in Stem Cell Differentiation. JSM Biotechnology and Biomedical Engineering. 2016. Article in Press.

Cameron B Pinnock, MSE; Elizabeth M Meier, MSE; Neeraj N Joshi, MD; Bin Wu, MD; Customizable Engineered Blood Vessels Using 3D Printed Inserts. Methods. 2016 Apr 15;99:20-7.

Elizabeth M. Meier MSE, Bin Wu, Mai T Lam PhD. The Inflammatory and Mechanical Effects of Porcine Small Intestine Submucosa Patches on Cardiac Tissue Post-Myocardial Infarction. Tissue Engineering Part A. *Submitted.*

Elizabeth M. Meier MSE, Bin Wu, Mai T Lam PhD. Effects of Strain Rate and Suturing on Mechanical Behavior of Skin. Biomechanics. *Submitted*